INSTABILITY OF CROSS-FLOW THROUGH CIRCULAR CYLINDERS

By

MINTER CHENG

Bachelor of Engineering
Feng Chia University
Taichung, Taiwan
Republic of China
1979

Master of Science
Oklahoma State University
Stillwater, Oklahoma
1985

Submitted to the Faculty of the Graduate College
of the Oklahoma State University
in partial fulfillment of the requirements
for the Degree of
DOCTOR OF PHILOSOPHY
May, 1991

INSTABILITY OF CROSS-FLOW THROUGH

CIRCULAR CYLINDERS

Thesis Approved:

Thesis Adviser

Dean of the Graduate College

ACKNOWLEDGEMENTS

The author wishes to express his deepest appreciation to his major advisor, Dr. Peter M. Moretti, for his experienced advice and constant guidance throughout this work. Appreciation is extended to Dr. Richard L. Lowery for his assistance of instrumentation problems. Gratitude is also extended to other committee members, Dr. David G. Lilley, Frank W. Chambers, and Dr. Kenneth J. Bell for their advice and criticism.

The author also like to recognize the financial support of the Electric Power Research Institute, technical monitor Mr. David A. Steininger.

Finally, the author wishes to express his sincere gratitude to his parents, Yuan-Chi and Pi-Ann Cheng, his wife, Suefen Chen, his brothers, George and Frank Cheng, and dear friends, Tom and Sue Moore, whose encouragement and support make all this possible.

TABLE OF CONTENTS

Chapter Page

LIST OF FIGURES

NOMENCLATURE

A	oscillation amplitude (a half of peak-to-peak)
C_n	nth cylinder in test model
D	circular cylinder diameter
E	hot-film anemometer output voltage
e'	fluctuation voltage
f	vortex shedding frequency
f_e	driving frequency of oscillation cylinder
f_n	natural frequency of cylinder
f_0	frequency for stationary flow condition
J_n	jet on the right hand side of nth cylinder
K_1, K_2	hot-film calibration constant
P	pitch distance
Re	Reynolds number
S	Strouhal number
U	free stream velocity
u'	fluctuation velocity
W_n	wake behind nth cylinder
ρ	fluid density
Superscripts	
$\bar{()}$	time-mean average
$()'$	fluctuation quantity

CHAPTER I

INTRODUCTION

1.1 Flow-Induced Vibration and Flow Instability

Fluid flow across a single or a group of circular cylinders not only is an important fundamental question in fluid dynamics but also has many practical applications in various areas of engineering and science. These areas include mechanical and aerospace engineering, power and process industries (turbine blades, heat exchanger tubes, power transmission lines), civil engineering (chimney stacks, bridges, buildings, radio telescopes, ice dams), and undersea technology (offshore drilling rigs, underwater pipelines, marine cables).

It is a long recognized fact that an uniform upstream fluid flow through a grid or a cascade of closely spaced circular cylinders is unstable. This instability is caused by the existence of multi-stable flow patterns which switch from one condition to another one at irregular time intervals. As the flow pattern switches, it changes the fluid forces acting on the cylinders. If the frequency of flow patterns switching is near to or coincides with the cylinder natural frequency, a severe vibration problem will be established. The instability provides a mechanism by which the energy of the flowing fluid is converted to cylinder vibrations.

In recent years, flow-induced vibration problems in heat exchangers have received a great deal of attention, since there has been a trend toward much larger heat exchangers, and toward increased shell-side velocities to improve heat transfer. In some cases, this has resulted in the occurrence of strong vibration in the tube banks, accompanied by intense

noise. The large amplitude vibration of the heat exchanger tubes can create fatigue and fretting failures and lead to plant shut-down. In the last two decades, the utility industry has lost in the order of $100 million to $1 billion due to vibration-related problems in heat-exchange equipments. The great majority of these problems occur as a result of flow instabilities. Therefore, flow instability is an important topic in flow-induced vibration research. Although the flow-induced vibration can be reduced through some proper techniques, the vibration cannot fully be removed. Thus basically, any heat exchanger system is subjected to some kind of flow-induced vibration.

1.2 Present Study Objectives

To predict the occurrence of vibration in a closely-spaced tube bundle subjected to crossflow, there must be an understanding of the phenomena that produce the exciting forces and of the dynamic response of the tubes. Therefore, a better understanding of the flow-induced vibration excitation mechanism for closely-spaced tube bundles is essential to the development of improved design methods for highly rated heat exchangers.

During the current decade, a great number of publications describing experimental and theoretical work have appeared in the literature. However, due to very complicated flow behavior in and behind tube arrays as well as a complexity of dynamic interaction between tube and fluid flow, to date the phenomenon of crossflow induced vibration is still far from being completely understood. Moreover, most of the published literature deals with the immediate problems of designers, relatively little fundamental research has been conducted.

In order to understand more clearly the characteristics of flow-induced vibration and the mechanism governing vibrational instability, the detailed flow behavior around a single and a group of circular cylinders needs to be investigated. The present study is carried out in this direction, using flow-visualization techniques and hot-film anemometer measurements to study wake formation, vortex formation, jet switching, and the lock-in

phenomenon of circular cylinders subjected to crossflow. It was hoped that this study would provide some deeper insight into flow-induced vibration mechanisms. Although this study is restricted to laminar flow at low Reynolds numbers, it offers a valuable tool for understanding the detailed structures in the above mentioned phenomena.

The present experiments were conducted on a free-surface water table, which includes a single cylinder, a normal cylinder pair, a single tube row with pitch-to-diameter ratios (distance between tubes' centers divided by the tube diameter) of 1.4, 1.33, and 1.25, and four-row tube arrays of 90, 60, 45, and 30 degree arrangements with pitch-to-diameter ratios of 1.4, 1.33, and 1.25 as testing models. The basic approach used in this study to achieve the above mentioned objectives is as follows:

1. Flow visualization by dye injection technique was used to highlight the important features and structures of the flow field.
2. A hot-film anemometer with the help of high speed data acquisition and a spectrum analyzer was used to perform measurements of the time-mean velocity, turbulence intensity, and vortex shedding frequency in the flow field of interest.
3. The spectra of fluctuation velocities were measured to obtain the shedding frequencies and were used to analyze the lock-in effect of a single cylinder and a normal cylinder pair.
4. Flow visualization technique was used to study the effect of tube displacement on flow instability.

1.3 The Present Contribution

The flow phenomena of fluid flow through a single and a group of circular cylinders have been visualized by dye injection techniques. Interpretation of these observations strongly suggested that complex instability exists in and behind closely-spaced tube rows and tube arrays. The emerging jets grouped together in a random manner, and flow pattern switched from one quasi-stable pattern to another one at irregular

time intervals. Lock-in behaviors of a single cylinder and a normal cylinder pair are investigated in this study. A new form of slanted onion-shape lock-in boundaries for a single cylinder with forced transverse vibration is observed and has not been found in other previous published results. Lock-in behavior of a large pitch ratio cylinder pair is similar to that of the single cylinder. A totally different lock-in behavior exists for a closely spaced cylinder pair. An even-number superharmonic lock-in is dominant in this case, in contrast to the single cylinder case which has odd-number superharmonic lock-in.

1.4 Outline of the Thesis

The first chapter of this five-chapter thesis is the introduction. Flow instability and its relation to flow-induced vibration is briefly described. The objectives of this study are also stated and justified.

A comprehensive literature survey of the flow behavior around a single cylinder, a normal cylinder pair, a single tube row, and a multi-tube-row array is described in Chapter II. A brief description of flow-induced vibration mechanisms is also stated.

A complete description of the experimental facility and measurement equipment is presented in Chapter III. The data acquisition, flow visualization techniques, and traversing & vibratory mechanisms are fully discussed.

Chapters IV and V give the conclusions of this research. The first presents results of the flow visualization and measurement techniques. These results are discussed thoroughly. Chapter V emphasizes the main conclusions to be drawn from this investigation.

CHAPTER II

SURVEY OF RELATED LITERATURE

Information regarding basic flow-induced vibration mechanisms and flow instability through a single and a group of circular cylinders has been extensively surveyed. Noteworthy results are included in the following summary where the emphasis is on instability flow.

2.1 Basic Flow-Induced Vibration Mechanisms

The initial investigation into flow-induced vibration problem was reported more than one hundred years ago, when Strouhal published his basic work concerning Aeolian tones. Lately, one of the most important flow-induced vibration problems deals with an array of circular cylinders subjected to crossflow. The observed flow-induced vibration phenomenon is very complex. At present, use of the fundamental principles of fluid and structural dynamics to solve this vibration problem has proved impossible. After several decades of research, it is generally accepted that the principal excitation mechanisms for the crossflow induced vibration [1-5] are turbulent buffeting, vortex shedding, and fluidelastic instability. They will be discussed separately under their headings.

2.1.1 Turbulent Buffeting

Cylinders in a tube array subjected to crossflow will encounter small amplitude vibration as a result of pressure fluctuations due to turbulence in the flow. In general, the energy associated with turbulent pressure fluctuations rather than being concentrated at a discrete frequency is normally distributed over a broad band of frequencies [1]. The

frequency spectrum distributes around a central dominant frequency which increases as the crossflow velocity increases. The cylinders selectively extract energy from the turbulence at their natural frequency and vibrate in a small amplitude and irregular manner corresponding to their amplification functions. The average amplitude increases in direct proportion to the dynamic head ($\rho U^2/2$) [1-5]. If the turbulence spectrum and spatial correlations in a cylinder array are known, structural response caused by turbulent buffeting can be predicted. However, the information about the turbulence within an array, its spectral distribution and level, is usually very limited, and it is very difficult to apply in practice. Over the years, this mechanism for induced vibration has received less attention than the others, because the other mechanisms often have a more serious effect on flow-induced vibrations.

2.1.2 Vortex Shedding Excitation

Fluid flow across a bluff body produces a series of vortices in the downstream wake as shown in Fig. 1. The vortices are shed alternately from each side of the body in a regular manner and alter the local pressure distribution. The structure experiences a time-varying lift force at the frequency of vortex shedding. This alternating force occurs more frequently as the flow velocity increases. If the vortex shedding frequency, which is the driving frequency, is close to or coincides with the natural frequency of the structure, vibration results. The vibration direction of the structure is predominantly perpendicular to the flow direction.

Quantitative experiments were first undertaken in 19th century by Strouhal, who defined the principal relationship

$$S = \frac{fD}{U}$$

where S is the Strouhal number, f is the vortex shedding frequency, D is the cylinder diameter, and U is the flow velocity. For a single cylinder, the vortex shedding occurs for

the ranges of Reynolds numbers $100 < Re < 5*10^5$ and $Re > 2*10^6$. The wake becomes completely turbulent, and no regular vortex shedding exists in the intermediate transcritical Reynolds number range. The vortex shedding Strouhal number is approximately equal to 0.2 for subcritical Reynolds number.

For closely-spaced tube rows and tube arrays, two or more values for Strouhal number may be found [6-8]. Experiments have shown that vortex shedding does not generally produce large amplitude tube vibration in tube arrays with pitch-to-diameter ratio of 1.5 or less [1], because the proximity of the tubes causes regular vortex shedding to degenerate into broad band turbulence. Moreover, for a closely-spaced tube bundle with tube motion, the flow area is being expanded and contracted synchronous with the frequency of vibration. This in turn changes the flow velocity which controls the frequency of vortex shedding. Since tubes only vibrate at a unique frequency, the vortex shedding then locks-in with the tube natural frequency.

In spite of years of effort, the basic interaction mechanisms between vortex shedding and structural vibration remain unsolved even for a single body. Vortex shedding for flow across multiple tubes is much more complicated and still needs further study.

2.1.3 Fluidelastic Instability

If the oncoming fluid flow to a group of circular cylinders exceeds a certain critical value (critical velocity), vibrational amplitudes increases drastically. Severe damage to the tubes usually results after a short period of time. Therefore, operation at a flow above the critical velocity is generally not acceptable. This instability is caused by the instantaneous displacement of one cylinder in an array from its normal equilibrium position. The displacement disturbs the flow field, and thereby upsets the force balance on adjacent cylinders, causing them also change their positions in a vibratory manner. The flowing fluid is capable of providing the vibrating cylinders driving forces which are proportional to the amplitude of displacement and square of the flow velocity. These driving forces result

in a certain amount of energy transferred to the cylinders per oscillation cycle. On the other hand, the damping forces remove a certain amount of energy per cycle. If during one cycle of oscillation, the energy fed to the cylinders from the flowing fluid exceeds that dissipated by damping, a fluidelastic instability will be established. This type of vibration is self-excited, and once initiated will grow in amplitude until a balance is reached between the net energy input and the dissipation by system damping. It thus depends upon both the velocity of the fluid and the motion of the structure for existence.

Extensive studies of fluidelastic instability of circular cylinders in crossflow have been reported since its concept was first introduced in the literature by Connors [9, 10] in late 1960's. A significant understanding of this problem now exists. Connors has developed a method for predicting the critical crossflow velocity by equating the excitation energy per oscillation cycle to that dissipated through damping. This prediction depends upon the natural frequency of the structure and the damping characteristics of the system. However, at present the estimation of system damping is still controversial due to the large number of parameters which interact in an unpredictable manner. It is still a problem to predict the instability phenomena from the fundamental principles of fluid dynamics and the theory of elasticity.

2.1.4 Summary of Flow-Induced Vibration Mechanisms

The effects of different mechanisms on flow-induced vibration of closely spaced tube bundles can be explained by analyzing the tube vibration amplitudes as a function of the flow velocity. Fig. 2 shows a qualitative example of measured vibration amplitudes of a tube bundle subjected to cross flow. At low flow velocity, the cylinder responds mainly to turbulent buffeting and its vibration amplitude goes up roughly in proportion to U^2. When the vortex shedding frequency becomes close to or coincides with the structure natural frequency, the vibratory response of the cylinder array exhibits a peak in the plot. At sufficiently high flow velocity, fluidelastic instability will generally develop. The

amplitude of vibrations increases sharply with increasing flow velocity until a balance is reached between the excitation energy and the dissipation by system damping.

2.2 Flow Behavior Around Cylinders

In the last two decades, a large number of publications describing experimental investigations as well as mathematical models for flow-induced vibration problems of circular cylinders subjected to crossflow have appeared in the literature. It appears from the substantial amount of literature that most of the researches have concentrated on the following subjects: dynamic instabilities [9-17], vortex shedding excitation [18-22], turbulent buffeting [23-26], acoustic resonance [27-31], vibration problems in heat transfer equipment [32-34], and design considerations [35-37]. Unfortunately, most experiments have not included a detailed description of flow characteristics. The following review concentrates mainly on flow visualizations and characteristic descriptions of flow around a single and a group of cylinders.

2.2.1 Single Cylinder

Flow around a circular cylinder has been a subject of fluid mechanics research for more than a century. There are many confusing phenomena involved in the interaction of flow with a cylindrical structure. Over the years, hundreds of papers, representing both experimental and theoretical studies, have been published and extensive reviews have been given by Morkovin [38], Mair & Maull [39], Berger & Wille [40], and more recently by Bearman [41]. Flow past a circular cylinder is probably one of the most extensively studied subjects, but it still remains not fully understood.

Based on experiments and qualitative observations, the flow phenomenon around a circular cylinder has been classified into several distinct regimes [1, 2, 38]. At very low Reynolds numbers, below about Re = 5, the flow follows the cylinder contours and does not separate. As Re is increased, in the range $5 \leq Re \leq 45$, the flow separates from the

back of the cylinder and form a pair of symmetric vortices. This is called as "twin-vortex" stage. As Reynolds number up to 150, the vortices decay slowly throughout the street length and the vortex street remains laminar as it travels downstream. This is the so-called stable region. Between Re = 150 and 300, the boundary layer is laminar over the front part of the cylinder; over the rear part the vortices breaking away from the cylinder become turbulent. In the subcritical region, $300 < Re < 3*10^5$, the laminar boundary layer separates from the cylinder and a strong and periodic vortex street exists. The Strouhal number in this region remains constant with a value of 0.20. In the transitional region, $3*10^5 < Re < 3.5*10^6$, the cylinder boundary becomes completely turbulent and the vortex shedding is disorganized. There is no regular vortex shedding exists. After the flow velocity exceeds this range, the von Karman vortex is formed again. The Strouhal number is 0.27 in this so-called supercritical range.

Recently performed experiments have shown that vortex shedding downstream from a flexible cylinder could be controlled by the natural frequency of the cylinder for a range of flow velocities. If a single elastically mounted cylinder is subjected to a gradually increasing crossflow velocity U, the vortex shedding frequency f increases roughly proportionately, keeping the Strouhal number nearly constant over a wide range of Reynolds numbers. But when the vortex shedding frequency f approaches the cylinder natural frequency f_n, f jumps to the same value as f_n, and remains there for a range of velocities [42, 43]. This is the so-called lock-in phenomenon. The Strouhal number no longer remains constant; instead, there is a significant motion of the cylinder at its natural frequency. However, when the flow velocity increases beyond a certain point, the vortex shedding frequency leaves the resonance value and rises again to the expected value predicted by the constant Strouhal number. This effect of the vortex shedding frequency f synchronizing with the cylinder natural frequency f_n (or resonance) over a range of velocities demonstrates that there is a feedback mechanism through which the response can influence the exciting function.

The above lock-in phenomenon with a flexible cylinder is known as free-vibration lock-in. In a corollary fashion, there is a range of excitation frequencies for a cylinder with forced transverse vibration, for which the forced oscillation and vortex shedding frequencies lock together and control the shedding process. This process is termed forced-vibration lock-in. Because the cylinder amplitude can be controlled independently, the latter mechanism lends itself to parametric studies of vortex shedding as a function of forcing frequency, amplitude and velocity.

The lock-in phenomenon has been extensively investigated for many years and a large number of papers have been devoted to this subject. The characteristics of lock-in can be summarized as follows:

(1) Frequency Demultiplication [42-45] -- Lock-in exists not only if the forced vibration frequency is near the shedding frequency itself but sometimes also if it is near an integer multiple of the shedding frequency.

(2) Hysteresis [42, 44] -- The lock-in velocity range for free-vibrations lock-in depends on whether the flow is increasing or decreasing.

(3) Parameter Sensitivity [44-46] -- Lock-in behavior depends on vibration amplitude and possibly also Reynolds number.

(4) Flow Structure [41, 44] -- The correlation length increases during lock-in.

Detailed descriptions and consequence of lock-in phenomena are reviewed and summarized by Griffin & Ramberg [47], Marris [48], and Sarpkaya [22]. Lock-in phenomena on a single cylinder with forced transverse vibration were studied by the author [49]. Onion-shaped lock-in boundaries were identified and its details will be described and discussed in Chapter IV.

2.2.2 Normal Cylinder Pair

The flow field around a pair of rigid circular cylinders is very complex, and has been studied extensively. Excellent reviews were published recently by Zdravkovich [50,

51]. Some objectives of the studies have been to measure the fluid force and/or pressure distribution acting on each cylinder, flow velocity profiles, vortex shedding frequencies, and to understand the resultant flow patterns. When one or both cylinders are elastic and vibrate, the flow field becomes significantly more complicated because of the interaction of the flow and the cylinder motion.

Most of the studies deal with the cylinders in tandem. The disturbed flow caused by the upstream cylinder striking the downstream cylinder can induce dynamic instability, called wake-induced flutter. In contrast to two cylinders in tandem, there is very limited information on two cylinders normal to flow. This literature survey mainly concentrates on the flow characteristics of a cylinder pair normal to crossflow.

Force measurements on a cylinder pair normal to flow have been made by Biermann & Herrnstein [52]. They expressed the results in terms of the interference drag coefficient, which is defined as the difference between the drag coefficient measured on one of the cylinders and the drag coefficient of the single cylinder at the same Reynolds number. They found that there was practically no interference for a cylinder gap of four diameters or more. For decreasing spacings, the interference drag could be either positive or negative depending on both Reynolds number and the cylinder gap.

Spivack [53] carried out a very detailed hot-wire investigation of the predominant frequencies in the flow field behind a pair of cylinders in side-by-side arrangement. For P/D greater than 2.0, the Strouhal number for each cylinder is the same as for the single cylinder. For P/D less than 2.0, two different frequencies are recorded. The upper frequency disappears for spacings less than 0.5D while the lower frequency decreases until the two cylinders are in contact. Similar results have been obtained by Bearman & Wadcock [54] and Jendrzejczk & Chen [55] by base pressure measurements.

One of the distinct features of the flow field is the bistable nature of the biased flow pattern. For $1.1 < P/D < 2.3$, Bearman & Wadcock [54] have found that the base pressure on the two cylinders is different and changes from one steady value to another, or

fluctuates between the two extremes. In this range of spacing, two bistable forces are experienced by the two cylinders. Ishigai, et al. [56] used the Schilieren optical method to visualize the bistable and biased flow pattern. They suggested that the biased flow was due to the Coanda effect. This was incorrect because the biased flow was also observed behind two flat plates placed normal to the flow [57].

Based on the experimental observations and measurements, the flow field for two identical cylinders normal to flow can be divided into four regimes:

No-Interference ($P/D > 4$): The flow pattern around each of two circular cylinders and the Strouhal frequency are the same as that around an isolated cylinder.

Coupled Vortex Streets ($2.2 < P/D < 4$): Although both wakes are equal in size and have the same frequency, the two vortex streets are coupled in an out-of-phase mode; i.e., the vortices are simultaneously formed and shed on the gap side and then simultaneously on the other side.

Biased Flow Pattern ($1.2 < P/D < 2.2$): Two asymmetric wakes are formed behind the cylinders. The gap flow is biased to one side and divides the wide and narrow wakes behind the cylinders. The biased flow in the gap is bistable and switches the narrow and wide wakes at irregular time intervals. Two Strouhal frequencies are associated with the two wakes.

Single Vortex Street ($1.2 \leq P/D$): When the two cylinders are fairly close to each other, they behave as a single bluff body, a single vortex street is formed behind the two cylinders. Because of the base bleed through the small gap, the two cylinders are strongly coupled by the flow field.

The existence of bistable flow patterns downstream from stationary cylinders provides the exciting forces for an initial displacement. The oscillating cylinders can resonate at their natural frequencies and the change-over of flow patterns can excite large amplitude oscillations. A similar jet switching mechanism of excitation was also found for a row of cylinders [58, 59].

The flow field around two cylinders is very complex. It depends on Reynolds number, cylinder arrangement, and upstream flow conditions. The interaction of fluid flow with cylinder oscillation is even more complicated. Based on the available information, the general characteristics of cylinder response in crossflow are not well understood in any of the various parameter ranges. Most of the experimental data were obtained for specific applications. At this time, it is not generally possible to predict the response of two cylinders in crossflow because the fluid forces acting on the cylinders cannot be calculated.

2.2.3 Single Tube Row

The flow field immediately downstream of a tube row is more complex than that of a single cylinder or a cylinder pair, because of the jets coming out from narrow gaps merging together in an irregular manner. Due to complex interference among jets, wakes, and vortex streets, an analysis of the entire flow field simultaneously has not been possible so far. There have been numerous papers about flow across a single cylinder and a cylinder pair, but for a tube row there are only a few reports available.

R. Gran Olsan (1936) and G. Cordes (1937) dealt with the flow phenomenon behind a row of rods having large pitch-to-diameter ratios and found no instability. Their work was mainly concerned with mixing in fully developed turbulent flow, and the flow was not truly two-dimensional in his experiments.

von Bohl [60] investigated the flow behind a single row of prismatic rods and determined that the jets emerging from between the rods were not stable, but tend to coalesce into pairs when the grid density (the ratio of obstructed area to total duct area) is more than about 0.37 to 0.46. His observations indicate a multi-stable pattern, since this pairing off was different at different times. In order to make consistent measurements, he favored one set of pairing by introducing a slight irregularity in the placement of the rods. This is the first complete theoretical and experimental investigation of this problem.

A thorough investigation of the stability of two-dimensional flow through a row of parallel rods was made by Corrsin [61]. He conducted his experiments by using a row of shaped brass rods that were streamlined on the upstream side but flat on the downstream side, having a grid density of 0.83. His velocity traverses showed somewhat irregular patterns rather than simple pairing of the initial jets; this appears to be evidence of complex flow patterns at such a high grid density. He explained that the physical mechanism of jet pairing-off depended upon the entrainment of fluid by individual jets from the wakes between them. In the same paper he also demonstrated that additional screens at a certain distance downstream could counteract the original instability while introducing new instabilities of their own.

Morgan [62] reviewed the instability of the flow through screens of low opening ratios and concluded that pairing of jets would occur downstream from rows of circular rods in crossflow with pitch-to-diameter ratio at 2 or less. Flow visualization photographs [6, 59, 63-67], vortex shedding frequency measurement [7, 8], and numerical analysis [68] demonstrated that flow instability downstream of a closely-spaced tube row and multi-stable flow patterns existed which could switch from one stable pattern to another one at irregular time intervals.

Flow visualization of a tightly-spaced tube row, using dye streaks in a closed water tunnel, appeared in a paper describing the paradox of flow-induced vibration by Moretti [69]. Severely divergent angles between the jets emerging from the tube row were observed. Two or more jets could be seen to join together, while a wide stagnant zone appeared between two combined jets. It was observed that for small pitch-to-diameter ratios, either the paired jets would pair-off again or larger groups of jets would coalesce. The flow pattern may change to different grouping of emerging jets at irregular time period. This "jet switching" mechanism is quite possibly another mechanism for flow-induced vibrations.

A complex instability of the parallel jets emerging from a single tube row with pitch-to-diameter ratio of 1.3, leading to a joining of groups of two or more jets had been observed in the author's previous experiments [70-72] by means of velocity traverse at various downstream positions. Between two groups of coalesced jets, there was a zone of recirculating. The coalesced groups of jets merged again for the second pairing so that, a very short distance from the tube row, the flow was no longer identifiable as having originated from a regular row of tubes. It was also shown that the pairing-off was different at different start-up to build up flow velocity. Sometimes, at irregular time intervals, the flow pattern switched from one quasi-stable state to another quasi-stable one. This confirmed that the flow downstream of a closely spaced tube row had multi-stable flow patterns, and that a minor disturbance of unknown origin could switch it from one configuration to another one. This phenomenon is wake-dominated and consequently not sensitive to Reynolds number within the subcritical regime.

As described above, in fluid flow through a circular cylinder row with the P/D ratio about 2 or less, the jets emerging from the cylinder gaps pair up as shown in Fig. 3. Jet switching also exists at this small P/D ratio. Fig. 4 shows two flow patterns describing jet-switching behavior. As reported by Roberts [58, 59] and Connors [9, 10], the jet switching is accompanied by a significant change in the drag forces of about 20%. Measurements of the drag forces show that a wide wake (diverging jets) behind a tube corresponds to a lower drag force while a narrow wake (converging jets) corresponds to a higher drag force. If the frequency of changing forces acting on the cylinders caused by the jet switching is near to or coincides with the cylinder natural frequency, a severe vibration problem will occur. This jet switching mechanism is a recent topic for flow-induced vibration research.

2.2.4 Tube Arrays

Cine films and still photographs of aluminum particle streaks in water tunnel tests conducted by Weaver & Abd-Rabbo [73, 74] were used to study flow development and behavior in arrays (square and staggered both) of flexible tubes in crossflow. The flow developments in the square and staggered arrays were quite different. Clear alternate vortex shedding has been found in staggered array but not in square array. On the other hand, large streamwise amplitude response due to symmetric vortex shedding from the first tube row was only observed in square array but did not occur in a staggered array.

Zdravkovich & Stonebanks [75] measured the instantaneous pressure distribution around tubes and found non-uniform flow downstream from equally-spaced single and two-row tube arrays. The biased gap flow was metastable, and abruptly changed direction at irregular time intervals. Again, they also supposed that the metastable phenomenon could be the mechanism of excitation of flexible tubes. Their observation of non-uniform flow patterns by using surface pressure distribution agreed with early investigations using other methods.

Funakawa et al. [76] visualized flow patterns of a three-row tube array in in-line and staggered arrangements. A hydrogen bubble method was used and the streamlines were recorded on video. They concluded that the exciting force was induced by the phase lag between wake switching or jet switching and the displacement. From fluid force measurement, a remarkable observation was that there were two critical flow velocity lines, an in-phase mode and an out-of-phase one, which intersected at the damping parameter of 10. Therefore, unstable vibration could oscillate in-phase at damping parameters of 10 or greater and oscillate out-of-phase at those below 10.

A five-row experiment using floating aluminum powder for flow visualization was conducted by Wallis [77]. Only two of his photographs involved small pitch-to-diameter ratios, but there was evidence of lateral flow deflections even in some of the tests with large

longitudinal pitch as long as the transverse pitch was only 1.5 diameters. He did not remark on this phenomenon, because he was principally concerned with observing the dead-water regions. Similar flow pattern photographs were shown in Werle's paper [78, 79].

Strong flow deflections and multi-stable behavior for four-row tube arrays are presented visually in the author's recent research [80]. These detailed flow behaviors will be described and discussed in Chapter IV.

CHAPTER III

EXPERIMENTAL FACILITY

This chapter describes the water table used in this study. The description of testing tube array models, dye injection technique, traversing mechanisms, hot-film anemometer, and data analysis are also included.

3.1 Water Table

The experiments were carried out on a closed-circuit free-surface water table, schematically illustrated in Fig. 5, which is available in the School of Mechanical and Aerospace Engineering of Oklahoma State University. Such a water table is specially suited for this kind of research. It has a 3-HP pump to drive flow and a 25 inch wide by 45 inch long glass table as the test section. Upstream of the test section, flow is conditioned through a settling chamber, a 2-1/2 inch wide by 1/8 inch hexagonal openings honeycomb, and three layers of fine mesh aluminum screens such that a low turbulence intensity (less than 1%) flat velocity profile, as shown in Fig. 6, is obtained. It can be seen that about 0.75 inch above the glass table the flow reaches 99% of its freestream velocity. Furthermore, flow visualization with dye threads shows parallel flow, without the large, slow "roller" eddies which normally tend to occur in this type of facility. In order to isolate the water table from the vibrating pump, rubber hoses are used as the connection between those two. The pump is set on a rubber pad to further reduce transmission of vibration through the ground. Good flow conditions were achieved even for an empty test section.

The water is recirculated from the settling chamber through the test section and then overflows a 3-inch high weir at the far end of the glass table into a storage tank. A 2-inch

outlet located at the bottom of the storage tank connects to the pump and allows the water to be pumped back to the 5 inch wide by 25 inch long by 36 inch high settling chamber. By using a by-pass loop, the flow velocity is adjustable. Its maximum mean flow velocity for the empty test section is 2.5 inch/sec. The testing models are set about 10 inches away from the leading edge of the test section. The low flow velocity is measured by counting the time of a particle passing through a known distance.

The lighting system used for flow visualization consists of four 300W electric lamps arranged in a pattern to minimize the shadows produced by the tubes. Because of the interference of traversing mechanism and lighting system, a 30 inch wide by 38 inch long mirror was installed at a 45 degree slant underneath the glass table. This arrangement allows observation through the glass from the bottom of the test section. Flow motion was visualized by means of the dye injection technique. The jet and wake patterns around the testing models were photographed by a motor-driven 35 mm camera or a 8 mm video camera.

3.2 Testing Tube Models

A single or a group of 1 inch diameter by 5 inch long solid brass circular rods were put vertically (free standing) on the flat glass of the water table, where they could be arranged in a various geometries by using templates. Four-row cylinder arrays of 90-degree (in-line square array), 60-degree (rotated equilateral triangular or parallel triangular array), 45-degree (staggered square array), and 30-degree (normal equilateral triangular array) geometries with pitch-to-diameter ratios of 1.4, 1.33, and 1.25 and single tube row with pitch-to-diameter ratios of 1.4, 1.33, and 1.25 were mainly used to study the flow behaviors by the flow visualization technique. A single cylinder and a normal cylinder pair were used to study flow-structure interaction and lock-in phenomenon by hot-film anemometer measurements.

A schematic drawing of principal tube array arrangements employed in this study is shown in Fig. 7. Eighteen to twenty brass rods, depending on the pitch-to-diameter ratios, spanned the test section and formed one row. Fig. 8 shows a schematic drawing of a single tube row spanning the test section. For the single-row arrangement, alternate red and green dyes were injected gently into the flow from the middle six tubes in the row, so that nearby jets and wakes could be distinguished clearly. For the four-row arrangement, dyes were injected into the flow from the middle six tubes of the upstream row, so that the flow development in and behind the tube array could be observed in detail.

3.3 Dye Injection Technique

Flow visualization is principally used for identification and characterization of the flow field. After several alternative techniques of visualization were tried out, the dye injection technique was selected in this study. A schematic of the dye injection tube is shown in Fig. 9. Food coloring dyes flow out gently from two rows of 0.02 inch diameter holes set thirty degrees apart on its surface. The dye injection tube is positioned with the holes facing the oncoming flow, thus letting stagnation point occur in the middle of those two rows of holes, so that the dye streaks will follow the motion of the shear layer on each side of the tube. For multi-row tube arrays, dye injection tubes were put at the upstream row of cylinders, so that the flow behavior in and behind the tube array could be observed. In order to improve the stability of dye streaks, milk is mixed with food dyes. This is because the butter fat in the milk reduces the diffusivity of dye streaks, so that farther downstream flow patterns can be observed clearly. Milk also has the advantage of good reflective properties [81]. The density of the mixture may be adjusted by mixing dye with alcohol. Red and green dyes were injected from alternate testing tubes in order to observe the individual wakes and distinguish the interferences from other tubes.

The dyes were injected through the holes in a controlled manner with no velocity component perpendicular to the tube surface so that the main stream was not disturbed. In

order to affirm the the reliability of results by this technique, a preliminary measurement was made on a single tube tested in the manner described above. The time period of dye vortex shedding was measured by a stop watch and the Strouhal number calculated was 0.21, which is in fairly good agreement with the well accepted value in the subcritical region.

A disadvantage of using the dye injection technique in a closed-circuit water table is that dye is accumulates and increasing contaminates the fluid. Therefore, the water table needs to be drained and refilled for each test run to maintain the clarity of observation.

3.4 Traversing Mechanism

A precise one-dimensional traversing mechanism has been built to locate the displaced tube at desired positions. It can be installed at different places to displace the tube longitudinally (along the flow direction) or transversely (perpendicular to the flow direction). A 1-inch diameter brass rod was mounted vertically with its bottom end free (1/64 inch gap between the cylinder end and the glass table); its top end was clamped to the traversing mechanism. A vibratory mechanism as shown in Fig. 10 can be connected with the traversing mechanism to oscillate transversely the moveable tube sinusoidally at desired amplitude and frequency. The vibratory mechanism was driven by an electric motor with an infinitely variable speed transmission connected to an adjustable eccentric disc. The 5-inch diameter disc has a 0.5 inch wide by 2 inch long slot cut at its center so that the degree of eccentricity can be controlled. The desired frequency and amplitude of the forcing oscillation can then be adjusted precisely by obtaining the desired frequency from the variable speed transmission while the amplitude is set by the degree of eccentricity of the disc. The cylinder and its mounting arrangement were sufficiently rigid to preclude deflection during forced oscillation.

3.5 Hot-Film Anemometer

A hot-film anemometer was used to measure the velocity profiles, turbulence intensities and vortex shedding frequencies. The sensors used in this study are a normal straight , DANTEC 55R11, and a right angle prong, DANTEC 55R13, cylindrical hot-film probes. These film sensors are thin nickel films deposited on 3-mm long quartz fibers by means of cathode sputtering. The fiber is 70-μm in diameter. Gold plating at the ends defined a sensitive length of 1.25 mm. A 2 μm thick quartz layer is sputtered onto the film for protection and the prongs are covered by a heavy lacquer coating. These probes are designed for measurements at medium temperatures in water and other conducting liquids. Hot-film probes are specially suited in flows with large velocity gradients or in flows with high turbulence intensity. Due to the greater sensor diameter, vortex shedding of the probe gives noise at velocities above approximate 50 cm/sec in water. In this study, the velocity range is much lower than that, therefore vortex shedding of the probe itself will not cause any problem. The DANTEC 55R11 probe is for general use, the DANTEC 55R13 probe is used in hard-to-get-at places, for instance when measurements are to be made inside the tube bundles. A 5-meter coaxial cable connects the probe support to the main bridge unit. A DISA type 55M01 anemometer and type 55M10 bridge system are used to operate the probe at constant temperature.

3.5.1 Calibration

The use of hot-wire or hot-film anemometer for measurements of flow velocity relies on laws governing convective heat transfer. A theoretical solution to the heat transfer problem of a uniformly heated cylinder in two-dimensional, incompressible, potential and non-viscous flow was formulated by L. V. King in 1914. But in practice, the heat transfer is generally too complicated to permit a theoretical calculation of the relation between the flow velocity and the heat flux from the probe. This relation must be found experimentally.

For conditions of thermal equilibrium, the rate of heat loss from the hot-wire or hot-film probe must be equal to the heating power generated by the electric current, that is, it must be equal to I^2*R. From a view-point of the user of the anemometer, primary interest is in the relation between flow velocity and electrically generated heating power. For a hot-wire probe operated at a specific overheating ratio, in a specific fluid, and at a specific temperature, the relation can be expressed by the equation

$$E^2 = K_1 + K_2U^n \tag{3.1}$$

where E is the output voltage of anemometer bridge,

U is the flow velocity, and

K_1, K_2 are calibration constants.

The hot-film probe calibration is carried out at a fixed temperature and relates the output anemometer voltage to the flow velocity. A calibrated two-dimensional planar water jet is used for the static calibration of the hot-film probe. The probe was placed at the potential core of the water jet during calibration. The selected flow velocity was obtained by modulating the flow controller. A relationship of the form in equation (3.1) was then used to fit the whole calibration curve to this equation using a least square curve fitting procedure. Since anemometer output voltage E is only a function of flow velocity U, the following relationship can be used to calculated the fluctuations in the velocity:

$$e' = \frac{\partial E}{\partial U} u' \tag{3.2}$$

where e' is the fluctuating voltage, and

u' is the fluctuating velocity.

Equations (3.1) and (3.2) can then be used to calculate the mean and the fluctuation velocities. By definition, the turbulence intensity I is the ratio of root-mean-square velocity to the time mean flow velocity. Therefore, the turbulence intensity can be expressed as follows

$$I = \frac{\sqrt{\overline{u'^2}}}{U}$$

3.5.2 Problems with Hot-Film Anemometer Measurements in Water Flow

Several problems were encountered in hot-film velocity measurement in water flow. The most serious problems are air bubble contamination and water temperature drift. Air usually dissolves in water through the air-water interface or cascade. Air bubbles will be formed on the solid surface and especially when its surrounding water is heated; as is the case for the water next to the hot-film probe. Additionally, as an air bubble moves with the water flow, it develops electrostatic charge and is attracted by the probe [82]. This problem is severe especially when the probe is hot. Once the air bubble adheres to the hot-film surface, it influences the heat transfer between the sensor and the fluid, and the hot-film calibration constants are no longer valid. Therefore, the output voltage from the anemometer is no longer related to the flow velocity by equation (3.1). One way to diminish the air bubble contamination problem is to keep the probe overheat ratio as low as possible while maintaining adequate sensitivity [82]. The overheat ratio used in this study is maintained at 1.06 (generally, the overheat ratio used in water flow is from 1.04 to 1.1), and the air bubble problem is solved.

Output voltage from the anemometer is dependent on the temperature difference between the sensor and the surrounding fluid. Because of the low overheat ratio, the hot-film measurement is extremely sensitive to water temperature change. A 0.01 degree Fahrenheit temperature change could cause a relatively large error of velocity measurement in water. To maintain a constant temperature within a limit of 0.01 degree is impossible. Equations (detail derivation is in Appendix A) based on temperature ratios that take into account the temperature differences are derived to modify the anemometer output voltage. The modified bridge voltage is given by:

$$E_c = \left(\frac{T_w - T_{f1}}{T_w - T_{f2}} \right)^{0.5} E_m \qquad (3.3)$$

the turbulence intensity can then be modified as

$$I = \frac{\sqrt{\overline{u'^2}}}{U} = \frac{2 * E_m * e_m'}{n\,[\,E_m^2 - A(\frac{T_w - T_{f2}}{T_w - T_{f1}})]} \qquad (3.4)$$

In order to affirm the reliability of these equations, a preliminary measurement of velocity profile downstream of a single stationary cylinder has been tested. The velocity profile calculated from equation (3.1) is slanted downwards from left to right because of the water temperature slowly increasing during the experiment. By using equation (3.3) to correct the anemometer output voltage due to temperature drift, the apparent downward trend in velocity has been pulled back to its true value. The comparison of the measured and modified velocity profiles is shown in Fig. 11. It demonstrates that these equations work well in this study.

3.6 Data Processing

An IBM compatible XT personal computer is used to sample the hot-film output voltage. A MetraByte DAS-20 Analog & Digital Interface Board and a MetraByte SSH-4 Simultaneous Sample & Hold Accessory Board are utilized to convert the 0-10 volt hot-film signals to 12 bit digital words. The P/C controls, via FORTRAN 77 code, the sampling rate and time. By using the Direct Memory Access technique, the data are transferred directly to memory. After all the data are taken, further FORTRAN programs are used to reassemble the samples, take average and root mean square values, then store the results. The maximum resolution is 0.024 millivolts and the maximum analog to digital conversion rate is 100,000 samples per second for this system.

One branch of the output signals of the anemometer was routed through a KROHN-HITE Model 330M band-pass filter to a Data Precision DATA 6100 Signal Analyzer. Spectral analysis of the signal was performed with 2048 points in the frequency domain, and 20 ensemble average was used to reduce the random errors.

CHAPTER IV

RESULTS AND DISCUSSIONS

In order to investigate flow behaviors of a single, a pair, a row, and an array of circular cylinders subjected to cross flow, a large number of experimental tests have been conducted. These experiments consist of flow visualization and hot-film anemometer measurements. The detailed experimental results will be presented in this chapter and compared with some available published results.

4.1 Flow Visualization

To obtain flow patterns in and behind the test models, the author conducted the experiments on a free-surface water table by using the dye injection technique. Alternate wakes are colored green and red respectively. This is done by filling different dyes into alternate hollow testing tubes and injecting dye from tube surface near the stagnation points. The flow patterns will be discussed separately for each test model.

4.1.1 Single Cylinder

This section primarily describes the flow behavior of a single cylinder either stationary or vibrating transversely to the oncoming flow. The flow pattern of the stationary cylinder is similar to the sketch in Fig. 1. Fluid flow follow the contour of the cylinder front side. Near the widest section of the cylinder, two rows of eddies (or boundary layers) separates from both sides of the cylinder surface. Three or four eddies on the same row roll up and form a vortex. Vortices are shed alternately from both sides of the cylinder and formed a regular pattern which is called a vortex street.

Ongoren & Rockwell [45] and Zdravkovich [83] have studied the vortex pattern when cylinder vibration occurs with frequencies near the vortex shedding frequency. However, the present study concentrates on the effects of cylinder vibration on the development of boundary layer eddies in the near wake region.

For small amplitude (A/D = 0.01) and low oscillating frequency ($f_e/f_0 \leq 0.3$), no evident change of flow pattern comparing with that of the stationary cylinder. As oscillating frequency reaches about 60% of the stationary vortex shedding frequency ($f_e/f_0 = 0.6$), it shows that eddies curling up closed to cylinder and the frequency of eddies is higher than the Karman vortex shedding frequency. As oscillating frequency about 1.7 times of the shedding frequency, boundary layer eddies synchronize with the cylinder oscillation. Eddies curl up when the cylinder moves to its maximum displacement on the opposite side. There is a substantial decrease in vortex formation length and the wake size is wider than that of the stationary cylinder. When $f_e/f_0 = 2.9$, the behavior of boundary layer eddies locking-in with the cylinder oscillation is weak, and no regular eddies exists in the near wake region. For further increases the oscillating frequency ($f_e/f_0 \geq 3.4$), boundary layer eddies lock-in with the cylinder oscillation again. However, eddies curl up when the cylinder moves to its maximum displacement on the same side. Eddies occur alternately in a very regular manner.

For large amplitude (A/D = 0.13) oscillation, the wake formation region has an angle of inclination to the freestream. The behavior resembles that of small amplitude oscillation except that the f_e/f_0 ratio for boundary layer eddies locking-in with the cylinder oscillation is lower for larger amplitude oscillations.

4.1.2 Normal Cylinder Pair

This section describes how the flows around two circular cylinders which are placed side-by-side in the approaching flow vary as their separation is reduced, from that past two independent cylinders to that past a single body. Intuitively, it seems reasonable

to assume that two cylinders in fluid flow should behave in a similar or even an identical manner to a single cylinder. This assumption is only valid when the two cylinders are sufficiently far apart.

For pitch ratio greater than the cylinder diameter (P/D > 2.2), the process of vortex formation for each cylinder is nearly identical to that of a single cylinder. The vortex shedding and vortex formation are coupled and are symmetric about the axis of the gap. Two cylinders develop their vortex streets equally at first. However, the two wakes interference with each other for farther downstream position since there is not enough spacing between them for their vortex streets to develop independently.

An instability of the fluid flow starts when the gap is less than about the cylinder diameter. The gap flow emerging between the cylinders is biased to one or the other of the cylinders and consequently forms a wide wake on the unbiased side and a narrow wake on the biased side. Zdravkovich [50] and Bearman & Wadcock [54] suggested that the biasing is due to a near-wake phenomenon rather than the position of boundary separation. The biased gap flow is bistable and changes direction at random time intervals. While the gap flow is biased to one side, the vortex shedding for each cylinder becomes uncoupled.

For locations on opposite sides of the narrow wake, vortices are out-of-phase indicating the existence of very distinction Karman vortex shedding. A small vortex street is formed. However, this small vortex street soon becomes indistinct and is destroyed by being swallowed up into the wide wake. In this case, two wakes merge together and form a single pair of von Karman vortex street in the downstream region. Vortices on opposite sides of the wide wake most of the time are in phase. Therefore, von Karman vortices are more difficult to observe. However, eddies on opposite sides of the gap between cylinder are always in phase.

For a pitch ratio less than 0.1, the gap flow is very weak and two cylinders can be treated as a single block. The shear layers separated from the outside of both cylinders,

interact with each other, and form a large scale Karman vortex. The vortex shedding from each individual cylinder no longer exists.

4.1.3 Fixed Single Tube Row

The flow behavior around a single circular tube row subjected to crossflow was studied by dye injection technique. The pitch-to-diameter ratios studied are 2.5, 2.2, 2.0, 1.4, 1.33, and 1.25; the upstream mean flow velocity is 1.55 in/sec. For pitch ratio P/D = 2.5, the vortex shedding from each cylinder of the tube row was exactly in the same manner as that for an isolated cylinder. There is a strong coupling among tubes. The vortices are developed almost synchronously in the whole row; the wakes downstream are parallel to each other until they all are mixed together. For P/D = 2.2, wide and narrow wakes occurred alternately in a very regular pattern but they were still parallel to each other.

When pitch ratio P/D $\leq$ 2.0, jet deflection appears and a large reversed flow region is formed behind the cylinder on the unbiased side. The degree of the deflection is evident especially when P/D is small. At P/D = 2.0, due to the deflection jet flows emerging from the cylinder gaps seemed to pair off immediately downstream. The paired jets were tilted and paired again farther downstream. Similar flow patterns are also shown in the photographs by Roberts [58] and Bradshaw [63].

At smaller pitch ratios, the jet deflections were more violent, and groups of three or more jets (not just only two) coalesced quite close to the tube row. Similar to the case of a close spaced normal cylinder pair, the tails of narrow wakes were found to fluctuate at a relatively regular high frequency, whereas, Karman vortices are more difficult to observe behind cylinders having wide wakes.

The flow pattern was found to switch from one stable configuration to another one due to flow disturbance. This indicates that multistable flow pattern exists downstream of a closely-spaced tube row. Similar behaviors were seen in the author's earlier wind-tunnel experiments [70-72].

4.1.4 A Statically Displaced Tube in a Single Tube Row

The traversing mechanism described earlier was used to displace the center cylinder in a single tube row either transversely or longitudinally. The effect of tube displacement on switching flow patterns among the multi-stable patterns was investigated by flow visualization technique. A single row of 13 1-inch diameter brass rods with pitch-to-diameter ratio at 2.0 spanned the whole width of the water table. Red and green food dyes were injected into the flow alternately from the surface of the middle six testing rods. One of the dye injection rods (fourth one in the plot) could be statically displaced. The following terminology has been used to describe the flow patterns, as shown in Fig. 12(a). C_n indicates the nth cylinder, J_n indicates the jet on the right-hand side of the nth cylinder, and W_n indicates the wake behind the nth cylinder. To describe the size of the wakes, the letters "N", "M", and "W" designate wakes which are narrow, medium, and wide, respectively.

4.1.4.1 In Transverse Direction. In this section, the flow pattern switch due to a transversely displaced tube in a single tube row is described. Five different initial stable flow patterns downstream of the six testing rods were studied and are discussed separately. (1) N-W-N-W-N-W Wake Combination (as shown in Fig. 12).

Initially, the flow pattern behaves in a very regular manner, wide and narrow wakes occur alternately downstream, as shown in Fig. 12(a). The moveable cylinder, C_4 has a wide wake. As C_4 displaces toward C_3, W_3 shrinks a little and deflects to its left, as shown in Fig. 12(b). As C_4 displaces farther about 0.55D from its origin, due to the left-direction flow J_3, W_2 changes from a wide wake to a narrow one and J_2 switches its direction in correspondence. Owing to W_2 changing from wide to narrow, J_1 switches toward its right and W_1 changes from narrow to wide. The flow pattern becomes a W-N-N-W-N-W combination, as shown in Fig. 12(c). If C_4 moves back to its origin from this position, the flow pattern sometimes reverts to its initial pattern and sometimes retains its

switched pattern. It is believed that at this position C_3 and C_4 start to act as a single block, for there is a combined wide wake of C_3 and C_4 at farther downstream.

As C_4 displaces farther left, for example, less than 0.1D away from C_3, the two cylinders can be treated as a single block and only a combined wide divergent wake behind them, as shown in Fig. 12(d) forms. There are two possible flow patterns after C_4 moves away from C_3. The first one is one in which W_3 retains narrow, the W-N-N-W-N-W combination, as shown in Fig. 12(e). The second one is one in which W_3 becomes wide, the W-N-W-N-N-W combination, as shown in Fig. 12(f). The reason for having two different flow patterns is simply that as C_4 leaves C_3 (even at low velocity), a low pressure region (or wake) exists between C_3 and C_4. This low pressure region will affect the flow behavior around the cylinders. If C_4 moves above certain velocity, the pressure at the low pressure region is low enough to draw J_3 toward its right, and let W_3 switch from narrow to wide. It also changes W_4 in correspondence.

(2) W-N-W-N-W-N Wake Combination (as shown in Fig. 13)

The initial flow pattern is similar to that of the previous case except that the whole flow pattern is shifted by one cylinder and C_4 now has a narrow wake downstream, as shown in Fig. 13(a). As C_4 displaces toward C_3, W_3 expands, W_4 shrinks and deflects to its right, as shown in Fig. 13(b). As C_4 and C_3 are closed together to less than 0.1D apart, as before, only a combined wide divergent wake behind them is seen as shown in Fig. 13(c). Due to the strong deflection of J_2 and J_4, W_1 and W_5 shrink and switch from wide to medium wakes. As C_4 returns to its origin, the flow reverts to its initial pattern.

(3) N-W-N-W-M-N Wake Combination (as shown in Fig. 14)

Initially, the system has an irregular flow pattern with wide, narrow, and medium wakes mixed together, as shown in Fig. 14(a). As C_4 displaces toward C_3, this situation becomes similar to that described in case (1). A wide wake cylinder moves toward a narrow wake cylinder, and the same behavior would occur as in case (1). As C_4 displaces right toward C_5, W_4 expands while W_5 remains as a medium wake and deflects to its

right, as shown in Fig. 14(b). As C_4 backs to its origin, the flow reverts to its initial pattern.

(4) M-N-W-M-N-W Wake Combination (as shown in Fig. 15)

The initial flow pattern is very similar to that of case (3). The pattern of N-W-M-N wakes shift one cylinder from the previous case, as shown in Fig. 15(a). As C_4 displaces toward C_3, W_3 and W_6 expand. In consequence, W_4 deflects to its right and W_2 shrinks a little. As C_4 displaces 0.4D left from its origin, J_2 deflects strongly to its left and shrinks W_2 farther. As a consequence W_1 changes from medium to wide, as shown in Fig. 15(b). As C_4 returns to its origin, the flow pattern retains its switched W-N-W-M-N-W pattern.

As C_4 displaces 0.27D from its origin toward C_5, W_5 shrinks and W_4 expands from medium to wide. Due to a whole sequence of flow pattern transition, W_3 changes from wide to narrow and W_1 changes from medium to wide in correspondence, as shown in Fig. 15(c). As C_4 displaces 0.4D right from its origin, C_4 and C_5 start to form as a single block. Owing to the wide wake behind C_4 and C_5, J_5 switches toward its right, W_6 changes from wide to narrow, and W_5 deflects to its right, as shown in Fig. 15(d).

(5) W-N-N-W-N-M Wake Combination (as shown in Fig. 16)

Similar to the previous case (4), the initial flow pattern is very irregular, as shown in Fig. 16(a). As C_4 displaces toward C_5, the same pattern would occur as when C_4 moves toward C_3 in case (1). As C_4 displaces toward C_3, W_3 and W_2 deflect to their left and W_1 shrinks a little but still remains as a wide wake. This is shown in Fig. 16(b). Then C_4 moves back to its origin, the flow reverts to its initial pattern.

4.1.4.2 In Longitudinal Direction. In this section, the flow pattern changes due to a tube displaced longitudinally in a single tube row is described. Four different initial stable flow patterns downstream of the middle six testing rods in the tube row are investigated. These are discussed separately.

(1) M-W-N-M-W-M Wake Combination (as shown in Fig. 17)

The initial flow pattern is very irregular, as shown in Fig. 17(a). As C_4 displaces downstream, W_4 expands in size and causes W_3 and W_5 to shrink. As C_4 is displaced 0.16D downstream, W_4 changes from medium to wide and W_5 changes from wide to narrow, as shown in Fig. 17(b). As C_4 is displaced farther downstream to 0.24D, W_4 expands and W_5 shrinks further; as a consequence, W_6 changes from medium to wide, as shown in Fig. 17(c). When C_4 returns to its origin, it retains its switched M-W-N-W-N-W pattern.

As C_4 is displaced upstream, W_4 changes from medium to narrow but W_3 and W_5 expand, and W_3 deflects to its right, as shown in Fig. 17(d). As is C_4 displaced farther upstream, there is no subsequent change. As C_4 returns to its origin, the flow reverts to its initial pattern.

(2) W-N-W-N-W-N Wake Combination (as shown in Fig. 18)

The initial regular flow pattern, shown in Fig. 18(a), is the same as that in case (2) of section 4.1.3.1. The cylinder was moved transversely in the previous section, but it was displaced longitudinally in this section. As C_4 is moved downstream, W_4 expands and results in W_3 and W_5 shrinking. As C_4 displaces 0.27D downstream, W_4 changes from narrow to wide but W_3 and W_5 changes from wide to narrow, as shown in Fig. 18(b). For farther displacement downstream, there is no subsequent change. As C_4 is returned back to its origin, the flow retains its switched W-N-N-W-N-N pattern.

When C_4 is displaced upstream, W_4 shrinks, W_3 and W_5 expand, and W_1 shrinks a little but still remains as a wide wake. For farther displacement upstream, there is no subsequent change. As C_4 returns to its origin, the flow reverts to its initial pattern.

(3) N-W-N-W-N-W Wake Combination (as shown in Fig. 19)

This combination is very similar to that of case (2) except the moveable cylinder C_4 has a wide wake downstream, as shown in Fig. 19(a). As C_4 displaces downstream, W_4 expands but W_3 and W_5 shrink and deflect away from W_4. W_2 and W_6 shrink a little but

still remain as wide wakes. For farther displacement downstream, there is no subsequent change. As C_4 is backed to its origin, the flow reverts to its initial pattern.

As C_4 displaces upstream, W_4 shrinks but W_3 and W_5 expand. When C_4 is displaced 0.24D upstream, W_4 switches from wide to narrow, W_5 changes to wide, and W_6 changes to narrow as a consequence. Although W_3 has a tendency to become a wide wake, the wide-wake effect of W_2, causes W_3 to look like a medium wake and inclines it to its right, as shown in Fig. 19(b). As C_4 is returned to its origin, W_3 changes back to narrow and the flow pattern is shown in Fig. 19(c).

(4) W-N-N-W-N-W Wake Combination (as shown in Fig. 20)

The initial irregular flow pattern shows very clearly that there are two or three jets merged into a group immediately downstream of the tube row even at the large pitch ratio (2.0),as shown in Fig. 20(a). As C_4 is displaced downstream, W_4 expands but W_3 and W_5 shrink. As C_4 is displaced 0.24D downstream, because of very strong wide wake effect of W_4, W_6 changes from wide to narrow. This is shown in Fig. 20(b). For farther displacement downstream, there is no subsequent change. When C_4 is back to its original position, the flow retains its new W-N-N-W-N-N pattern.

With C_4 displaced upstream, W_4 shrinks but W_4 and W_5 expand. As C_4 is displaced 0.24D upstream, the flow pattern of C_3 to C_6 is the mirror image of that for C_2 to C_5 in case (3), as shown in Fig. 20(c). For farther displacement upstream, there is no subsequent change. As C_4 is backed to its origin, again like that of case (3), W_5 changes to narrow and the flow pattern is that shown in Fig. 20(d).

4.1.5 Four-Row tube Arrays

Observation of low patterns of stationary four-row tube arrays arranged in 90, 30, 45, and 60 degree geometries at pitch-to-diameter ratios of 1.4, 1.33, and 1.25 were carried out systematically. Sketches of the flow patterns, based on visual observation of dye streaks, are described separately according to each geometry as below. This part of the

experimental results was presented in the "1989 ASME Pressure Vessel and Piping Conference" [80].

4.1.5.1 Ninety-Degree Geometry. Fig. 21 shows the flow patterns of the tube array with pitch ratio P/D = 1.25, The Reynolds number is 2,800 based on the gap flow velocity and the cylinder diameter. At least nine different flow patterns are observed, including violent deflections of the gap flow in the upstream row. The wake regions between each rows are fully turbulent and the turbulence increases deeper inside the tube array. For the first two rows, the flow pattern can be seen clearly. However, due to the development of turbulence, the detailed flow behavior is difficult to examine after the third row but the bulk flow direction still can be clearly identified.

The stagnation points of tubes in the same row are not necessarily all at the same side, as shown in Fig. 21(h). In some cases, the stagnation points switch from one side to the opposite side for subsequent downstream rows as shown in Fig. 21(a), 21(d)-21(f). It is interesting to see almost an exact mirror image in the flow patterns of Figs. 21(b) and 21(c) for the first three rows. Behind the tube bundle, a flow pattern similar to that of a single tube row is seen. The gap flows group together in an irregular way with wide stagnant zones appearing between the combined jets, but they are not always at the same locations for different flow patterns. An examination of Wallis' [77] flow visualization photographs, confirms the existence of flow deflections. In addition, his results also show evidence of shift stagnation points after the first row. Since the turbulence develops very fast for high flow velocity and small pitch ratio, the flow pattern is hard to see by using dye injection technique in this geometry for freestream flow velocity over 1.5 inch/sec.

Figs. 22 and 23 show the flow patterns of tube arrays with pitch ratios P/D of 1.33 and 1.4. The flow patterns are not unlike those of Fig. 21. However, it is found that the flow is less sensitive to disturbance, and gap flow deflection is more moderate at these larger pitch ratios.

4.1.5.2 Thirty-Degree Geometry. Figs. 24 to 26 show the flow patterns of the tube arrays with pitch ratios of 1.25, 1.33, and 1.4. The plots show flow deflections building up progressively row-by-row. Flow patterns are very similar in the first three rows for different pitch ratios and flow velocities. The gap flow of the upstream row is divided into two approximately equal parts by the next downstream row. The size of dead-water (or vortex formation) region behind each tube is strongly dependent on the pitch ratio and flow velocity. It is larger for higher flow velocity or larger pitch ratio. von Karman vortices are definitely formed even for very small pitch ratios. After the last row, the characteristic grouping of the emerging jets, similar to that seen after a single row, is evident. The flow pattern of this geometry is much more stable than that of 90-degree geometry. Also, for a larger pitch ratio, the flow is comparatively less sensitive to disturbance.

4.1.5.3 Forty-Five Degree Geometry. For this geometry, three pitch ratios and various velocities are tested. The flow pattern is stable and insensitive to disturbance. The only differences between flows for different pitch ratios and velocities is the size of dead-water region. The gap flow of the upstream flow is divided into two approximately equal parts by the downstream row, as shown in Fig. 27. The configuration of flows in the dead-water region is similar to that of 30-degree geometry. von Karman vortex streets can be clearly seen behind each cylinder. Downstream of the tube array, all gap flows are almost parallel to each other until they mix together.

4.1.5.4 Sixty-Degree Geometry. Figs. 28 to 30 show the flow patterns of the tube array with pitch ratios of 1.25, 1.33, and 1.4. Dead-water region configuration is similar to that of 90-degree geometry and the mixing behavior is weak even for 1.25 pitch ratio. The plots show strong shifts of stagnation points to one side or the other on the third row and very strong deflection of groupings in the wake. These grouping are very sensitive to downstream disturbances, and switch readily from one pattern to another. Gap flow

deflection behavior in tube array is not found for all tested pitch ratios and flow velocities. In the same way, the flow is less sensitive to disturbance for large pitch ratios.

4.1.6 Summary of Flow Visualization Observations

Flow visualization studies give better perception and understanding of the actual flow development in a tube array. A relationship between jet instability tube and displacement has also been discovered. From the experimental results, some conclusions are outlined below.

4.1.6.1 Single Cylinder. The flow pattern downstream of a stationary cylinder as observed by dye injection technique is similar to those well known results. Vortices are shed alternately from both sides of the cylinder and form a regular pattern known as the Karman vortex street.

Above a certain frequency of a forced transversely vibrating cylinder, boundary layer eddies synchronize with the cylinder motion. At low frequencies, eddies curl up when the cylinder moves to its maximum displacement on the opposite side. For a higher oscillation frequency, the lock-in behavior of boundary layer eddies and cylinder motion is very weak. The eddies lock-in with cylinder oscillation again for a higher oscillation frequency and curl up when the cylinder moves to its maximum displacement on the same side.

4.1.6.2 Normal Cylinder Pair. For $P/D \geq 2.2$, the process of the vortex formation for each of the cylinders is exactly the same as that of the single cylinder. When P/D becomes smaller, an instability starts. The jet flow between two cylinders deflects and the deflection to either side can take place with equal probability. Due to the biased jet flow, the sizes of the vortex formation region for the two cylinders are different. For pitch ratio less than 0.1, two cylinders can be treated as a single block and a large scale Karman vortex street exists downstream.

4.1.6.3 Single Tube Row. Flow visualization results for a fixed tube row and a statically displaced tube in tube row are summarized as follows:

(1) Irregular flow patterns existed downstream of a regular spaced tube row at a P/D ratio less than 2.2. Different "wide, medium, and narrow" wake combinations were observed at different start-ups but under the same test conditions. This indicated the existence of multi-stable flow patterns.

(2) The flow pattern could switch from one stable pattern to another one at irregular time intervals. This indicated that instability existed in small pitch ratio arrangements and this is presumably related to flow-induced vibration.

(3) The characteristic feature of the biased flow is the narrow wake on the biased side and wide wake on the opposite side. No two wide wakes are adjacent to each other, but three narrow wakes in a series bounded by two wide wakes was observed.

(4) Across wide wakes, eddies curling up are always in phase. Across narrow wakes, the curling eddies have phase shifts which depends on pitch ratio.

(5) Although some literature [6, 56] have indicated that von Karman vortex formation only can be seen downstream of narrow wakes, in the author's observation, strong well-organized vortices appear even farther downstream of a wide wake.

(6) Tube displacement plays an important role in switching the flow among multi-stable patterns.

(7) A tube transverse displacement can switch the deflection of a jet which is not necessarily adjacent to the displaced tube, but may be one tube column away from it.

(8) Flow pattern is more sensitive to a tube displaced longitudinally than displaced transversely.

(9) For a tube displaced downstream, its wake expands but the nearby wakes shrink. On the other hand, for a tube displaced upstream, its wake shrinks but the nearby wakes expand. In other words, in a single tube row, the upstream tubes always have narrow

wakes, the downstream tubes always have wide wakes. This confirms Roberts' model [58, 59].

(10) As a tube with a wide wake is displaced closer to a tube with a narrow or medium wake, the wide wake becomes wider but the other wake becomes narrower.

4.1.6.4 Four-Row Tube Arrays. The existence of flow deflections in regular tube arrays has now been clearly established. Deflection becomes severe at small pitch-to-diameter ratios. The flow visualization results are summarized as follows:

(1) Because the mixing behavior depends on flow velocity, the flow pattern is hard to visualize by dye injection technique at high flow velocity. Therefore, the author's flow visualization study was only conducted on freestream flow velocities less than 1.5 inch/sec.

(2) Strong deflections and multi-stable behavior are most common with the 90-degree arrangements. Instabilities start at the first row of cylinders and lead to flow deflections within the array. As in the case of single rows, small downstream perturbations switch the flow among several alternative patterns.

(3) The 45-degree arrangement appears to be comparatively stable, and the flow downstream remains almost parallel.

(4) The 60-degree arrangement shows strong shifts of stagnation points to one side or the other in the third row, and very strong deflection of groupings in the wake. Wallis' [77] flow visualization photographs confirm these observations.

(5) For 30-degree arrangements, the flow deflections are built up gradually row-by-row. Small Karman vortex streets were observed even for small pitch ratios. The grouping of the emerging jets downstream of the array is similar to that of the single row case.

(6) Observations confirm that the wake flow behind a closely-spaced four-row in-line or staggered tube banks is statically unstable. The flow pattern downstream of the tube array is similar to that of the single row case.

(7) The 90 and 60 degree arrangements are very sensitive to downstream disturbance. On the other hand, the 45 degree arrangement is most resistant to disturbance. In general, the flow is less sensitive to disturbance for large pitch ratios. The flow is more sensitive to downstream disturbance than upstream disturbance. This agrees with the observation that flow appears wake-dominated in all experiments on tube rows and tube arrays.

(8) The flow patterns in the last three rows of a four-row bank differ from those shown for three-row banks by Funakawa et al. [76]. This might be attributed either to their moving tube or to the difference in the number of rows.

(9) The flow pattern switches at irregular time intervals, analogous to the jet switching instability of a single tube row. Any jet switching changes the forces acting on a cylinder and it might provide a mechanism for flow-induced vibration in tube bundles.

(10) The size of the dead-water region behind each tube in 30 and 45 degree arrangements is smaller than that in 90 and 60 degree arrangements. It follows that 30 and 45 degree arrangements may have better heat transfer coefficients.

4.2 Hot-Film Measurements

This section presents experimental results of using a hot-film anemometer to investigate vortex shedding frequencies, time-mean velocity profiles, and turbulence intensities in flow fields. The scope of the investigation included the familiar single cylinder, two cylinders, a single tube row, and a four-row tube array in a crossflow. Red and green food dyes were injected from the surface of testing tubes not only to show the flow patterns but also to determine the best locations for flow measurements. The probe was arranged parallel to the cylinder and perpendicular to the flow.

4.2.1 Single Cylinder

Fig. 31 shows one particular result of Strouhal number measurements for a single cylinder at different positions downstream. It was found that same frequency was obtained at the shear-layer after the first eddies "curling-up" and in the wake region. Tested at different flow velocities, the calculated Strouhal numbers were in a range from 0.19 to 0.21, which is in quite good agreement with the generally accepted value in the subcritical region. A broad band flow frequency spectrum with no unique peaks exists in the recirculation zone; this is to be expected because the flow has no periodic behavior in this mixing region. Multiple frequencies were found at the point where two shear-layers merge together. Near to the separation point, there was a low frequency region where the frequency value depended on the flow velocity. It might have resulted from the development of the Bloor-Gerrard frequency.

The von Karman vortex streets formed in the wake of a cylinder with forced transverse oscillation were studied using a hot-film anemometer. Good signals were obtained by placing the hot-film probe parallel to the cylinder, 4-D downstream and 2.5-D across from the cylinder center. The hot-film output was analyzed by a frequency spectrum analyzer to measure the vortex shedding frequency f in the vortex wake.

The driving frequency ratio f_e/f_0 (driving frequency / stationary vortex shedding frequency) was varied from 0 to 4.5. The amplitude ratio, A/D (half peak-to-peak oscillation amplitude / cylinder diameter), was varied from 0 to 0.75 at two different Reynolds numbers of 1500 and 1650. Because of the hysteresis effect, lock-in frequency differs depending upon whether the driving frequency is increasing or decreasing. The driving frequency was increasingly adjusted in this experiment.

Variation of shedding frequency as a function of cylinder forced oscillation frequency is shown in Fig. 32 for amplitude ratios (A/D) of 0.05, 0.145, and 0.235, respectively, with the Reynolds number at 1500. Since the velocity is constant, the

expected vortex shedding frequency f_0 (for a stationary cylinder) is constant. It should be noted that the measured frequencies f in the wake lie almost on the horizontal line ($f/f_0 = 1$) and the vortex-shedding frequency is unaffected by the excitation. This is true for many values of the excitation frequency f_e. However, there is a range where the observed frequencies fall on a line from the origin with a slope of unity. Then the vortex-structure in the wake has lock-in to the excitation.

According to these figures, lock-in also occurs at excitations which are superharmonics of the shedding frequency. Then the values of measured frequency fall on a line from the origin with a slope of one-third. Lock-in regions for the odd-number superharmonic of the shedding frequency are very marked; even-number superharmonics are narrower. Several investigators have observed a similar subharmonic like resonance when $f/f_n = 3$ for the oscillations of an elastically supported circular cylinder in a uniform crossflow [84, 85].

A further observation which can be made is that the frequency of vortex shedding tends to slightly decline with increasing excitation frequency and vibration amplitude. From flow-visualization experiments we have conducted, we believe this to be related to the widening of the wake (and of the von Karman vortex street) resulting from high-frequency or large amplitude lateral oscillation.

The figures described above are plotted from peaks in the frequency spectra observed downstream. At low driving frequency, the observed vortex shedding remains unaffected by the forced oscillatory motion ($f/f_0 = 1$), and the forcing-frequency motion is not observable in the wake. At somewhat higher driving frequencies, the wake spectrum shows the existence of two clearly distinguishable peaks, as shown in Fig. 33. One of them is caused by von Karman vortex shedding, the other by the forced oscillation. The first one is determined by the constant flow velocity in agreement with the Strouhal relation, while the other varies with the forcing frequency. Flow-visualization indicates that two vortex-shedding patterns can exist superposed on each other in the near wake

region; farther downstream the eddies tend to merge or separate into a more regular vortex street.

By further increasing the forced oscillation frequency towards f_0, only a single peak is observed as shown in Fig. 34; the wake oscillates at the cylinder driving frequency and the separate peak for the von Karman vortex shedding is lost. This is the region of complete lock-in.

Another double-value region exists at a driving frequency a little higher above the complete lock-in region. This double-value phenomenon was observable only in the vicinity of the first lock-in region and not for superharmonic lock-in regions.

As the driving frequency is increased above the first lock-in region, the shedding frequency ratio f/f_0 becomes less than unity, as noted above, especially at the larger amplitude ratios. The third-superharmonic lock-in region has a substantial width at all three amplitude ratios, but begins at smaller excitation frequencies for large amplitude ratios. Thus it seems to dip downward towards the origin with increasing amplitude ratio. At amplitude ratios of 0.05 and 0.145, a narrow lock-in region appears to exist when f_e/f is 1.5 (not an integer!). This phenomenon does not appear at larger amplitude ratios and may be spurious.

The lock-in region for synchronization of vortex shedding with transverse vibration was obtained at many A/D ratios and for two Reynolds numbers, 1500 and 1650, as shown in Fig. 35. For small amplitude cylinder motion, the width of the lock-in region increases with increasing amplitude. For small amplitude vibration, it is similar to other published results [44-46]. However, as amplitude ratio (A/D) increases further, the lock-in range becomes narrower again! The slanted onion shape of the lock-in region has not been previously seen. Although it appears counter-intuitive at first, it is in harmony with the observation that free vibrations due to cross-flow tend to be limited in amplitude.

Examination of Fig. 35 shows that the lock-in region is not symmetric with respect to $f_{lockin}/f_e = 1$; the lower frequency lock-in boundary is farther away from the center

frequency than is the higher frequency lock-in boundary. Reynolds number has a strong influence on the upper lock-in boundary, but a very minor effect on the lower lock-in boundary. The maximum frequency-ratio point at the higher lock-in boundary occurs at lower amplitude ratio than the minimum frequency-ratio point at the lower lock-in boundary. Finally, as shown by the slant of the onion-shaped region, larger amplitudes again tend to depress the frequency of vortex shedding.

4.2.2 Normal Cylinder Pair

The time mean velocity profiles at various downstream positions for a cylinder pair with pitch ratio of 1.4, as shown in Fig. 36, are interesting. The gap flow emerging between the cylinders is biased to one cylinder and consequently forms a wide wake on the unbiased side and a narrow one on the biased side. Fig. 36(d) and 36(h) show two different velocity profiles at 1.25D downstream. Wide and narrow wakes shift with each other. This demonstrates bistable flow patterns and also verifies the flow visualization results. The velocity profiles also show that the size of the wide wake slowly increases, whereas, it decreases for the narrow one. Two wakes gradually merge together and form a single wide divergent wake at a 2.5D downstream position.

The frequency of vortex formation in the flow about a pair of parallel cylinder at various separations was investigated with a hot-film anemometer. The frequency of vortex shedding was detected at a position outside the wake of each cylinder. The narrow wake had a unique well-defined high frequency peak associated with the vortex formation in that wake; a typical oscillogram and a spectrum are shown in Fig. 37. The frequencies in the wide wake were more difficult to capture, but a very low frequency was observed. An oscillogram and spectrum of the wide wake are shown in Fig. 38. The vortex shedding frequency of a wide wake was smaller than that of a narrow wake. A typical plot of Strouhal numbers in the vicinity of a normal cylinder pair having P/D = 1.5 is shown in Fig. 39.

The measurement of the shedding frequency of two circular cylinders displaced in a plane normal to the freestream are presented non-dimensionally in Fig. 40 in the form of Strouhal number S vs. pitch ratio. For pitch ratios greater than 2.2, the Strouhal number values of both cylinders are identical to that of a single cylinder. As the gap is decreased, high and low Strouhal numbers associated with narrow and wide wakes are noted. For the narrow wake, the Strouhal number is sharply increases until it reaches its maximum at P/D = 1.5, then slowly decreases with further decreases in pitch ratio. For the wide wake, the Strouhal number sharply decreases to its minimum at P/D = 1.4 then retains at about equals 0.1. For P/D less than 0.1, only one wide wake exists.

Since the flow field of two cylinders is much more complex than that of a single cylinder, very little is known of the lock-in behavior of a cylinder pair. In this study, only one cylinder of the cylinder pair is forced to oscillate transversely, and two pitch ratios are tested. The first case is with P/D = 3.0; in this case the wakes behind each cylinder are almost identical. The other case is with P/D = 1.5, and wide and narrow wakes occur downstream.

Very interesting results of lock-in behavior for a cylinder pair were observed. Fig. 41 shows the variation of shedding frequency as a function of the cylinder forced oscillation frequency for a cylinder pair at P/D = 3.0. The lock-in behaviors of the two cylinders are similar to each other and similar to that of a single forced oscillation cylinder. This implies that the lock-in behavior of the forced oscillation tube in a large pitch ratio cylinder pair is similar to that of a single cylinder. Lock-in also exists for the fixed cylinder in the cylinder pair adjacent to the forced oscillation one. This demonstrates that lock-in behavior not only occurs with cylinders in free oscillation and forced oscillation, and must also occur in the oscillation flow [86-88]. The lock-in region for the forced vibrating tube is wider than that of the fixed tube which is subjected to periodic disturbance in its flow field.

The variation of shedding frequency as a function of the cylinder forced oscillation frequency for both wide and narrow wakes at P/D = 1.5 is shown in Fig. 42. Since these two wakes have different vortex shedding frequencies, the plots are normalized to their own stationary shedding frequency.

A totally different lock-in behavior occurs for a normal cylinder pair having P/D = 1.5. For the wide wake, no "complete lock-in" region was found. A wide double value region exists where one value relates to the forced oscillation frequency and the other relates to vortex shedding frequency. The vortex shedding frequency is the same as that of the stationary wide wake in the cylinder pair ($f/f_0 = 1$).

For the narrow wake, complete lock-in and wide superharmonic lock-in regions exist. Unexpectedly, the superharmonic lock-in behavior is in contrast to that in the single cylinder case. For a single cylinder, lock-in regions for odd-number superharmonics of the shedding frequency are primary, but for the narrow wake of the cylinder pair, the even-number superharmonics dominate lock-in behavior.

4.2.3 Single Tube Row

For a single tube row, there were 18 1-inch brass rods put vertically on the water table with a pitch-to-diameter ratio of 1.4. Only the flow pattern downstream of the middle six tubes was investigated. The Strouhal number for each cylinder in the tube row is shown in Fig. 43. For the three narrow wake regions, the vortex shedding frequencies were approximately the same and the Strouhal number was about 0.4. For the wide wakes, the vortex shedding frequencies depended upon the size of wake, and the Strouhal number varied from 0.07 to 0.13.

Fig. 44 shows velocity profiles at three different downstream positions from the middle six tubes of the single tube row measured by the hot-film anemometer. The pitch ratio is 1.25 and the upstream flow velocity is 1.5 inch/sec. In this case the flow starts out as several uniform jets. At 0.5D downstream of the tube row, the emerging jets begin to

group together. It is evident that two groups of jets are formed at 1.0D downstream, one with set having three jets and the other having two jets. It confirms flow visualization observations and also confirms the author's previous wind tunnel experiments [70-72].

The relationship of Strouhal number vs. tube displacement was studied for a single tube row with pitch ratio of 2.0. Vortex shedding frequencies for the middle five testing rods were measured by the hot-film anemometer. The middle rod was displaced across the flow by using a traversing mechanism and the vortex shedding frequencies were recorded for every 0.05 inch displacement.

The flow patterns along with the tube displacement are shown in Fig. 45. The complex behavior of the flow pattern changes is described in Section 4.1.4.1. In the sequence of C_3 displacements, W_1 almost remains the same size, W_2 expands slowly, and W_3 shrinks continuously until it emerges with W_2 and forms a single wake. The sizes of W_4 and W_5 change slowly until they both become medium wakes. The plot of variation of Strouhal number vs. cylinder displacement, shown in Fig. 45, strongly demonstrates that the Strouhal number of each cylinder in a tube row depends upon the wake size; wide wakes have lower shedding frequencies and narrow wakes have higher frequencies.

4.2.4 Four-Row Tube Arrays

In very complicated and high turbulent flow, such as the flow around the cylinders in the tube bank in the present study, it is very difficult to obtain highly reliable data on the mean and turbulent fluctuating velocities. However, such data may be very useful in analyzing the flow-induced vibration mechanisms of the tube bank. Therefore, the mean velocity and turbulence intensity were measured with a hot-film anemometer for a four-row tube array having P/D = 1.5 and 90 degree arrangement at a gap Reynolds number equal to 4000. Due to the limitation of the traversing mechanism, only the central three columns were measured. The hot-film probe could be traversed crosswise with the flow and flow

data were recorded in 1/64 inch increments. In this manner, precise mean velocity and turbulence intensity profiles could be obtained.

Fig. 46 shows typical examples of the mean velocity and stream-wise turbulence intensity profiles. Fig. 46(a) represents the results measured at a cross section midway between the first and second rows. It shows a very large velocity gradient and a high turbulence intensity in the region behind each tube. On the other hand, still deeper inside the tube bank, the velocity gradient is not so steep though the turbulence intensity increases a lot. At 1D downstream the tube bank, all the wakes merged together, no distinct velocity peak was observed. As expected the maximum turbulence intensity occurred in the shear layer region.

The time histories and their spectra of fluctuation flow velocity at various positions in the tube bank is shown in Fig. 47. At the gap flow of the first row, at point 1, the fluctuation is mainly due to the freestream turbulence and a broad band spectrum was observed. A relative high amount of energy is concentrated on a narrow frequency band for the gap flow of the first three rows, at points 2, 4, 5, 7,and 8. The Strouhal number based on the freestream velocity and tube diameter was 0.31, which is in fairly good agreement with Fitzhugh's [89] and Chen's [18] result. Comparing the fluctuation velocities at point 3, 6,and 10, it clearly shows that flow becomes more and more turbulent the deeper inside the tube bank and a broad spectrum is associated with it. At point 10, where the gap flow is leaving the tube bank, the flow becomes fully turbulent and the peak is less evident.

4.2.5 Summary of the Measurement Results

4.2.5.1 Single Cylinder. The results of observations of the vortex shedding frequencies of a single transverse vibration cylinder at Reynolds number 1500 and 1650 are summarized as follows:

(1) The vortex shedding frequency becomes locked-in to excitation frequency in the vicinity of the "expected" shedding frequency ($f/f_e = 1$). When the driving frequency equals to a multiple of the natural shedding frequency, lesser extent lock-in regions also exist. This result confirms some previous published results [42-45].

(2) The odd-number superharmonics have wider lock-in regions than even-number superharmonics. This phenomenon was interpreted in terms of a "wall-jet" effect of the moving boundary by Ericsson [90], as illustrated in Fig. 48. At odd-number harmonics, the vortex shedding is enhanced by the cylinder motion, whereas for even-number harmonics, it is opposed by the cylinder motion. Thus, one would expect that odd-number harmonics lock-in is dominate. Stansby [44] and Ongoren [45] obtained similar results finding that lock-ins occur at $f_e = f_0$ and $f_e = 3f_0$, but no clear sign of lock-in at $f_e = 2f_0$.

(3) Double-value shedding frequency spectra only exist when the driving frequency is near, but not too near, to the natural shedding frequency. This, however, was not observed near superharmonics.

(4) The vortex shedding frequency of a forced vibrating cylinder is less than that of stationary one. The vibrating cylinder sheds vortices at both ends of its vibration cycle, and widens the wake; this causes a reduction in the shedding frequency.

(5) Lock-in frequency range is a function of the cylinder vibration amplitude and Reynolds number. At small amplitudes, this dependence is basically the same as the finding of Koopmann [46] and Bublitz [91].

(6) Over a large range of the amplitude parameter, an onion-shape lock-in region was discovered. This phenomenon has not been observed by others. It can be demonstrated by flow visualization that the periodic behavior in the wake is weak for large oscillation frequency. The center frequency of the lock-in region is skewed towards lower frequencies, which is the results of a reduction in the vortex shedding frequency for large vibration amplitude.

(7) Reynolds number has strong effect on the upper frequency lock-in boundary, but only a minor effect on the lower frequency lock-in boundary.

4.2.5.2 Normal Cylinder Pair. For a normal cylinder pair at P/D < 2.2, one wide and one narrow wake pattern exists. The vortex shedding frequency is lower for the wide wake and is higher for the narrow wake. The lock-in behavior of large pitch ratio cylinder pair is similar to that of the single cylinder. A different lock-in behavior exists for the closely-spaced cylinder pair: lock-in for even-number superharmonic, rather than odd-number superharmonic, of the shedding frequency is primary. This phenomenon is in contrast to that observed with a single cylinder. Lock-in also occurs for a stationary cylinder which is next to an oscillating one as shown in Fig. 41. This confirms the results of Chen & Ballenge [86] and Mujumdar & Douglas [87] that lock-in exists in an oscillating freestream.

4.2.5.3 Single Tube Row. The fluid flow downstream of a closely-spaced tube row has complex instability. It is caused by the emerging jets coalescing together in a random manner, and the flow pattern switches from one stable configuration to another one at irregular time intervals. Strouhal numbers downstream of each cylinder in the row depends upon the size of each wake. Velocity profiles at various downstream positions also show wide and narrow wake random combinations and jet grouping together in an irregular way. A statically displaced tube in tube row is very effective in switching the flow patterns, therefore, the Strouhal number of each cylinder is changed correspondingly.

4.2.5.4 Four-Row Tube Arrays. A 90-degree arrangement at P/D = 1.5 four-row tube array was tested in this study. A reverse flow in the wake inside the tube array was shown by the W-shape velocity profiles. A regular vortex shedding and a narrow band peak in the turbulence spectrum were observed right after the first row. Deeper inside the tube array, the flow is more complex. The fluctuation velocity oscillograms clearly show the turbulence development inside the tube array. A clear peak is evident in the turbulence spectrum through the first three rows, but the peak is less evident for the fourth row. This

implies that one or two tube row models can not adequately represent full heat exchanger tube arrays.

CHAPTER V

CLOSURE

5.1 Conclusions

The present research is concerned with the instability of flow around a single cylinder, a normal cylinder pair, a tube row, and a four-row tube array in cross flow. This is an area in which there is a need for more fundamental research, particular by regarding the interaction between the cylinders and the surrounding fluid.

Flow visualization by dye injection technique was used to highlight the important features and structures of the flow field. A hot-film anemometer with the help of a high speed data acquisition system and a spectrum analyzer was used to perform measurements of the time-mean velocity, turbulence intensity, and vortex shedding frequency in the flow field of interest.

The pitch-to-diameter ratio plays the most important role in flow instability in tube rows and tube arrays. Measurements show that when the gap between cylinders less than about one cylinder diameter, instability occurs. In addition, decrease the pitch ratio increases the instability. Cylinder arrangement is another important factor in the flow instability in multi-row tube arrays. 90 and 60 degree arrangements are very sensitive to downstream disturbance, while a 45 degree arrangement is the most resistant to disturbance.

A more detailed experiment consisted of investigating lock-in behavior of a single cylinder and a normal cylinder pair. The lock-in behaviors of the single cylinder generally agree with the available published results. A slanted onion-shaped lock-in region was

observed by the author which had not been identified in previous literature. The lock-in behavior of a large pitch ratio cylinder pair is similar to that of the single cylinder. For a closely spaced cylinder pair, the lock-in regions of even-number superharmonic of the shedding frequency are in marked contrast to the single cylinder case.

The fluctuation velocity oscillograms clearly show the turbulence development inside the tube array. A clear peak is evident in the turbulence spectrum at the first three rows, the peak is less evident for the fourth row. This implies that one or two tube rows can not adequately represent full heat exchanger tube arrays.

5.2 Recommendations for Future Research

The efforts to get more and detailed information on the instability flow phenomenon around circular cylinders and their interactions with the mechanical structures should be intensified. Further fundamental research should be extended in several areas to obtain a better knowledge of flow instability. First, in order to obtain a better understanding of the interaction between the cylinder and its surrounding fluid, the flow structures around a single oscillation cylinder and the lock-in behaviors in transverse and longitudinal directions will require more detailed investigations. This would involve measurements of the time-mean and fluctuation properties in the flow field; flow visualization should also be used. Secondly, the flow structures and lock-in behaviors of an oscillation tube in a tube row or a tube array should be studied to make a better understanding of the proximity effect of flow instability. Third, the instability phenomenon in tube rows or tube arrays related to tube motion should be studied systematically, by flow visualization and measurements both. This would give a more complete understanding of the dynamic response of structures in the flow.

A SELECTED BIBLIOGRAPHY

[1] Blevins, R. D., Flow-Induced Vibration, 2nd edition, Van Nostrand Reinhold Company, New York, 1990.

[2] Chen, S. S., Flow-Induced Vibration of Circular Cylindrical Structures, Hemisphere Publishing Corporation, 1987.

[3] Chen, S. S., "Flow Induced Vibrations", Pressure Vessels and Piping: Design Technology -1982- A Decade of Progress, ASME, 1982, pp. 301-312.

[4] Chenoweth, J. M., Flow-Induced Tube Vibrations in Shell-And-Tube Heat Exchangers, Final Report of Research on Heat Exchanger Tube Vibration, Contract No. EY-76-C-03-1273, Energy Research and Development Administration (ERDA), Feb. 1977.

[5] Savkar, S. D., "A Brief Review of Flow Induced Vibrations of Tube Arrays in Cross-Flow", Journal of Fluids Engineering, vol. 99, Sep. 1977, pp. 517-519.

[6] Ishigai, S., and Nishikawa, E., "Experimental Study of Structure of Gas Flow in Tube Banks with Tube Axes Normal to Flow, Part II; On the Structure of Gas Flow in Single-Column, Single-Row, and Double-Rows Tube Banks", Bulletin of the JSME, vol. 18, no. 119, 1975, pp. 528-535.

[7] Borges, A. R. J., "Vortex Shedding Frequencies of the Flow Through Two-Row Banks of Tubes", Journal of Mechanical Engineering Science, vol. 11, no. 5, 1969, pp. 498-502.

[8] Ramamurthy, A. S., Lee, P. M., and Ng, G. P., "Velocity Scales for Constrained Flows", Aeronautical Journal, vol. 79, 1975, pp. 38-41.

[9] Connors, H. J., An Experimental Investigation of the Flow-Induced Vibration of Tube Arrays in Cross Flow, Ph.D Dissertation, University of Pittsburgh, 1969.

[10] Connors, H. J., "Fluidelastic Vibration of Tube Arrays Excited by Cross Flow", Symposium on Flow-Induced Vibration in Heat Exchangers, ASME, Dec. 1970, pp. 42-56.

[11] Chen, S. S., "Guidelines for the Instability Flow Velocity of Tube Arrays in Crossflow", Journal of Sound and Vibration, vol. 93, no. 3, 1984, pp. 439-455.

[12] Lever, J. H., and Weaver, D. S., "On the Stability Behaviour of Heat Exchanger Tube Bundles: Part 1-Modified Theoretical Model", Symposium on Flow-Induced Vibrations, ASME, vol. 2., Dec. 1984, pp. 83-97.

[13] Chen, S. S., "Instability Mechanisms and Stability Criteria of a Group of Circular Cylinders Subjected to Cross-Flow", Journal of Vibration, Acoustics, Stress, and Reliability in Design, vol. 105(1), 1983, pp. 51-59.

[14] Paidoussis, M. P., and Price, S. J., "The Mechanisms Underlying Flow-Induced Instabilities of Cylinder Arrays in Cross Flow", Journal of Fluid Mechanics, vol. 187, 1988, pp. 45-59.

[15] Connors, H. J., "Fluidelastic Vibration of Heat Exchanger Tube Arrays", Journal of Mechanical Design, vol. 100, April 1978, pp. 347-353.

[16] Paidoussis, M. P., "Fluidelastic Vibration of Cylinder Arrays in Axial and Cross Flow - State of Art -", Flow-Induced Vibration Design Guidelines, ASME, PVP-52, 1981, pp. 11-46.

[17] Blevins, R. D., "Fluid Elastic Whirling of Tube Rows and Tube Arrays", Journal of Fluids Engineering, vol. 99, 1977, pp. 457-461.

[18] Chen, Y. N., "Flow-Induced Vibration and Noise in Tube-Bank Heat Exchangers Due to von Karman Streets", Journal of Engineering for Industry, vol. 90(b), 1968, pp. 134-146.

[19] Chen, Y. N., "Flow-Induced Vibrations of In-Line Tube Banks", Symposium on Flow-Induced Vibrations, vol. 3, ASME, 1984, pp. 163-170.

[20] Chen, Y. N., and Weber, M., "Flow-Induced Vibrations in Tube Bundle Heat Exchangers with Cross and Parallel Flow", Symposium on Flow-Induced Vibration in Heat Exchangers, ASME, Dec. 1970, pp. 57-77.

[21] Chen, Y. N., "Fluctuating Lift Forces of the Karman Vortex Streets on Single Circular Cylinders and in Tube Bundles", Journal of Engineering for Industry, vol. 94, 1972, pp. 603-628.

[22] Sarpkaya, T, "Vortex-Induced Oscillations, A Selective Review", Journal of Applied Mechanics, vol. 46, 1979, pp. 241-258.

[23] Fitzpatrick, J. A., and Donaldson, I. S., "Row Depth Effects on Turbulence Spectra and Acoustic Vibrations in Tube Banks", Journal of Sound and Vibration, vol. 73(2), 1980, pp. 225-237.

[24] Owen, P. R., "Buffeting Excitation of Boiler Tube Vibration", Journal of Mechanical Engineering Science, vol. 7(4), 1965, pp. 431-439.

[25] Sandifer, J. B., and Bailey, R. T, "Turbulent Buffeting of Tube Arrays in Liquid Crossflow", Symposium on Flow-Induced Vibrations, vol. 2, ASME, 1984, pp. 211-226.

[26] Savkar, S. D., "Buffeting of Cylindrical Arrays in Cross-Flow", Symposium on Flow-Induced Vibrations, vol. 2, ASME, 1984, pp. 195-210.

[27] Blevins, R. D., "Review of Sound Induced by Vortex Shedding from Cylinders", Journal of Sound and vibration, vol. 92(4), 1984, pp. 455-470.

[28] Parker, R., "Acoustics Resonances in Passages Containing Banks of Heat Exchanger Tubes", Journal of Sound and Vibration, vol. 57(2), 1978, pp. 245-260.

[29] Funakawa, M., and Umakoshi, R., "The Acoustic Resonance in a Tube Bank", Bulletin of the JSME, vol. 13(57), 1970, pp. 348-355.

[30] Paidoussis, M. P., Symposium on Flow-Induced Vibrations, vol. 5, "Turbulence-Induced Noise and Vibration of Rigid and Compliant Surfaces", ASME Winter Annual Meeting, New Orleans, Louisiana, Dec. 9-14, 1984.

[31] Paidoussis, M. P., Symposium on Flow-Induced Vibration and Noise, vol. 3, "Flow-Induced Vibration and Noise in Cylinder Arrays", ASME Winter Annual Meeting, Chicago, Illinois, Nov. 27-Dec. 2, 1988.

[32] Ginniff, M. E., Symposium of International Conference on Vibration in Nuclear Plant, vol. 1, sec. 1, "Vibration Behaviour of Fuel and Fuel Components", The British Nuclear Energy Society, Keswick, U. K., May, 1978.

[33] Paidoussis, M. P., Symposium on Flow-Induced Vibrations, vol. 3, "Vibration in Heat Exchangers", The ASME Winter Annual Meeting, New Orleans, Louisiana, Dec. 9-14, 1984.

[34] Paidoussis, M. P., Symposium on Flow-Induced Vibration and Noise, vol. 5, "Flow-induced Vibration in Heat-Transfer Equipment" ASME Winter Annual Meeting, Chicago, Illinois, Nov. 27-Dec. 2, 1988.

[35] Chen, P. Y., Flow-Induced Vibration Design Guidelines, ASME, PVP-52, 1981.

[36] Kissel, J. H., "Flow-Induced Vibrations in Heat Exchangers", Machine Design, vol. 45(11), May 1973, pp. 104-107.

[37] Eisinger, F. L. "Prevention and Cure of Flow-Induced Vibration Problems in Tubular Heat Exchangers", Flow-Induced Vibrations, ASME, 1979.

[38] Morkovin, M. V., "Flow Around Circular Cylinders-A Kaleidoscope of Challenging Fluid Phenomena", Symposium on Fully Separated Flows, ASME, Philadelphia, Pa. May 1964, pp. 102-118.

[39] Mair, W. A., and Maull, D. J., "Bluff Bodies and Vortex Shedding - A Report on Euromech 17", Journal of Fluid Mechanics, vol. 45(2), 1971, pp. 209-224.

[40] Berger, E., and Wille, R. "Periodic Flow Phenomena", Annual Review of Fluid Mechanics, vol. 4, 1972, pp. 313-340.

[41] Bearman, P. W., "Vortex Shedding from Oscillating Bluff Bodies", Annual Review of Fluid Mechanics, vol. 16, 1984, pp. 195-222.

[42] Bishop, R. E. D., and Hassan, A. Y., "The Lift and Drag Forces on a Circular Cylinder Oscillating in a Flowing Fluid", Proceedings of the Royal Society (London), Series A, 277, 1964, pp. 51-75.

[43] Toebes, G. H., "The Unsteady Flow and Wake Near an Oscillating Cylinder", Trans. ASME, Journal of Basic Engineering, vol. 91, Sep. 1969, pp. 493-505.

[44] Stansby, P. K., "The Locking-On of Vortex Shedding Due to the Cross-Stream Vibration of Circular Cylinders in Uniform and Shear Flows", Journal of Fluid Mechanics, vol. 74, part 4, 1976, pp. 641-665.

[45] Ongoren, A., and Rockwell, D., "Flow Structure from an Oscillating Cylinder, Part 1. Mechanisms of Phase Shift and Recovery in the Near Wake", Journal of Fluid Mechanics, vol. 191, 1988, pp. 197-223.

[46] Koopmann, G. H., "The Vortex Wakes of Vibrating Cylinders at Low Reynolds Numbers", Journal of Fluid Mechanics, vol. 28, part 3, 1967, pp. 501-512.

[47] Griffin, O. M., and Ramberg, S. E., "The Vortex Street Wakes of Vibrating Cylinders", Journal of Fluid Mechanics, vol. 66, 1974, pp.553-576.

[48] Marris, A. W., "A Review on Vortex Streets, Periodic Wakes, and Induced Vibration Phenomena", Journal of Basic Engineering, vol. 86, 1964, pp. 185-196.

[49] Cheng, M., and Moretti, P. M., "Lock-in Phenomena on a Single Cylinder with Forced Transverse Vibration", accepted by Symposium of Flow-Induced Vibration and Wear, ASME Pressure Vessel and Piping Conference, 1991.

[50] Zdravkovich, M. M., "Review of Flow Interference Between Two Circular Cylinders in Various Arrangements", Journal of Fluids Engineering, vol. 99, 1977, pp. 618-633.

[51] Zdravkovich, M. M., "Classification of Flow-Induced Oscillations of Two Parallel Circular Cylinders in Various Arrangements", Symposium on Flow-Induced Vibrations, vol. 2, ASME, 1984, pp. 1-18.

[52] Biermann, D., and Herrnstein, W. H., "The Interference Between Struts in Various Combinations", NACA Reports 468, 1933.

[53] Spivack, H. M., "Vortex Frequency and Flow Pattern in the Wake of Two Parallel Cylinders at Varied Spacing Normal to an Air Stream", Journal of the Aeronautical Science, vol. 13, 1946, pp. 289-301.

[54] Bearman, P. W., and Wadcock, A. J., "The Interaction Between a Pair of Circular Cylinders Normal to a Stream", Journal of Fluid Mechanics, vol. 61(3), 1973, pp. 499-511.

[55] Jendrzejczk, J. A., and Chen, S. S., "Fluid Forces on Two Circular Cylinders in Crossflow", Flow-Induced Vibration - 1986, ASME PVP vol. 104, 1986, pp. 1-13.

[56] Ishigai, S., Nishikawa, E., Nishimura, K., and Cho, K., " Experimental Study on Structure of Gas Flow in Tube Banks with Tube Axes Normal to Flow, Part 1, Karman Vortex Flow from Two Tubes at Various Spacings", Bulletin of the JSME, vol. 15(86), 1972, pp. 949-956.

[57] Hayashi, M., Sakurai, A., and Ohya, Y., "Numerical and Experimental Studies of Wake Interference of Two Normal Flat Plates at Low Reynolds Numbers", Memoirs of the Faculty of Engineering, Kyushu University, vol. 43, No. 2, June 1983, pp. 165-177.

[58] Roberts, B. W., "Low Frequency, Aeroelastic Vibrations in a Cascade of Circular Cylinders", Mechanical Engineering Science Monograph, no. 4, The Institution of Mechanical Engineers, Sep. 1966.

[59] Roberts, B. W., "Low-Frequency, Self-Excited Vibration in a Row of Circular Cylinders Mounted in an Airstream", Ph.D. Dissertation, University of Cambridge, July 1962.

[60] von Bohl, J. G., "Das Verhalten Paralleler Luftstrahlen", Ingenieur-Archiv, 11(4), 1940, pp. 295-314.

[61] Corrsin, S., "Investigation of the Behavior of Parallel Two-Dimensional Air Jets", NACA ACR no. 4H24, Nov. 1944.

[62] Morgan, P. G., "The Stability of Flow Through Porous Screens", Journal of the Royal Aeronautical Society, vol. 64, June 1960, pp. 359-362.

[63] Bradshaw, P., "The Effect of Wind-Tunnel Screens on Normally Two Dimensional Boundary Layers", Journal of Fluid Mechanics, vol. 22(4), 1965, pp. 679-688.

[64] Higuchi, H., "An Experimental Investigation of the Flow field Behind Grid Models", AIAA-86-2460-CP, AIAA 9th Aerodynamic Decelerator & Balloon Technology Conference, Albuquerque, New Mexico, Oct. 1986.

[65] Honji, H., "Viscous Flows Past a Group of Circular Cylinders", Journal of the Physical Society of Japan, vol. 34, no. 3, March 1973, pp. 821-828.

[66] Honji, H., "Formation of a Reversed Flow Bubble in the Time-Mean Wake of a Row of Circular Cylinders", Journal of the Physical Society of Japan, vol. 35, no. 5, Nov. 1973, pp. 1533-1536.

[67] Hara, F., "A Flow Visualization Study of a Single Row of Circular Cylinders Vibrating in Water and Two-Phase Cross Flows", Symposium on Flow-Induced Vibration and Noise, vol. 1, ASME, 1988, pp. 75-89.

[68] Hayashi, M., Sakurai, A., and Ohya, Y., "Wake Interference of a Row of Normal Flat Plates Arranged Side by Side in A Uniform Flow", Journal of Fluid Mechanics, vol. 164, 1986, pp. 1-25.

[69] Moretti, P. M., "Caught in a Cross Flow - The Paradox of Flow-Induced Vibrations", Mechanical Engineering, vol. 108, no. 12, 1986, pp. 56-61.

[70] Cheng, M., "Experimental Study of the Flow Field Downstream of a Single Tube Row", M. S. Report, School of Mechanical and Aerospace Engineering, Oklahoma State University, Stillwater, Oklahoma, 74078-0545, Nov. 1985.

[71] Moretti, P. M., and Cheng. M., "Instability of Flow Through Tube Rows", Journal of Fluids Engineering, vol. 109, June 1987, pp. 197-198.

[72] Cheng, M., and Moretti, P. M., "Experimental Study of the Flow Field Downstream of a Single Tube Row", Journal of Experimental Thermal and Fluid Science, vol. 1, no. 1 Jan. 1988, pp. 69-74.

[73] Weaver, D. S., and Abd-Rabbo, A., "A Flow Visualization Study of a Square Array of Tubes in Water Cross-Flow", Symposium on Flow-Induced Vibrations, vol. 2, ASME, 1984, pp. 165-177.

[74] Abd-Rabbo, A., and Weaver, D. S., "A Flow Visualization Study of Flow Development in a Staggered Tube Array", Journal of Sound and Vibration, vol. 106(2), 1986, pp. 241-256.

[75] Zdravkovich, M. M., and Stonebanks, K. L., "Intrinsically Non-Uniform and Metastable Flow in and Behind Tube Arrays", Symposium on Flow-Induced Vibration and Noise, vol. 1, ASME, 1988, pp. 61-73.

[76] Funakawa, M., Ishimatsu, T., Kumon, K., and Edakuni, K., "Excitation Mechanism of Unstable Fluid-Elastic Vibration in Tube Array", Journal of the Japanese Society of Mechanical Engineers, ser. C, vol. 51, no. 471, 1985, pp. 2997-3003. (Translated by Electric Power Research Institute).

[77] Wallis, R. P., "Photographic Study of Fluid Flow Between Banks of Tubes", Engineering, vol. 148, Institution of Mechanical Engineers, Oct. 1939, pp. 423-426.

[78] Werle, H., "Hydrodynamic Flow Visualization", Annual Review of Fluid Mechanics, vol. 5, 1973, pp. 361-382.

[79] Werle, H., "SUR L'ECOULEMENT AUTOUR D'UN FAISCEAU TUBULAIRE", Revue Francaise de Mecanique, no. 41, 1972, pp. 7-19.

[80] Cheng, M., and Moretti, P. M., "Flow Instabilities in Tube Bundles", Flow-Induced Vibration - 1989, ASME PVP-154, July 1989, pp. 11-15.

[81] Clayton, B. R., and Massey, B. S., "Flow Visualization in Water: A Review of Techniques", Journal of Science Instruments, vol. 44, 1967, pp. 2-11.

[82] Lamas, C. G., Fundamentals of Hot-Wire Anemometry, Cambridge University Press., 1986.

[83] Zdravkovich, M. M., "Modification of Vortex Shedding in the Synchronization Range", Journal of Fluids Engineering, vol. 104, Dec. 1982, pp. 513-517.

[84] Shirakashi, M., Ishida, Y., and Wakiya, S., "Higher Velocity Resonance of Circular Cylinder in Crossflow", Journal of Fluids Engineering, vol. 107, Sep. 1985, pp. 392-396.

[85] Durgin, W. W., March, P. A., and Lefebvre, P. J., "Lower Mode of Circular Cylinders in Cross-Flow", Journal of Fluids Engineering, vol. 102, June 1980, pp. 183-190.

[86] Chen, C. F., and Ballengee, D. B., "Vortex Shedding from Circular Cylinders in An Oscillating Freestream", AIAA Journal, vol. 9, no. 2, 1971, pp. 340-342

[87] Mujumdar, A. S., and Douglas, W. J. M., "The Vortex Wakes of Stationary Cylinders Exposed to An Oscillating Turbulent Stream", Journal of Basic Engineering, vol. 92, no. 3, Sep. 1970, pp. 665-666.

[88] Hatfield, H. M., and Morkovin, M. V., "Effect of An Oscillating Free Stream on the Unsteady Pressure on a Circular Cylinder", Journal of Fluids Engineering, vol. 95, June 1973, pp. 249-254.

[89] Fitz-Hugh, J. S., "Flow-Induced Vibration in Heat Exchangers", Proceedings of International Symposium on Vibration Problems in Industry, paper no. 417, Keswick, Apr., 1973.

[90] Ericsson, L. E., "Karman Vortex Shedding and The Effect of Body Motion", AIAA Journal, vol. 18, no. 8, 1980, pp. 935-944.

[91] Bublitz, P., "Unsteady Pressures and Forces Acting on An Oscillating Circular Cylinder in Transverse Flow", Symposium of Flow-Induced Structural Vibrations, Karlsruhe (Germany), 1972, pp. 443-453.

APPENDIXES

APPENDIX A

MODIFICATION OF HOT-FILM OUTPUT DUE TO TEMPERATURE DRIFT

It is well known that hot-wire/film anemometry is based on measurement of the convection heat transfer from an electrically heated sensor to the surrounding fluid. The amount of heat transferred mainly depends upon the flow velocity and the temperature difference between the sensor and the fluid. Therefore, for any anemometer output voltage change, both flow velocity and fluid temperature need to take into account. Generally, for velocity measurements by a constant temperature type anemometer, the fluid temperature is assumed to be a constant and the anemometer bridge voltage can be interpreted as a directed measure of the flow velocity. However, during experiments, it is very difficult to keep fluid temperature as a constant which calibration was carried out. Any change in fluid temperature will create a change in bridge output and result misinterpretation of the flow velocity. Furthermore, in conjunction with a low overheat ratio, such as used for measuring water flow velocity, the variation of fluid temperature can be easily the most important source of error in hot-wire/film velocity measurements.

There are several methods for taking temperature into account if it is varying during experiments including: (a) calibrating the probe over the expected temperature range which may occur in the experiment, monitoring temperature separately and correcting the data graphically; (b) using a compensating coil in the same flow stream with the active probe and keeping the overheat ratio constant; (c) placing two active sensors operated at different temperatures simultaneously and differencing the outputs to get temperature and velocity independently.

An analytical correction formula, follow the similar procedure developed by P. W. Bearman (1971), has been derived in this study to modify the hot-film velocity measurements which are influenced by the fluid temperature change. This correction equation shows to be satisfactory for the velocity measurement in water and its detailed derivation is shown as follows.

The heat transfer from the hot film sensor is described by King's law (King, 1914) and is usually written as

$$Nu = A' + B'Re^n \tag{1}$$

where Nu is the Nusselt number, Re is the Reynolds number, and A', B' are constants.

For hot-wire heat balance, heat generated by electric current must be equal to heat transfer through convection

$$\frac{E^2}{R_w} = h\pi DL(T_w - T_f) \tag{2}$$

where R_w is wire resistance, E is anemometer bridge output voltage, h is convection heat transfer coefficient, D is probe diameter, L is probe length, and subscripts w and f mean wire and fluid properties. Rearrange equation (2) as follows

$$\frac{E^2}{R_w \pi LK_f(T_w - T_f)} = \frac{hD}{K_f} = Nu$$

Therefore,

$$A' + B'Re^n = \frac{E^2}{R_w \pi LK_f(T_w - T_f)} \tag{3}$$

and

$$E^2 = \pi LK_f R_w (T_w - T_f)A' + \pi LK_f R_w (T_w - T_f)B'(\rho UD/\mu)^n$$

where K_f, ρ, and μ are functions of fluid temperature.

If the fluid temperature change is slow and does not change much during each measuring period, the changes of the K_f, ρ, and μ can be neglected. Then equation (3) can be simplified as

$$E^2 = (T_w - T_f)A'' + (T_w - T_f)B''U^n$$

or

$$E^2 = A(T) + B(T)U^n$$

where A and B are functions of $(T_w - T_f)$ only.

For temperature at calibration temperature T_{f1},

$$E^2 = A + BU^n \tag{4}$$

For temperature at T_{f2} away from T,

$$E_m^2 = A_1 + B_1U^n \tag{5}$$

where

$$\frac{A}{A_1} = \frac{B}{B_1} = \frac{(T_w - T_{f1})}{(T_w - T_{f2})} \tag{6}$$

Substitute equation (6) in equation (5) gives

$$E_m^2 = A(\frac{T_w - T_{f2}}{T_w - T_{f1}}) + B(\frac{T_w - T_{f2}}{T_w - T_{f1}})U^n$$

Compare with equation (4), obtain

$$E_m^2 = (\frac{T_w - T_{f2}}{T_w - T_{f1}})E^2$$

Therefore, the corrected bridge voltage can be modified as

$$E_c = (\frac{T_w - T_{f1}}{T_w - T_{f2}})^{0.5} E_m$$

where subscripts c and m identify the corrected and measured values. Any ambient temperature change will affect fluctuation voltage as well as the mean bridge voltage. Therefore,

$$e'_c = (\frac{T_w - T_{f1}}{T_w - T_{f2}})^{0.5} e'_m$$

The turbulence intensity

$$\frac{\sqrt{\overline{u'^2}}}{U} = \frac{2*E*e'}{n(E^2 - A)}$$

can be modified as follows

$$I = \frac{\sqrt{\overline{u'^2}}}{U} = \frac{2*E_m*e_m'}{n[\, E_m^2 - A(\frac{T_w - T_{f2}}{T_w - T_{f1}})]}$$

APPENDIX B

FIGURES

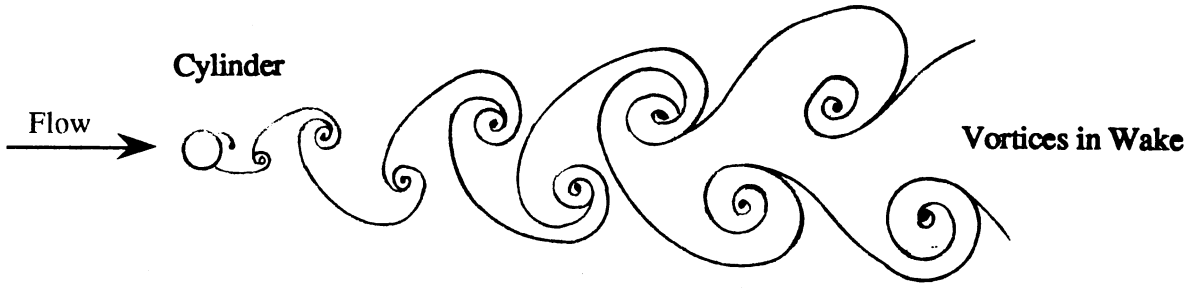

Figure 1. Sketch of Vortex Shedding Resulting from Flow across a Circular Cylinder

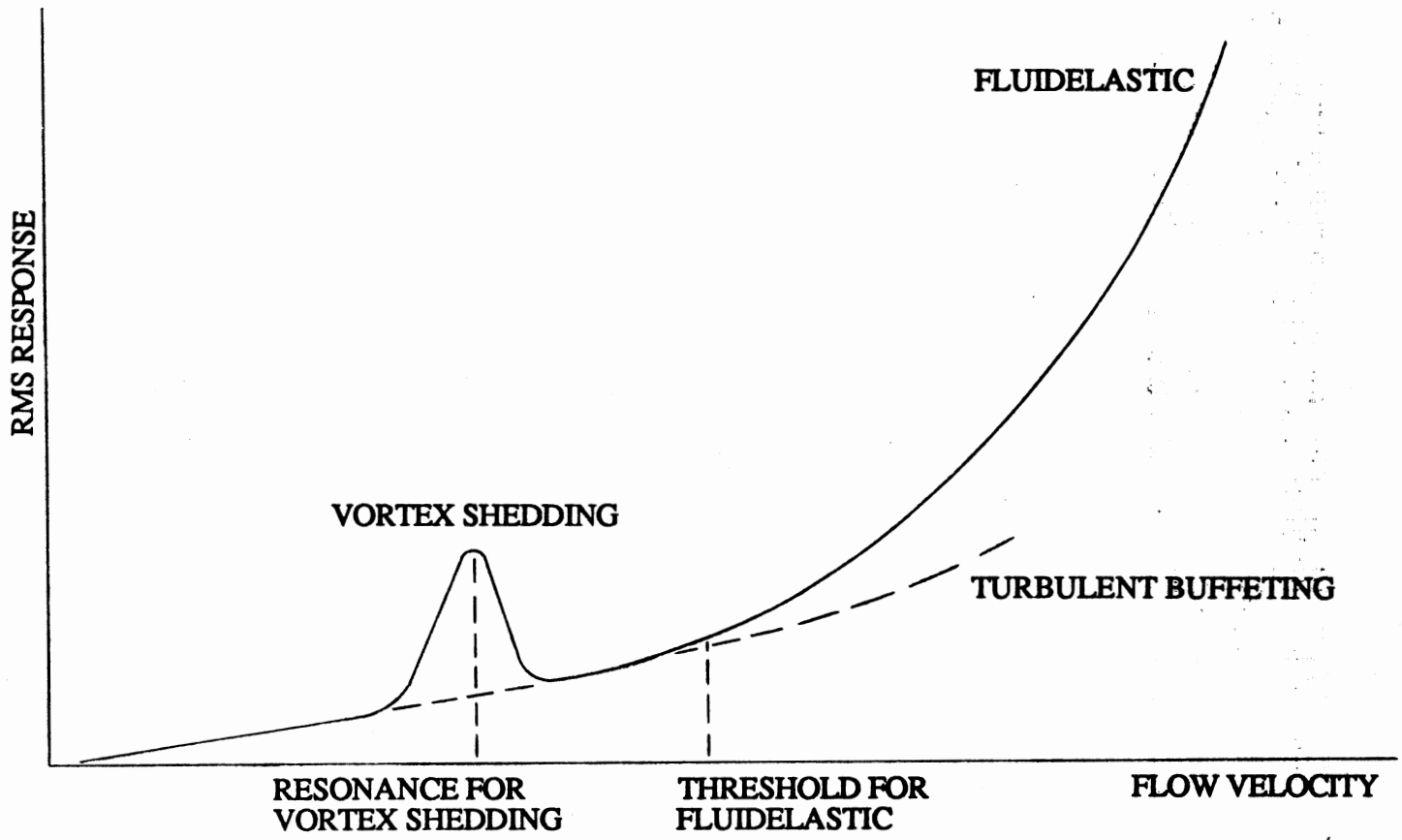

Figure 2. Ideal Response of a Cylinder in a Cylinder Array
Subjected to Crossflow

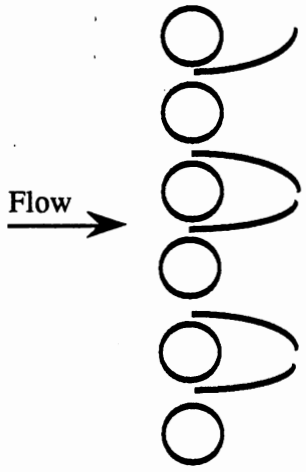

Figure 3. Jet Pairing of a Single Tube Row

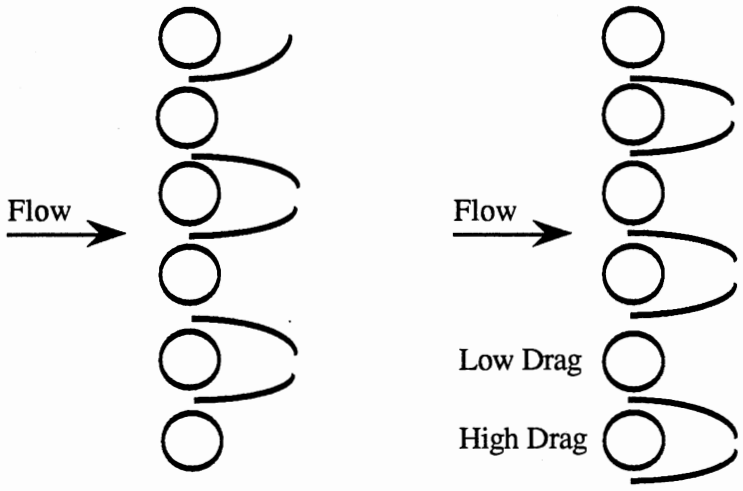

Figure 4. Jet Switching Caused by Disturbance

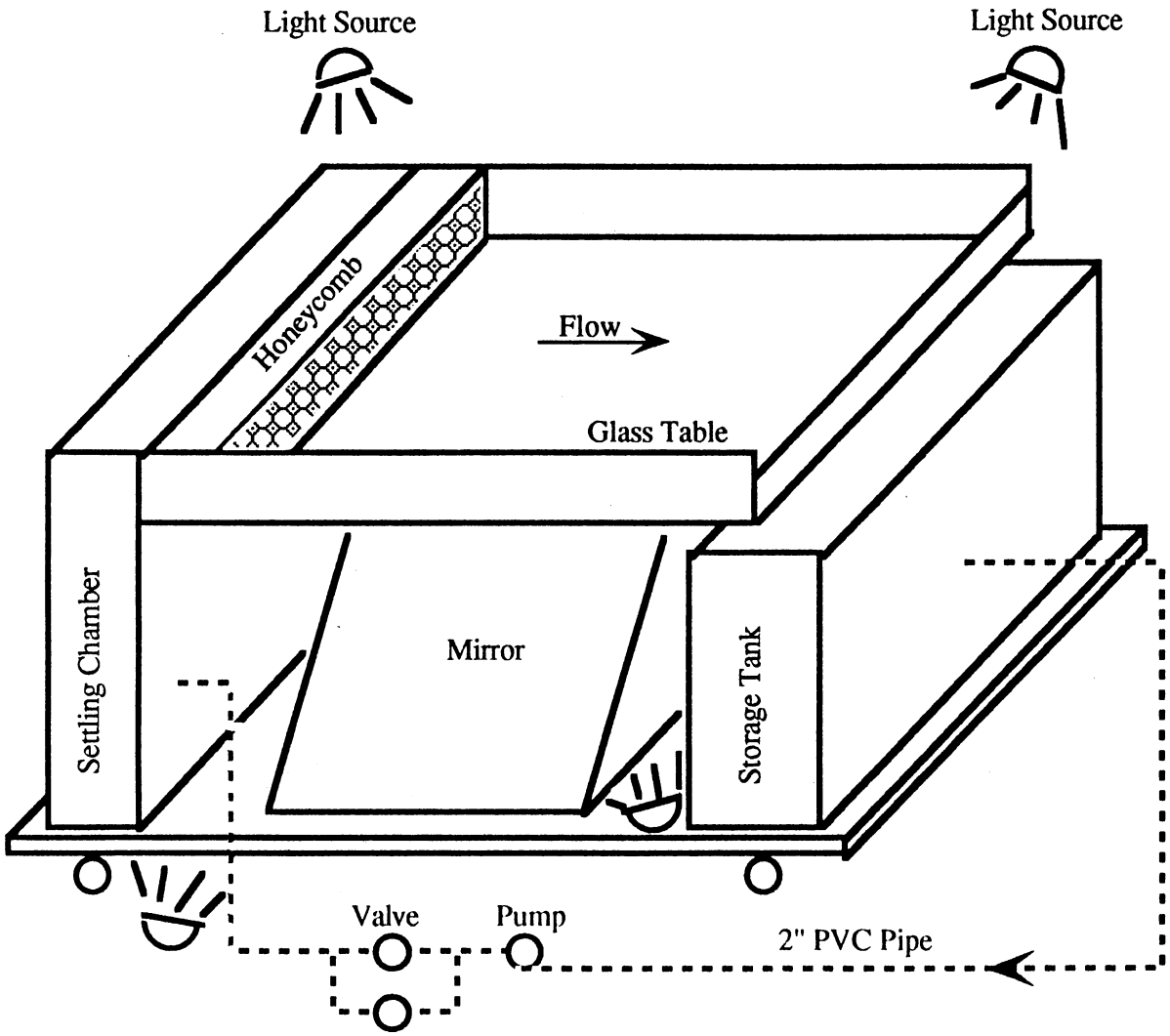

Figure 5. Schematic of Water Table Setup

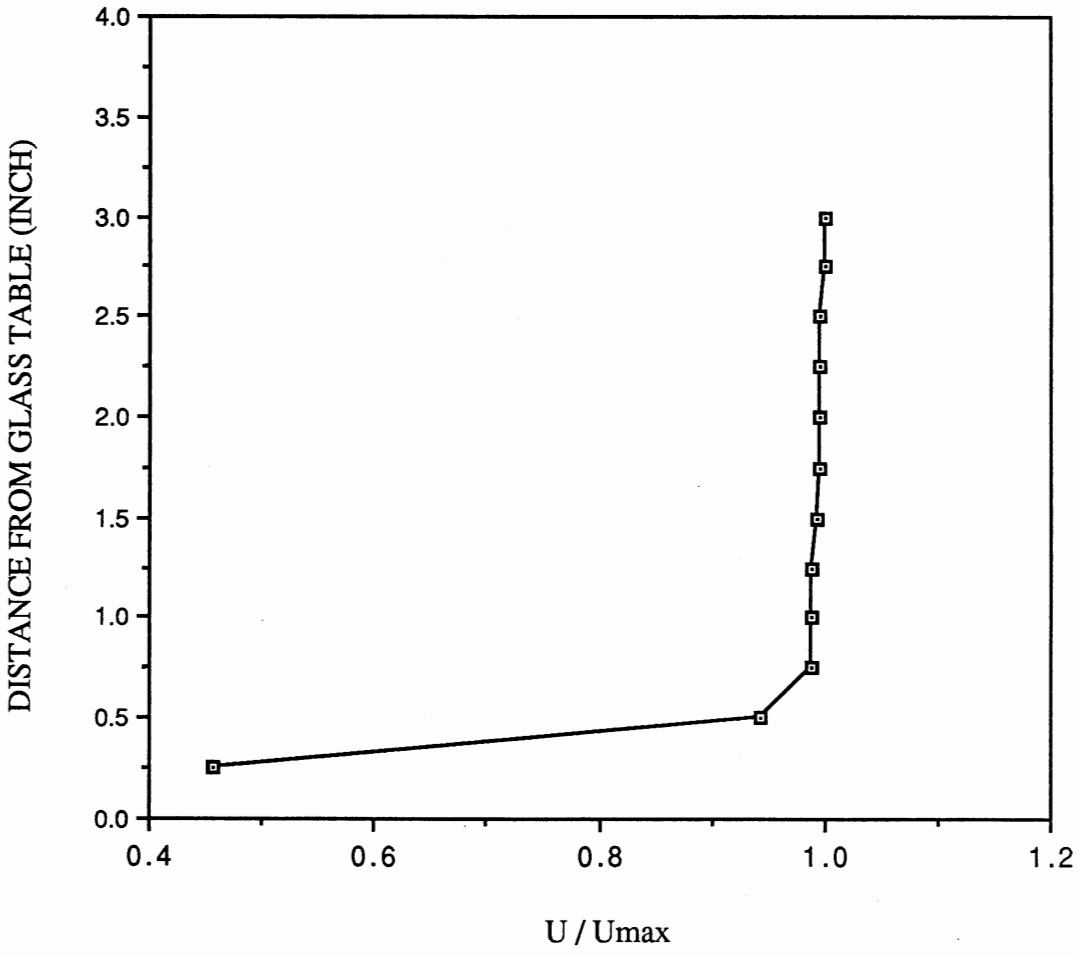

Figure 6. Velocity Profile of Water Table at U = 1.5 inch/sec

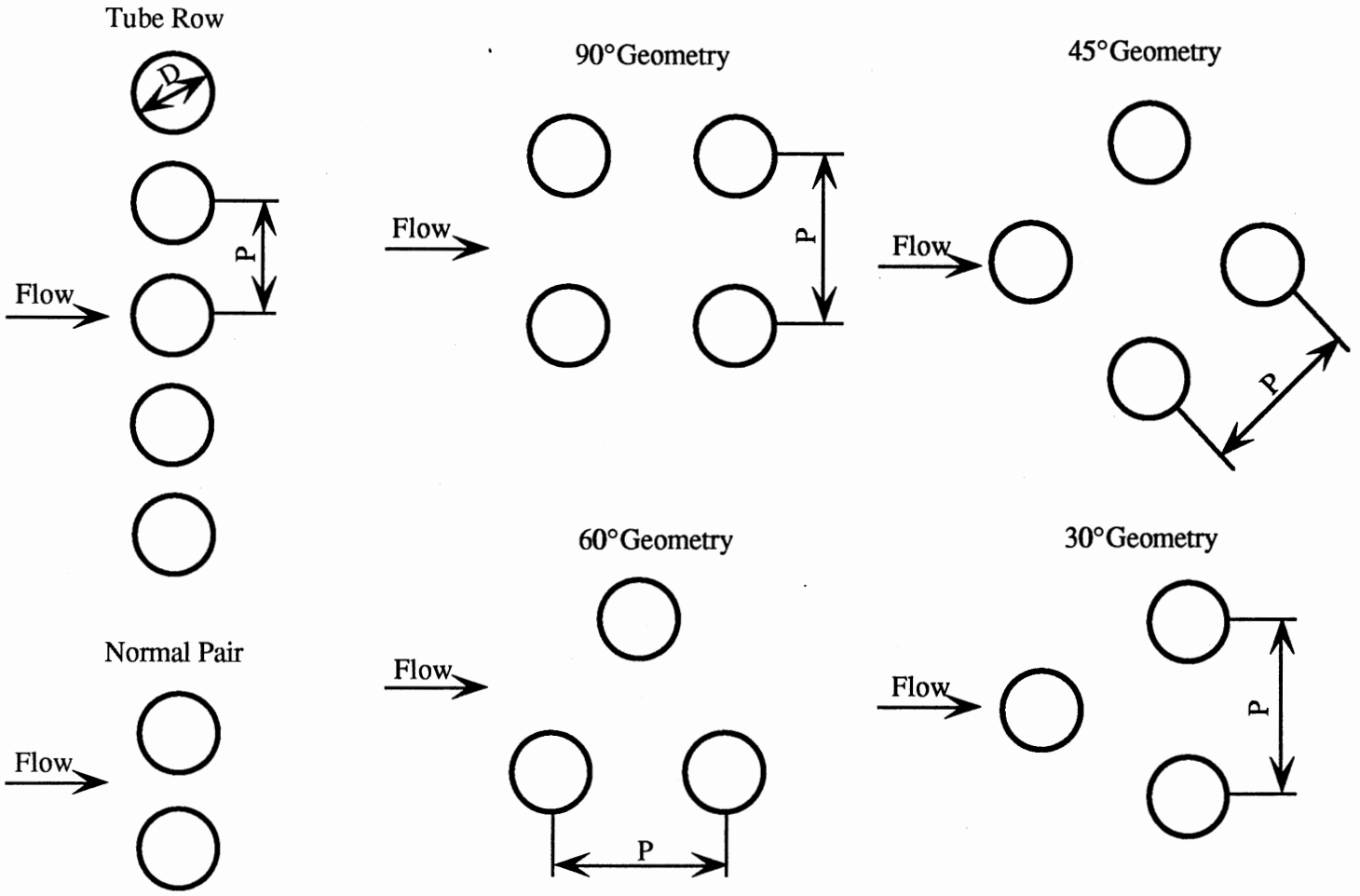

Figure 7. Schematic of Tube Array Arrangements

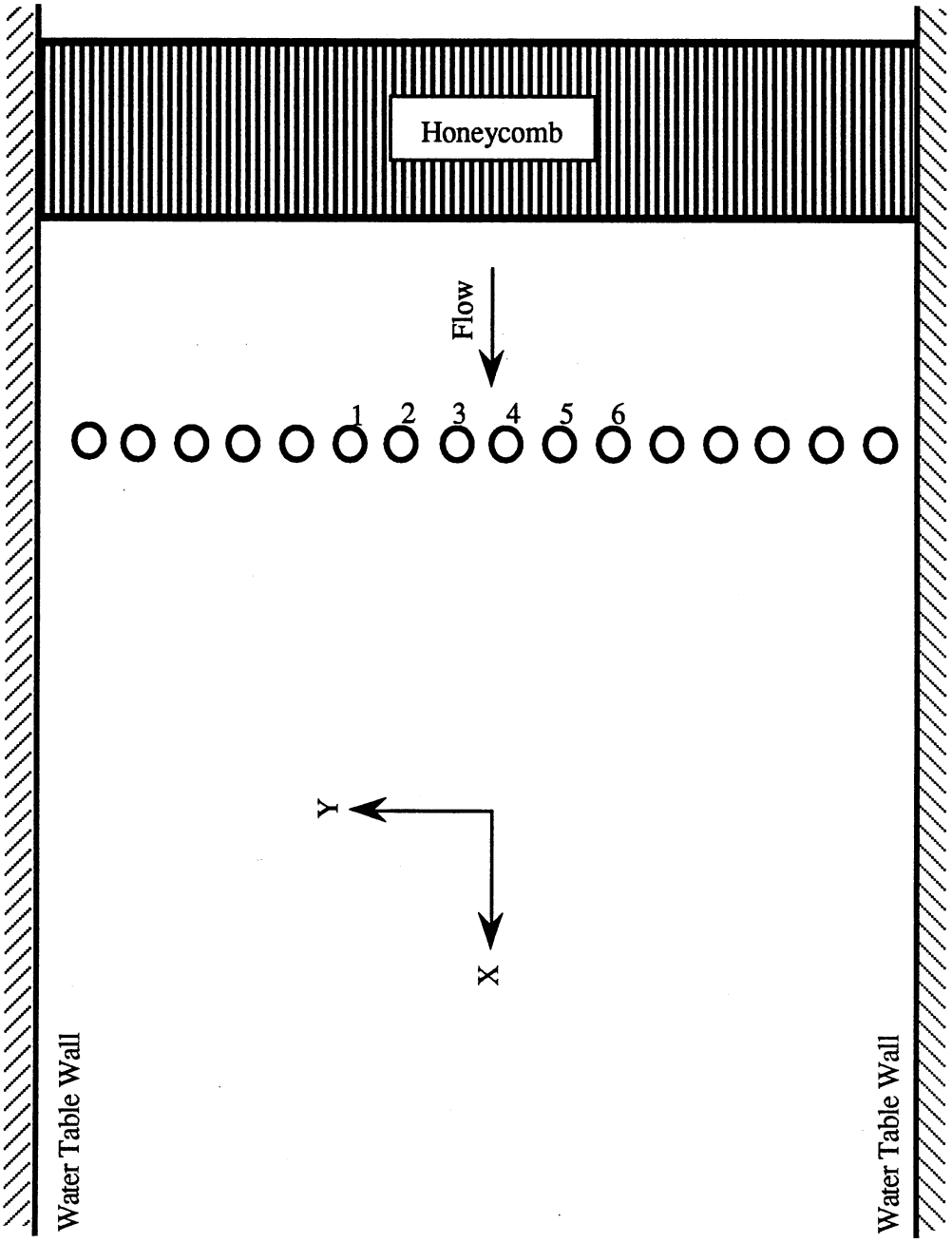

Figure 8. Schematic of a Single Tube Row on the Water Table

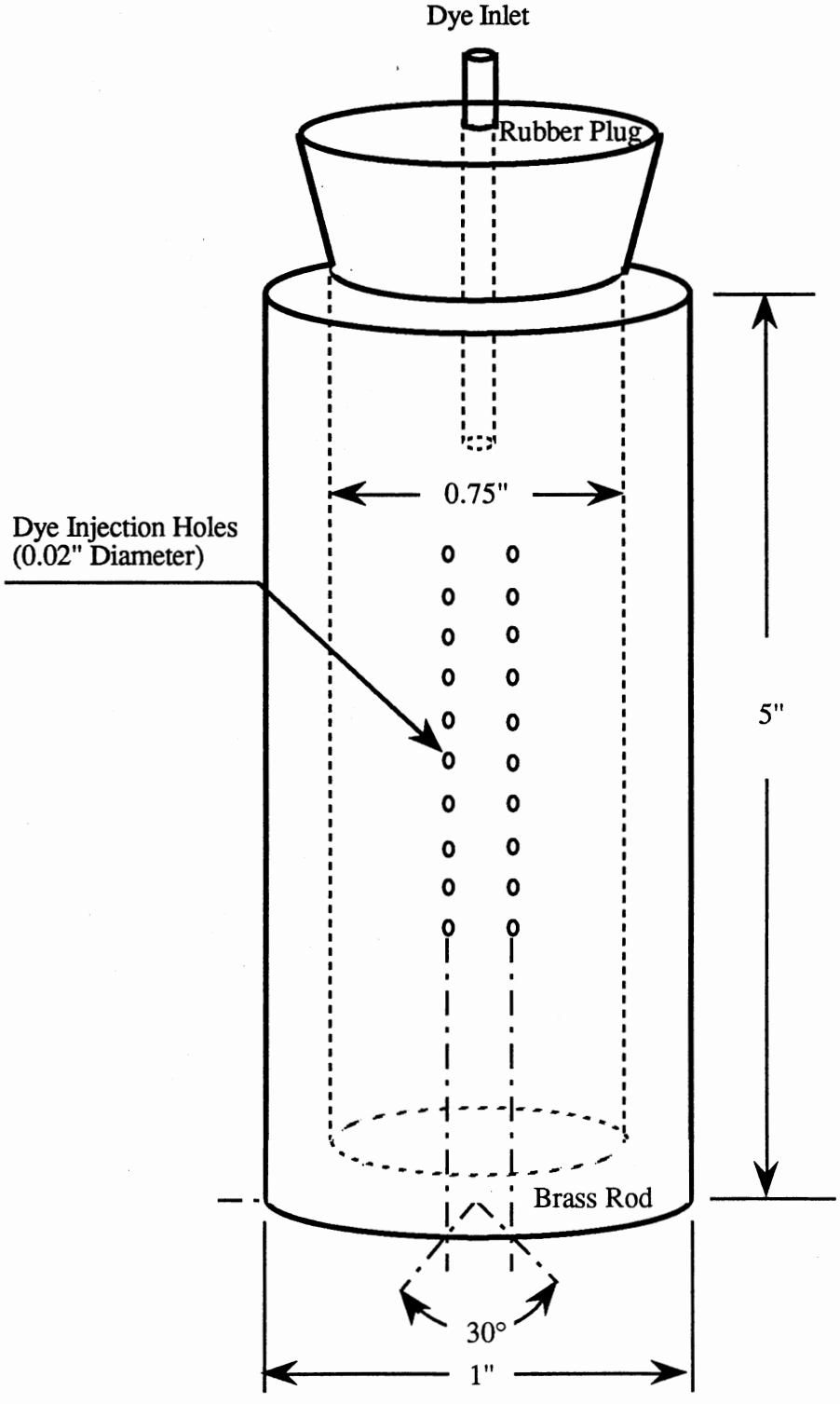

Figure 9. Schematic of Dye Injection Tube

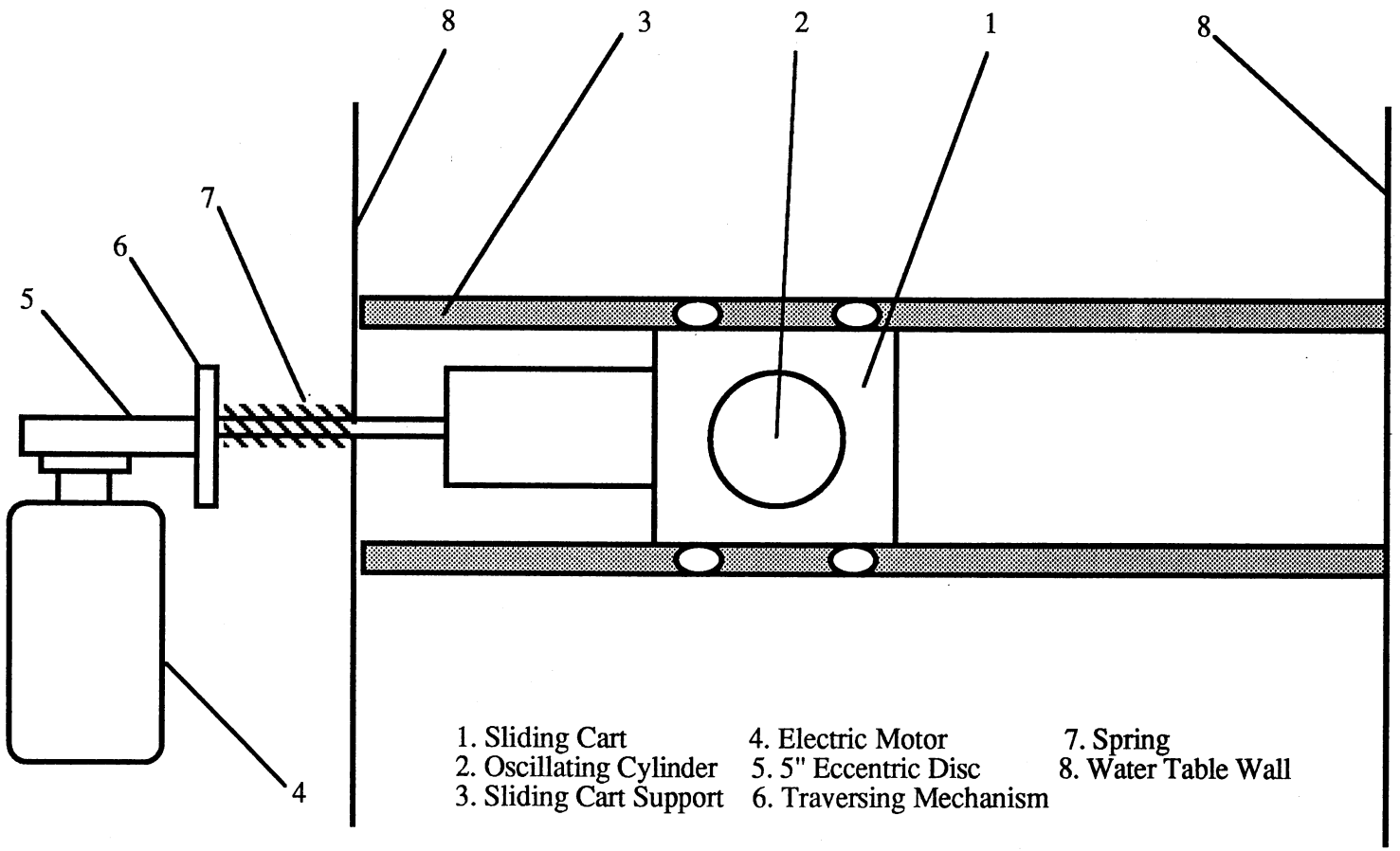

Figure 10. Schematic of Traversing & Vibratory Mechanisms

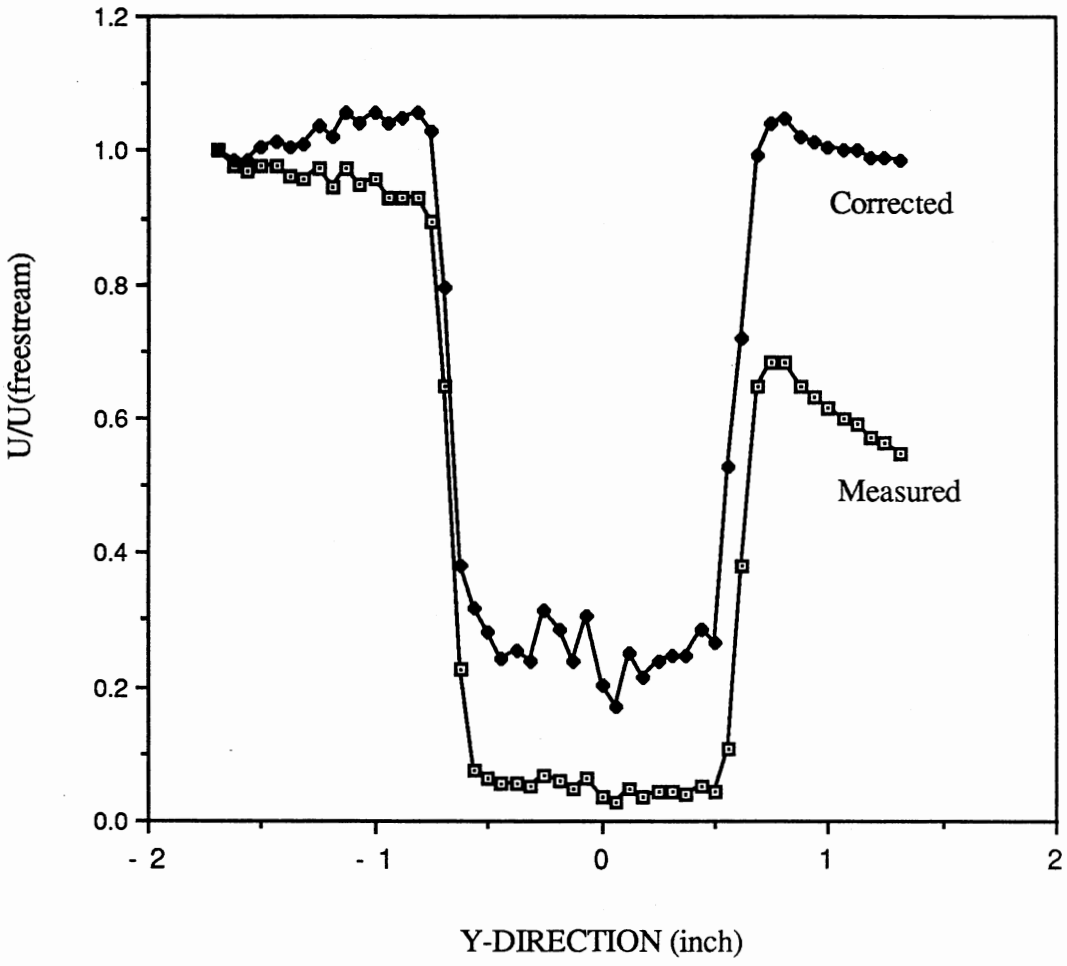

Figure 11. Measured & Corrected Velocity Profiles Downstream of a Stationary Cylinder

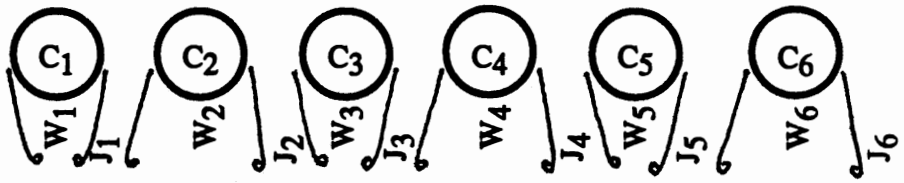

(a) INITIAL STABLE PATTERN

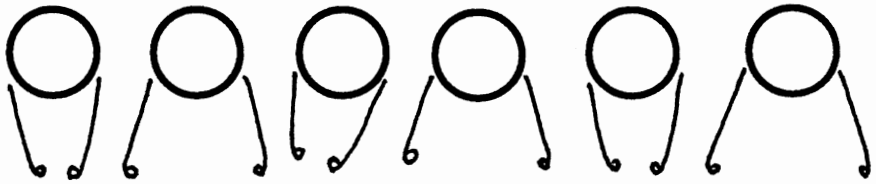

(b) C_4 DISPLACED LEFT

(c) C_4 DISPLACED 0.55D LEFT

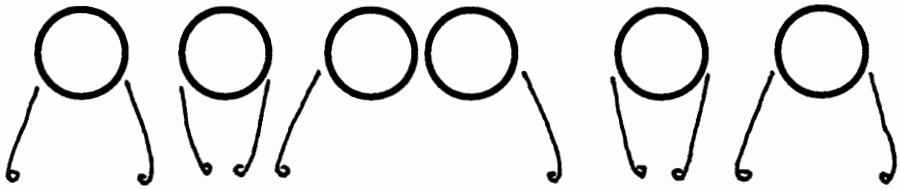

(d) C_4 VERY CLOSE TO C_3 (LESS THAN 0.1D)

Figure 12. Flow Pattern Change due to a Transversely Displaced Tube in a Single Tube Row at Initial Stable Pattern as N-W-N-W-N-W Combination

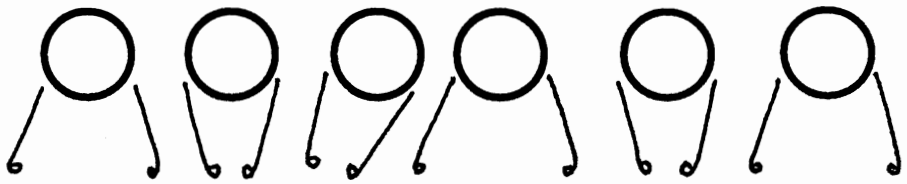

(e) FLOW PATTERN 1 - AS C_4 MOVES AWAY FROM C_3
(W-N-N-W-N-W)

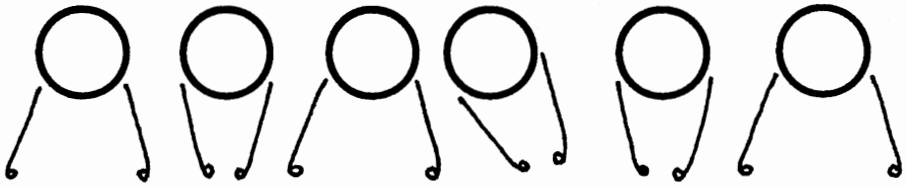

(f) FLOW PATTERN 2 - AS C_4 MOVES AWAY FROM C_3
(W-N-W-N-N-W)

Figure 12. (Continued)

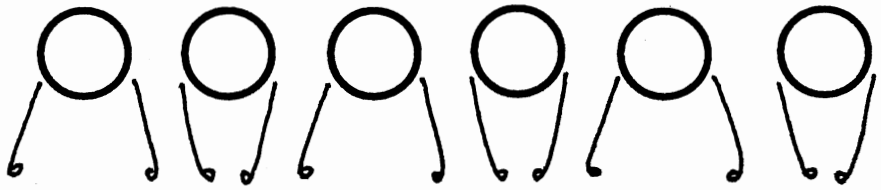

(a) INITIAL STABLE PATTERN

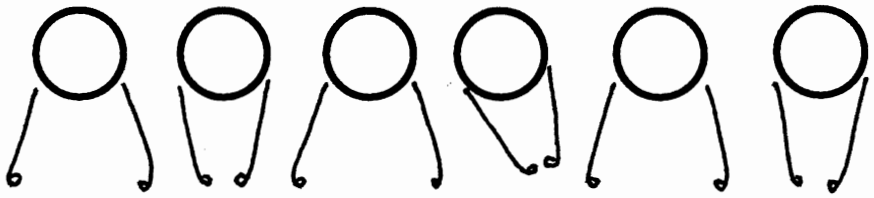

(b) C_4 DISPLACED LEFT

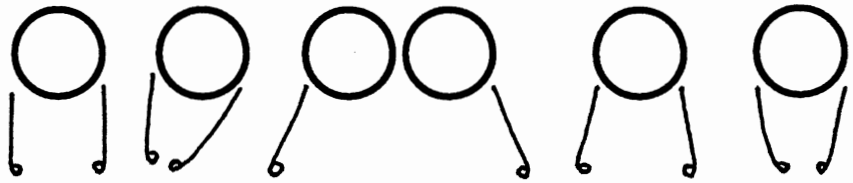

(c) C_4 VERY CLOSE TO C_3 (LESS THAN 0.1D)

Figure 13. Flow Pattern Change due to a Transversely Displaced Tube in a Single Tube Row at Initial Stable Pattern as W-N-W-N-W-N Combination

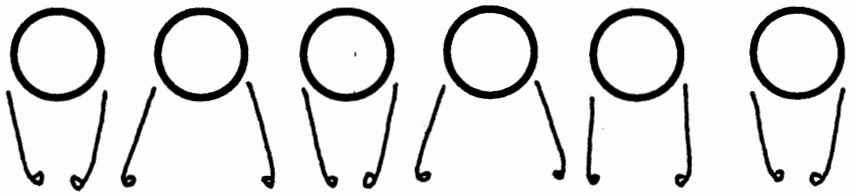

(a) INITIAL STABLE PATTERN

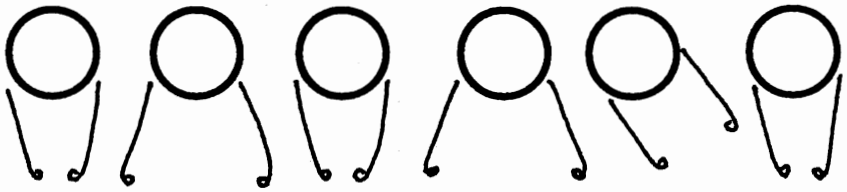

(b) C_4 DISPLACED RIGHT

Figure 14. Flow Pattern Change due to a Transversely Displaced Tube in a Single Tube Row at Initial Stable Pattern as N-W-N-W-M-N Combination

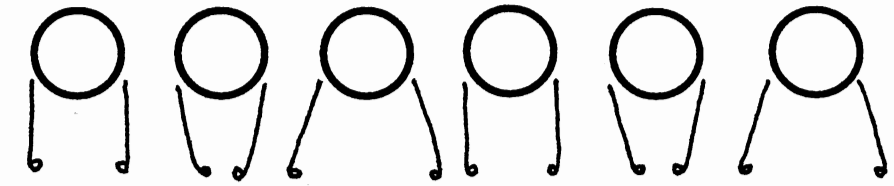

(a) INITIAL STABLE PATTERN

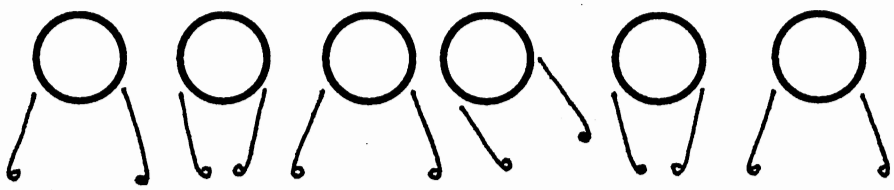

(b) C_4 DISPLACED 0.4D LEFT

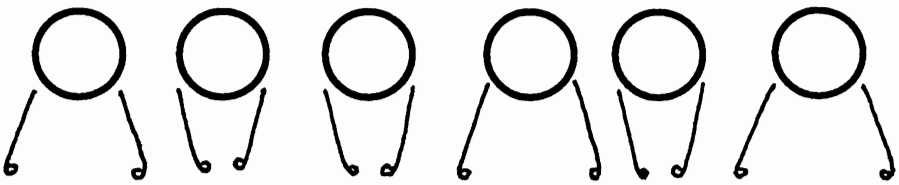

(c) C_4 DISPLACED 0.27D RIGHT

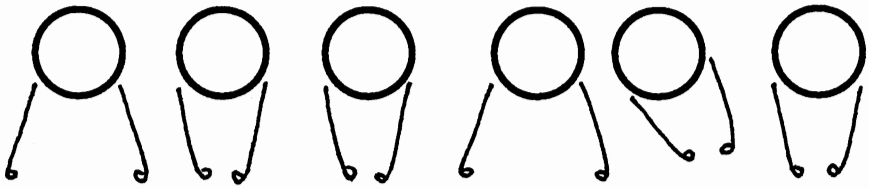

(d) C_4 DISPLACED 0.4D RIGHT

Figure 15. Flow Pattern Change due to a Transversely Displaced Tube in a Single Tube Row at Initial Stable Pattern as M-N-W-M-N-W Combination

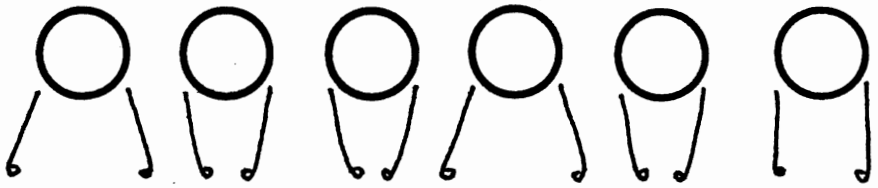

(a) INITIAL STABLE PATTERN

(b) C_4 DISPLACED LEFT

Figure 16. Flow Pattern Change due to a Transversely Displaced Tube in a Single Tube Row at Initial Stable Pattern as W-N-N-W-N-M Combination

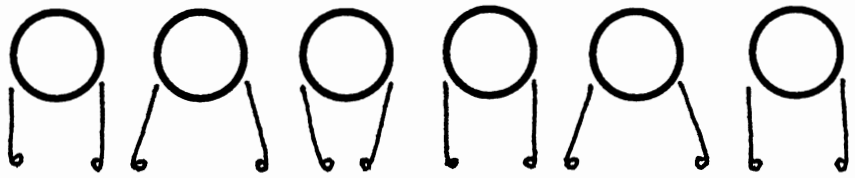

(a) INITIAL STABLE PATTERN

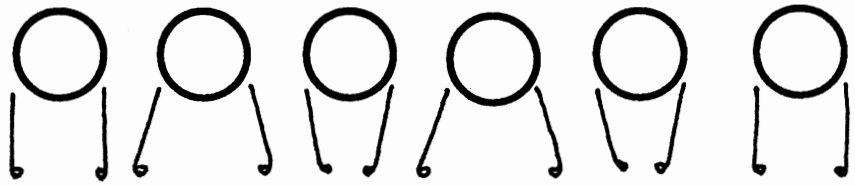

(b) C_4 DISPLACED 0.16D DOWNSTREAM

(c) C_4 DISPLACED 0.24D DOWNSTREAM

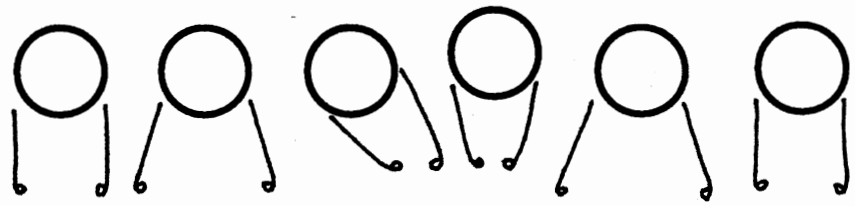

(d) C_4 DISPLACED UPSTREAM

Figure 17. Flow Pattern Change due to a Longitudinally Displaced Tube in a Single Tube Row at Initial Stable Pattern as M-W-N-M-W-M Combination

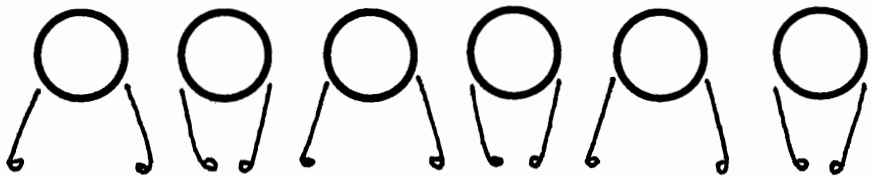

(a) INITIAL STABLE PATTERN

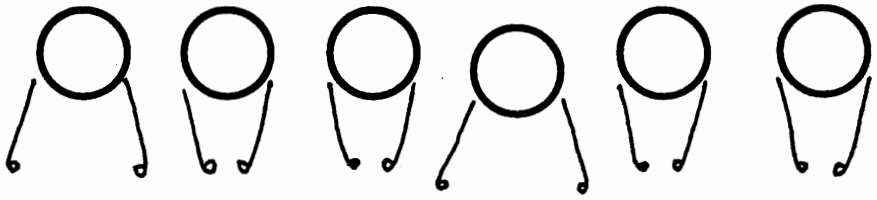

(b) C_4 DISPLACED 0.27D DOWNSTREAM

Figure 18. Flow Pattern Change due to a Longitudinally Displaced Tube in a Single Tube Row at Initial Stable Pattern as W-N-W-N-W-N Combination

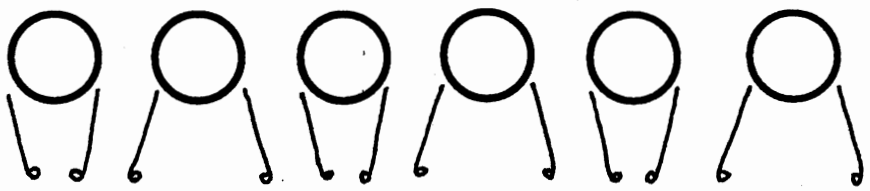

(a) INITIAL STABLE PATTERN

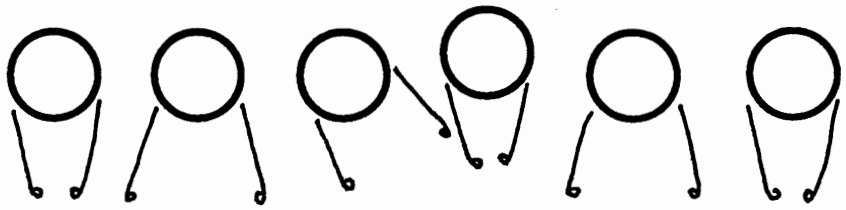

(b) C_4 DISPLACED 0.24D UPSTREAM

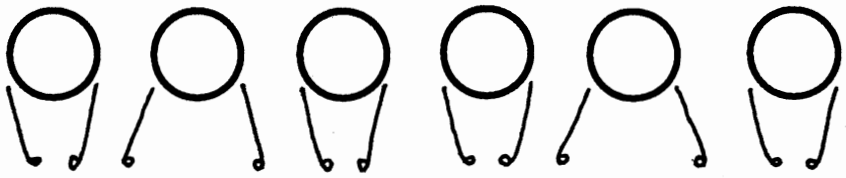

(c) C_4 BACKS TO ITS INITIAL ORIGIN

Figure 19. Flow Pattern Change due to a Longitudinally Displaced Tube in a Single Tube Row at Initial Stable Pattern as N-W-N-W-N-W Combination

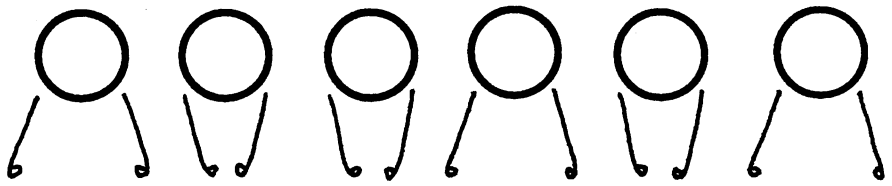

(a) INITIAL STABLE PATTERN

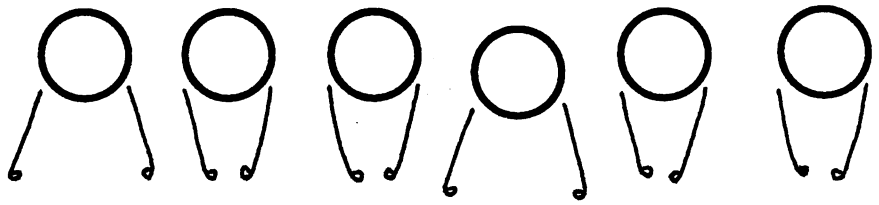

(b) C_4 DISPLACED 0.24D DOWNSTREAM

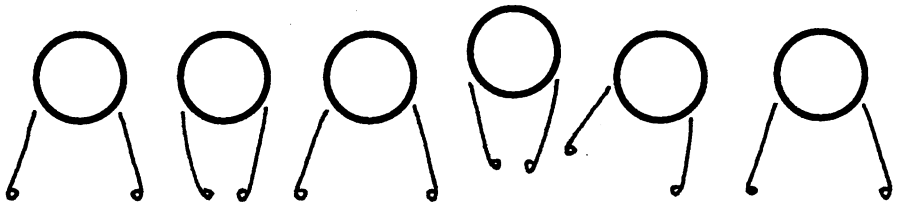

(c) C_4 DISPLACED 0.24D UPSTREAM

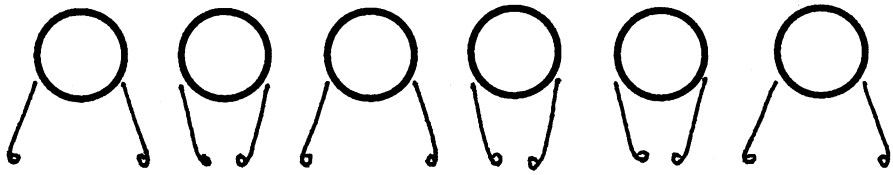

(d) C_4 BACKS TO ITS INITIAL ORIGIN

Figure 20. Flow Pattern Change due to a Longitudianlly Displaced Tube in a Single Tube Row at Initial Stable Pattern as W-N-N-W-N-W Combination

(a)

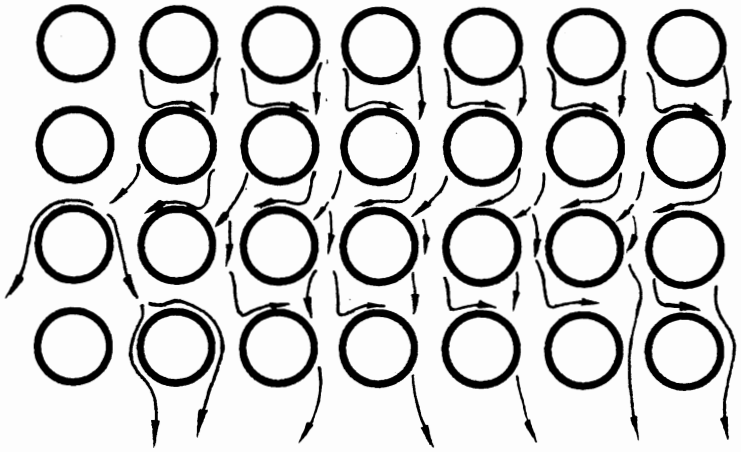

(b)

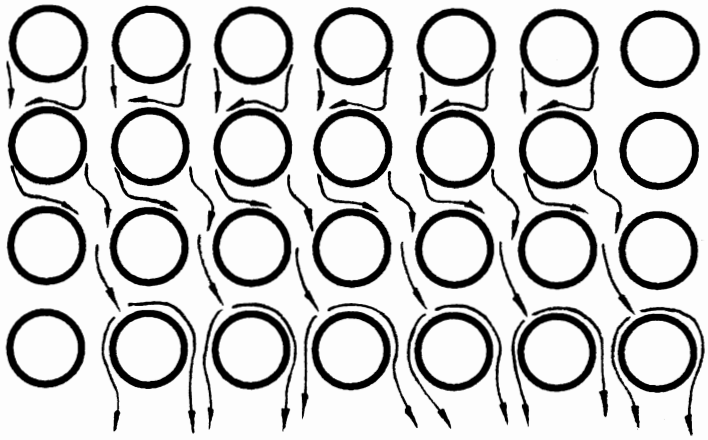

Figure 21. Flow Patterns of Tube Arrays with 90^{o} Arrangement and P/D=1.25 at Re=2840

(c)

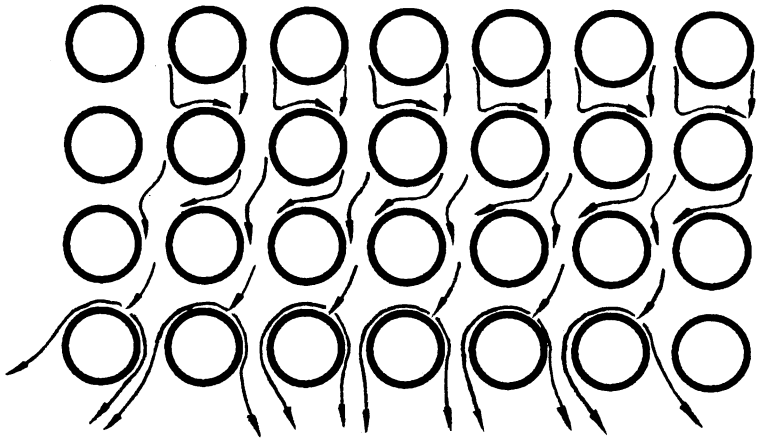

(d)

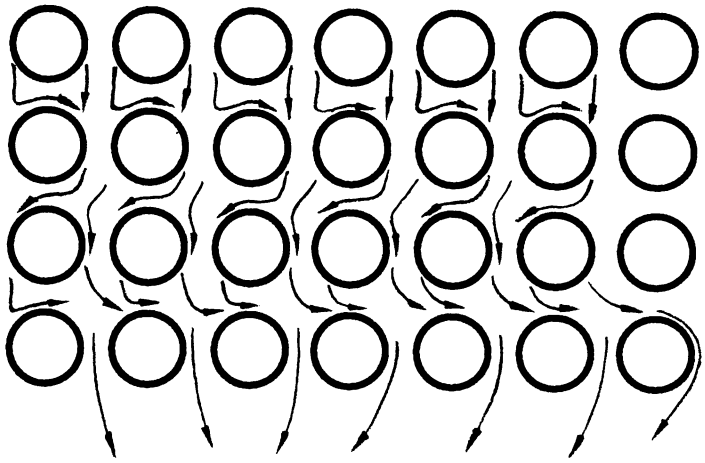

Figure 21. (Continued)

(e)

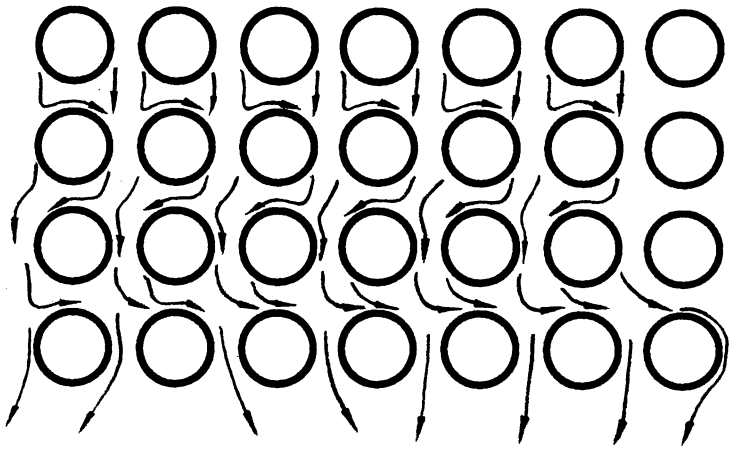

(f)

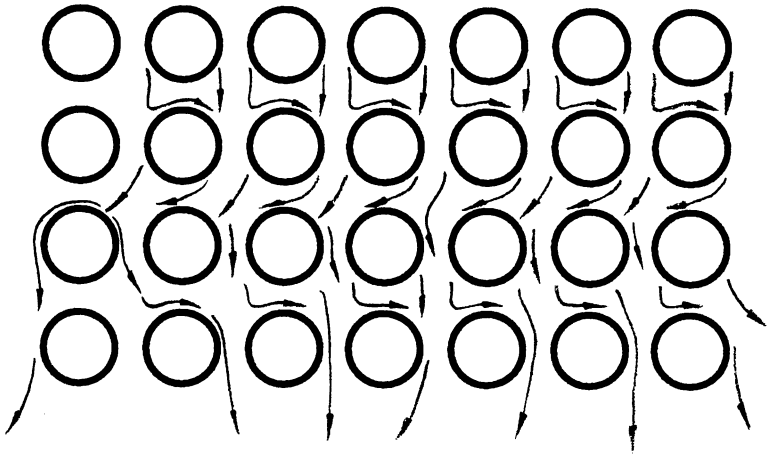

Figure 21. (Continued)

(g)

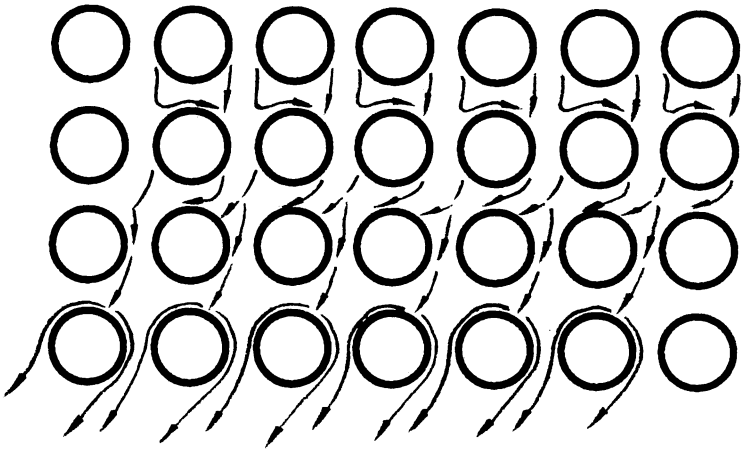

(h)

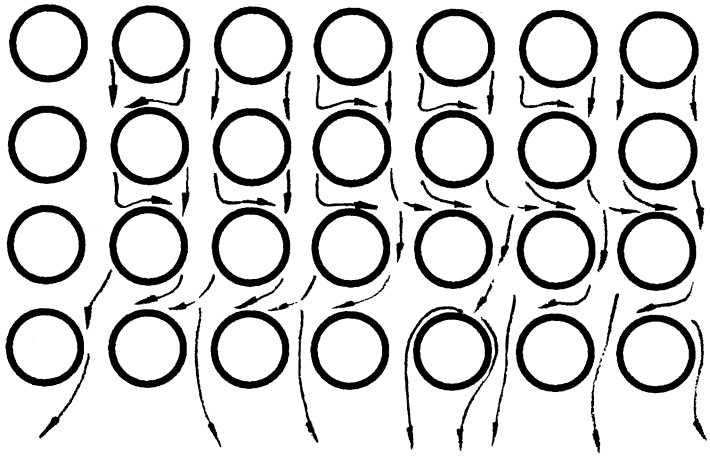

Figure 21. (Continued)

(i)

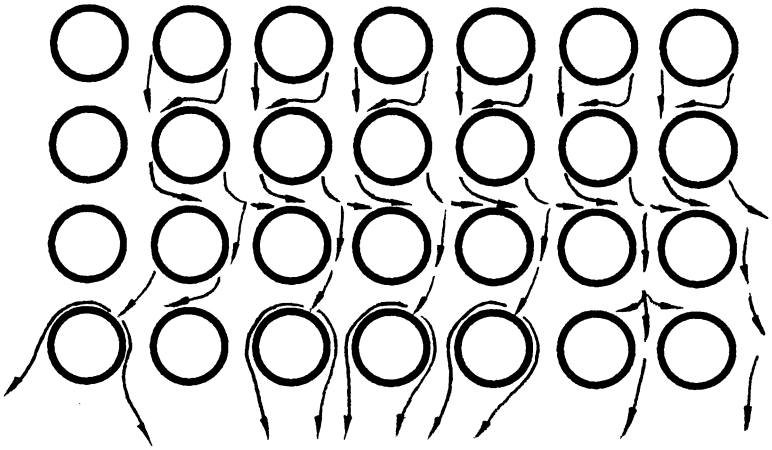

Figure 21. (Continued)

(a)

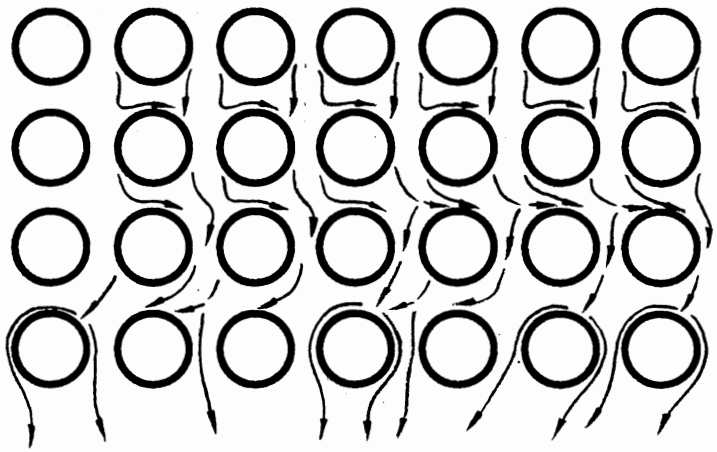

(b)

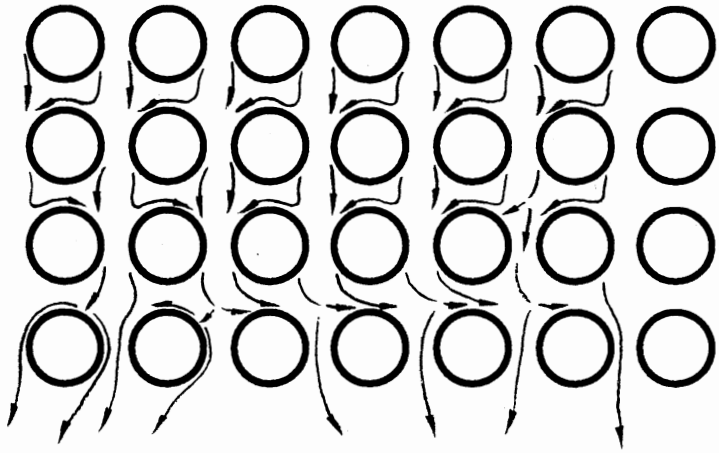

Figure 22. Flow Patterns of Tube Arrays with 90^{o} Arrangement and P/D=1.33. (a)-(f) Re=2600, (g)-(h) Re=7100.

(c)

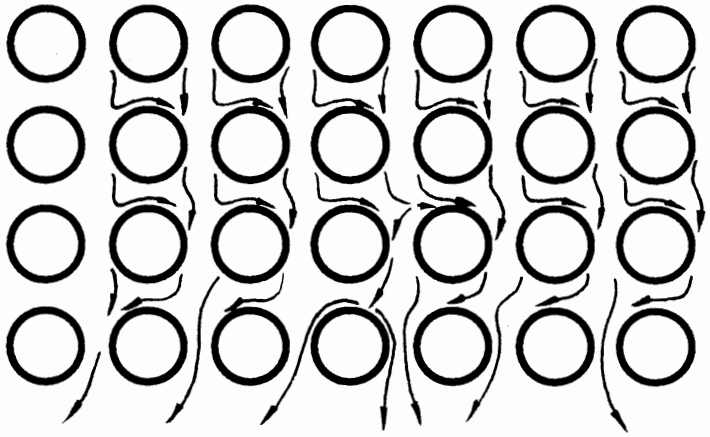

(d)

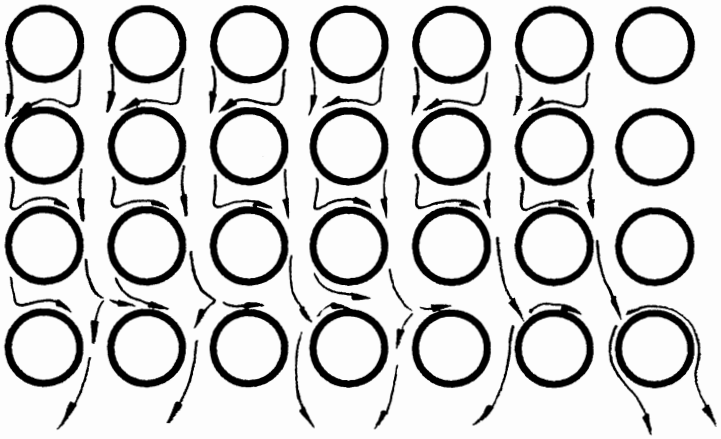

Figure 22. (Continued)

(e)

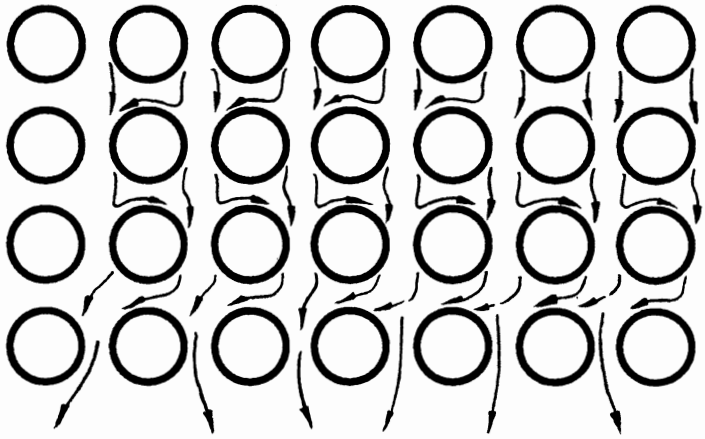

(f)

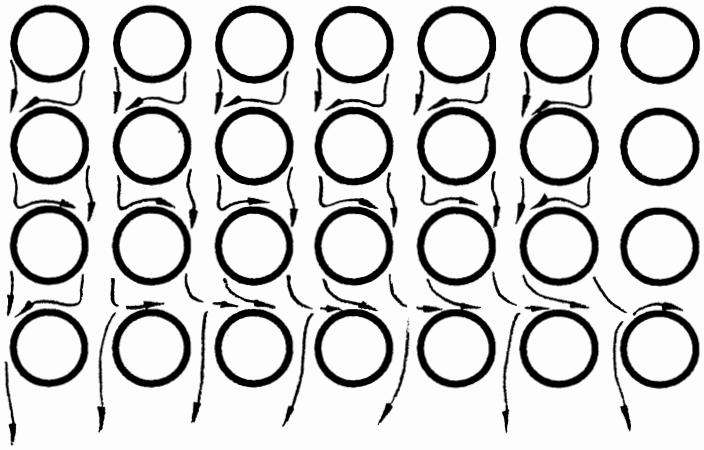

Figure 22. (Continued)

(g)

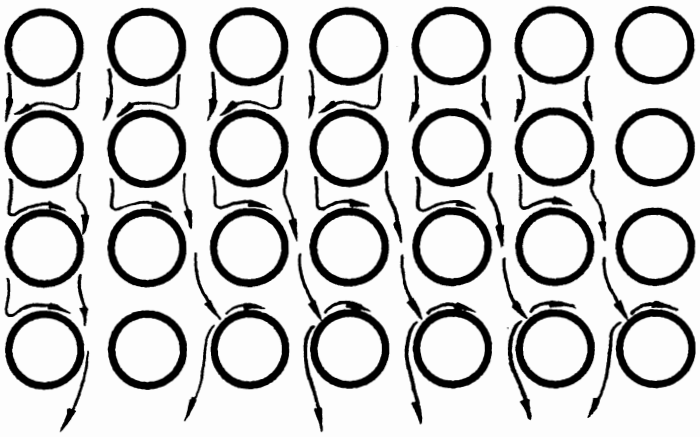

(h)

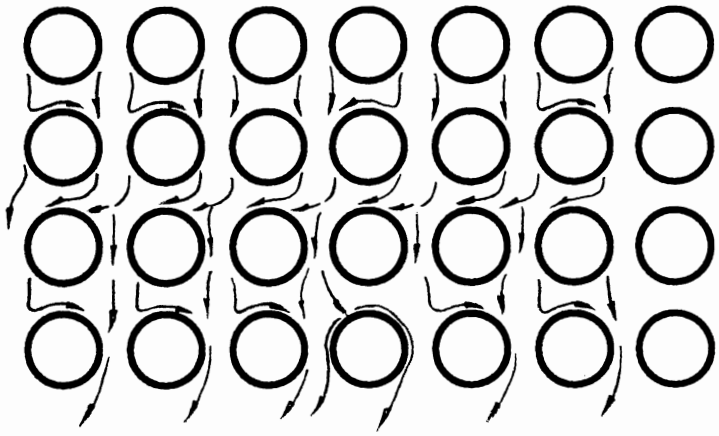

Figure 22. (Continued)

(a)

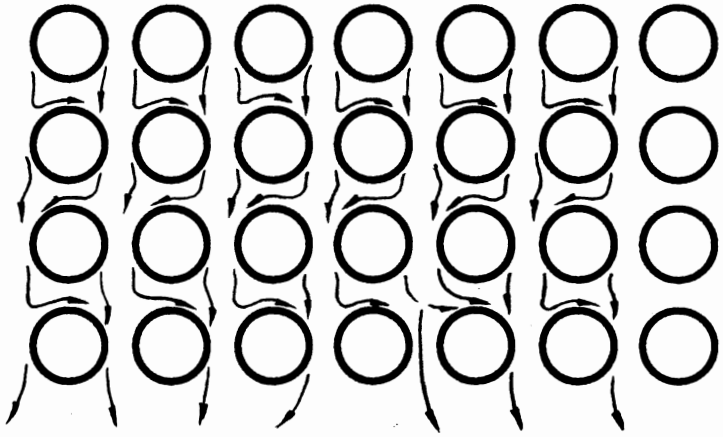

(b)

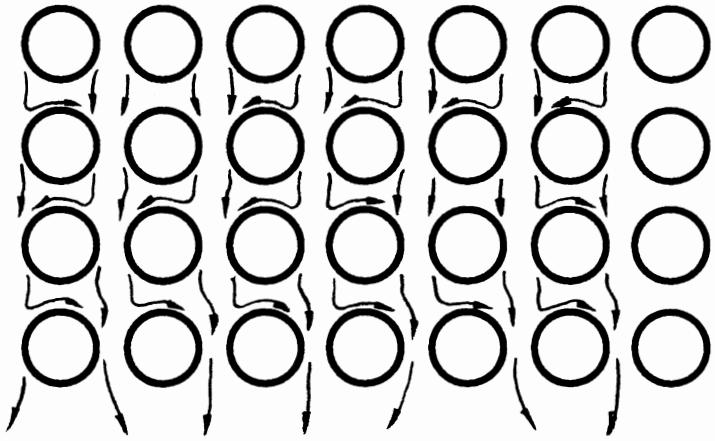

Figure 23. Flow Patterns of Tube Arrays with 90° Arrangement and P/D=1.4. (a)-(f) Re=2400, (g) Re=4830,. (h) Re=5830.

(c)

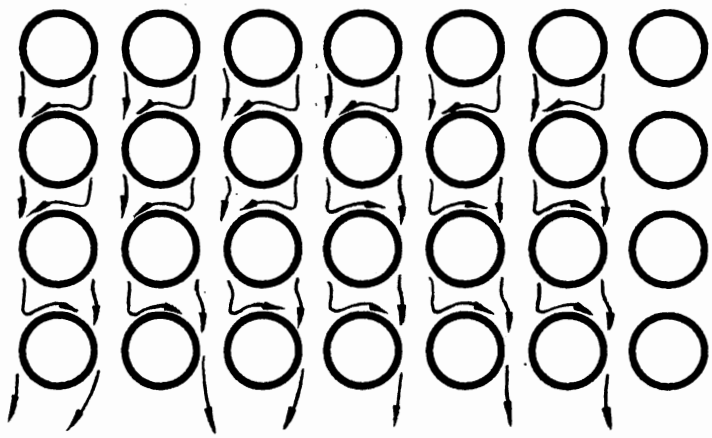

(d)

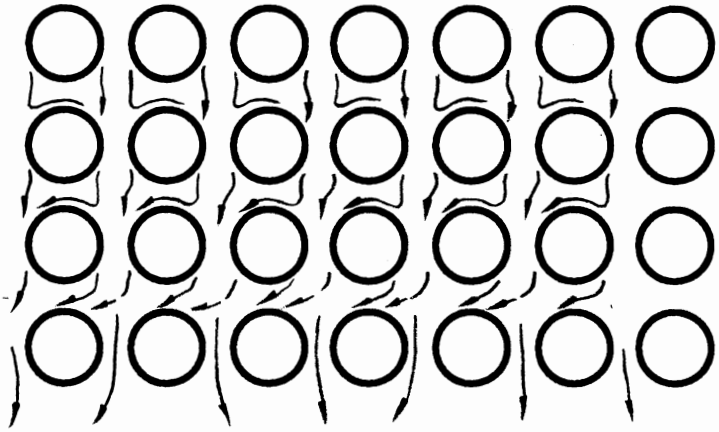

Figure 23. (Continued)

(e)

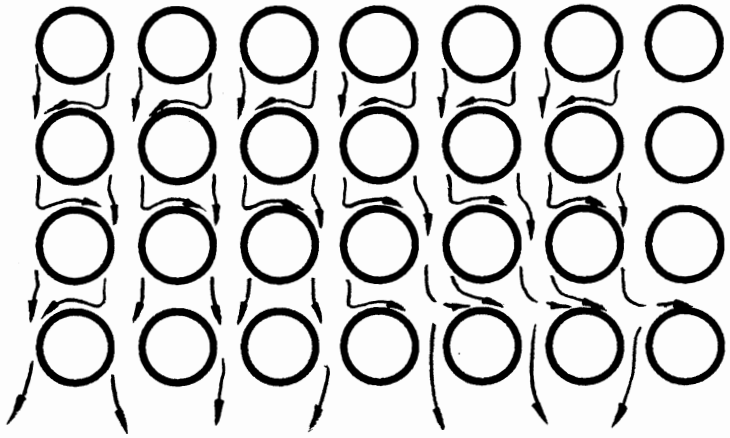

(f)

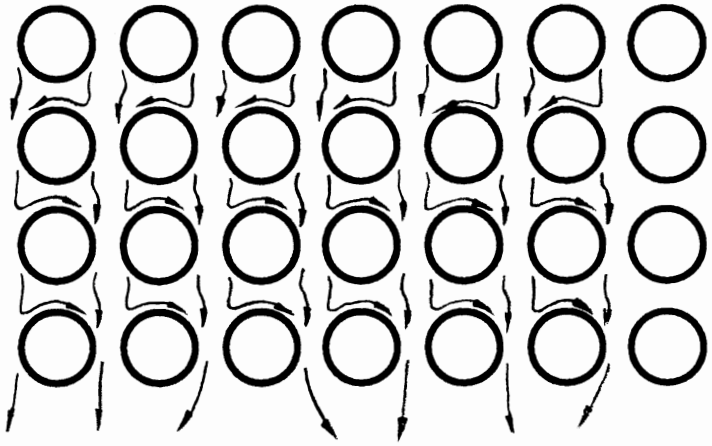

Figure 23. (Continued)

(g)

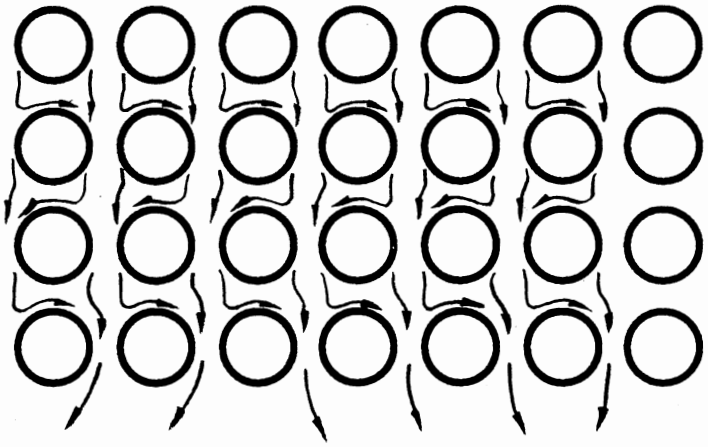

(h)

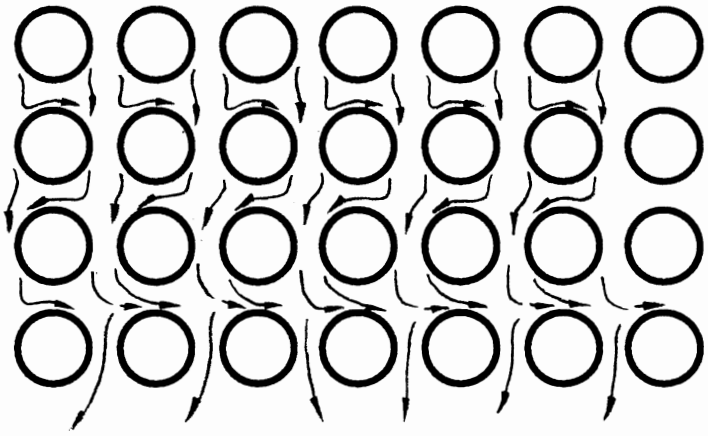

Figure 23. (Continued)

(a)

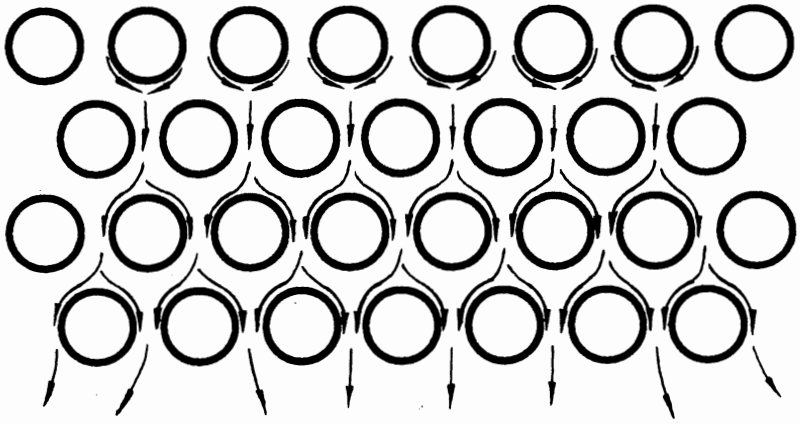

(b)

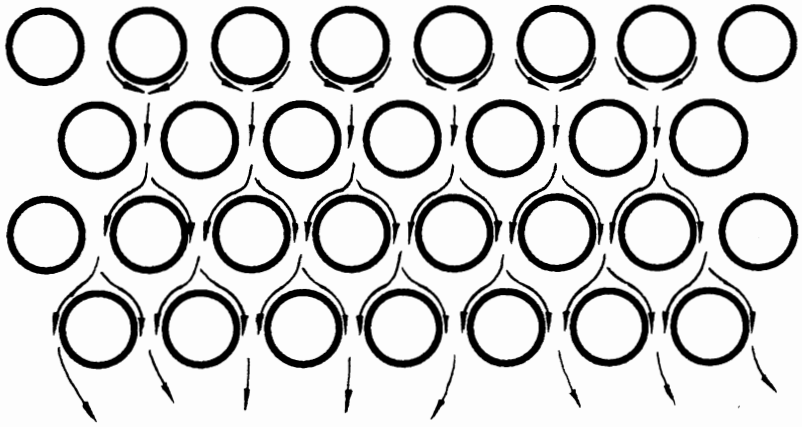

Figure 24. Flow Patterns of Tube Arrays with 30° Arrangement and P/D=1.25. (a)-(e) Re=2670, (f) Re=8350.

(c)

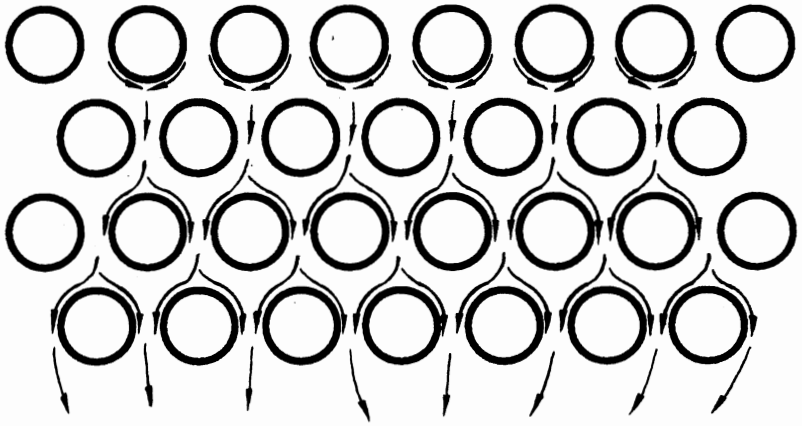

(d)

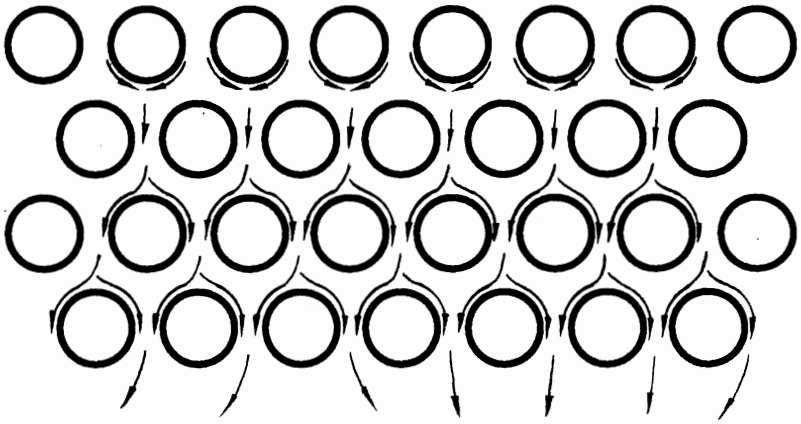

Figure 24. (Continued)

(e)

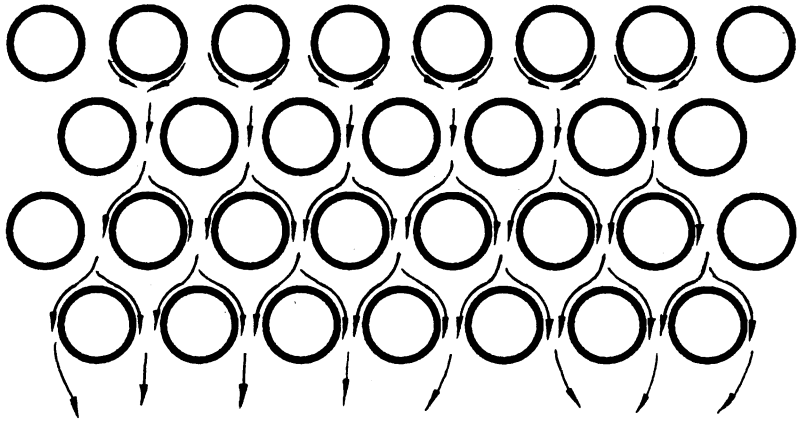

(f)

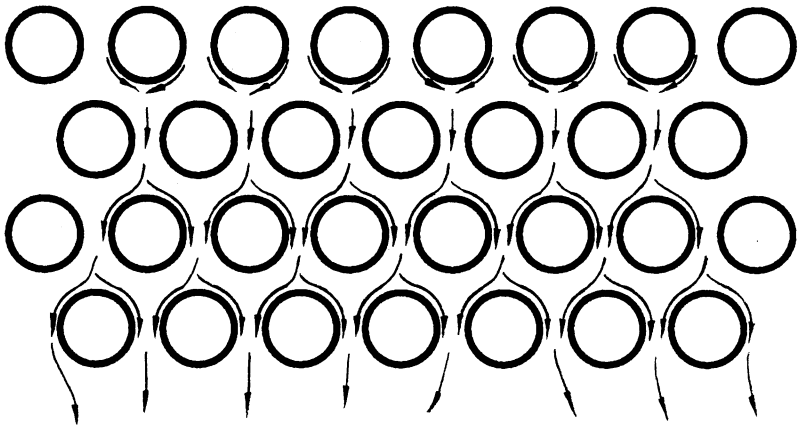

Figure 24. (Continued)

(a)

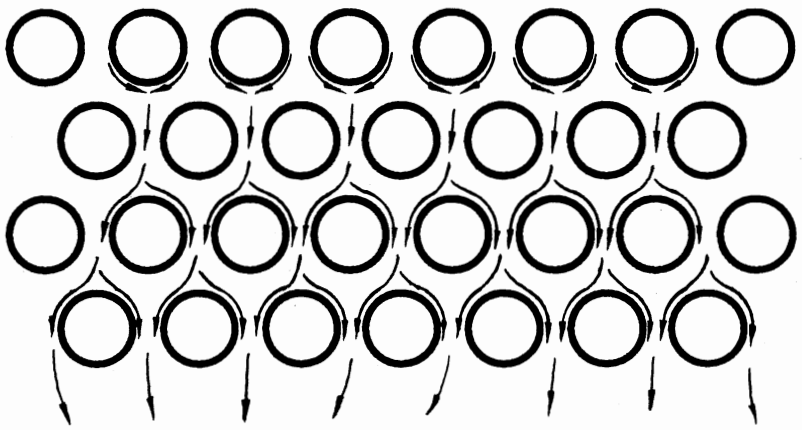

(b)

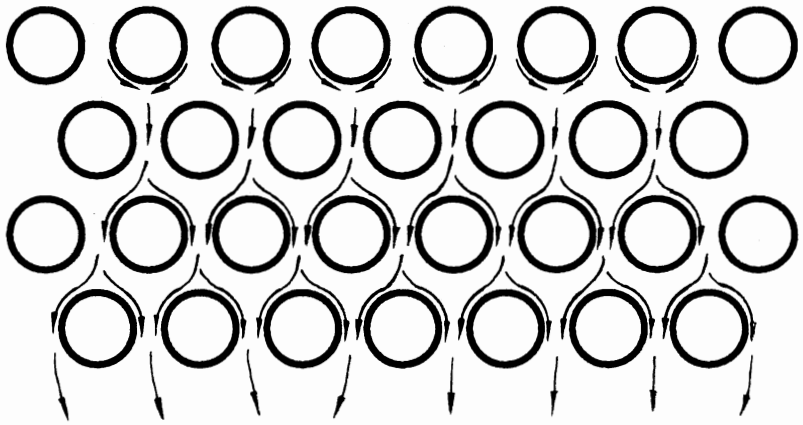

Figure 25. Flow Patterns of Tube Arrays with 30^{o} Arrangement and P/D=1.33. (a)-(b) Re=2400, (c) Re=4100.

(c)

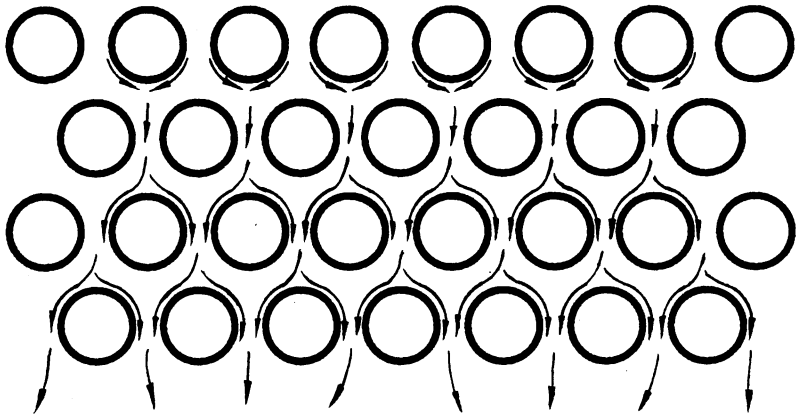

Figure 25. (Continued)

(a)

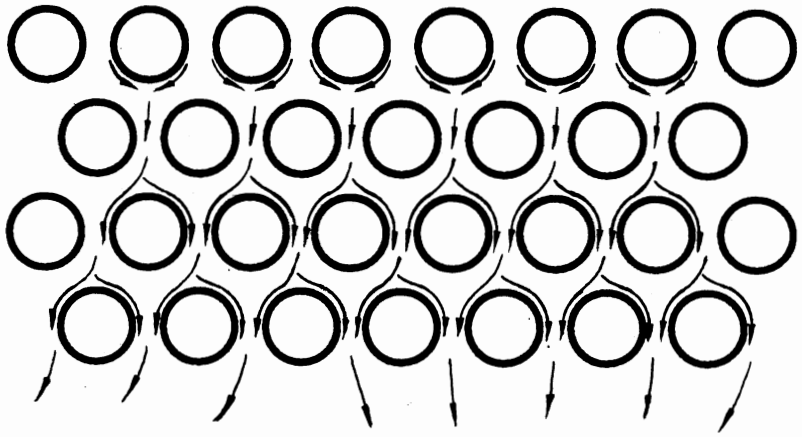

(b)

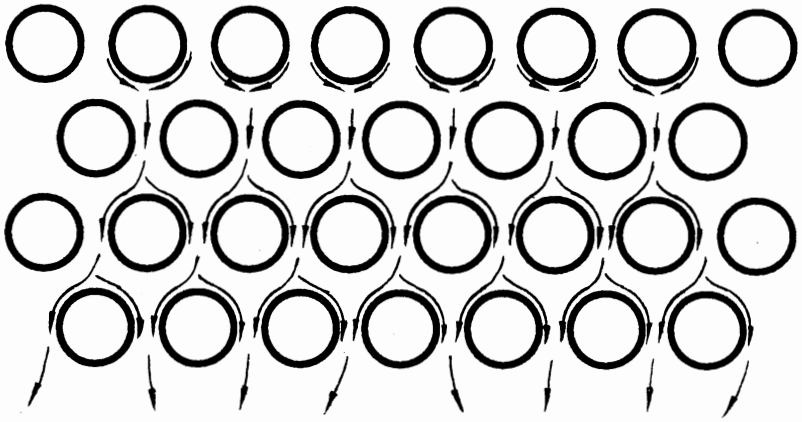

Figure 26. Flow Patterns of Tube Arrays with 30^{o} Arrangement and P/D=1.4. (a)-(b) Re=2240, (c) Re=4450.

(c)

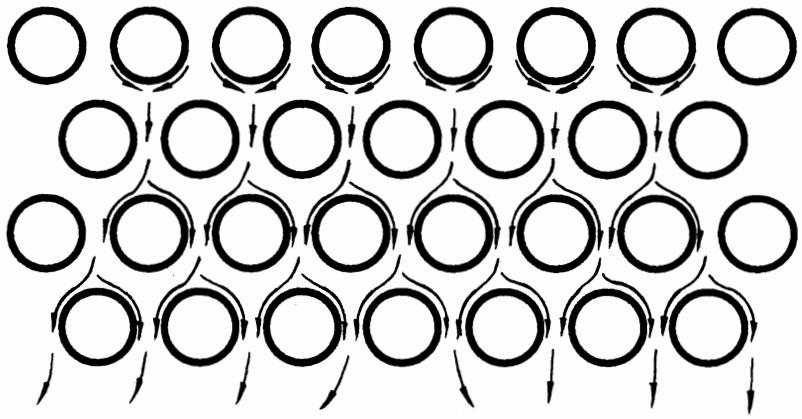

Figure 26. (Continued)

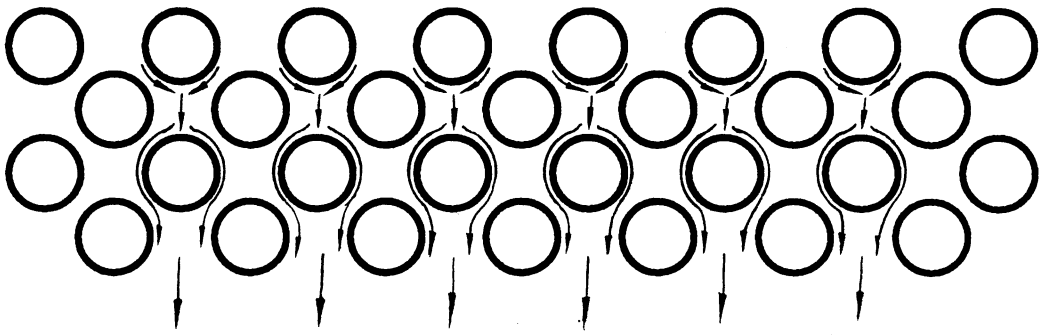

Figure 27. Flow Pattern of Tube Arrays with 45° Arrangement

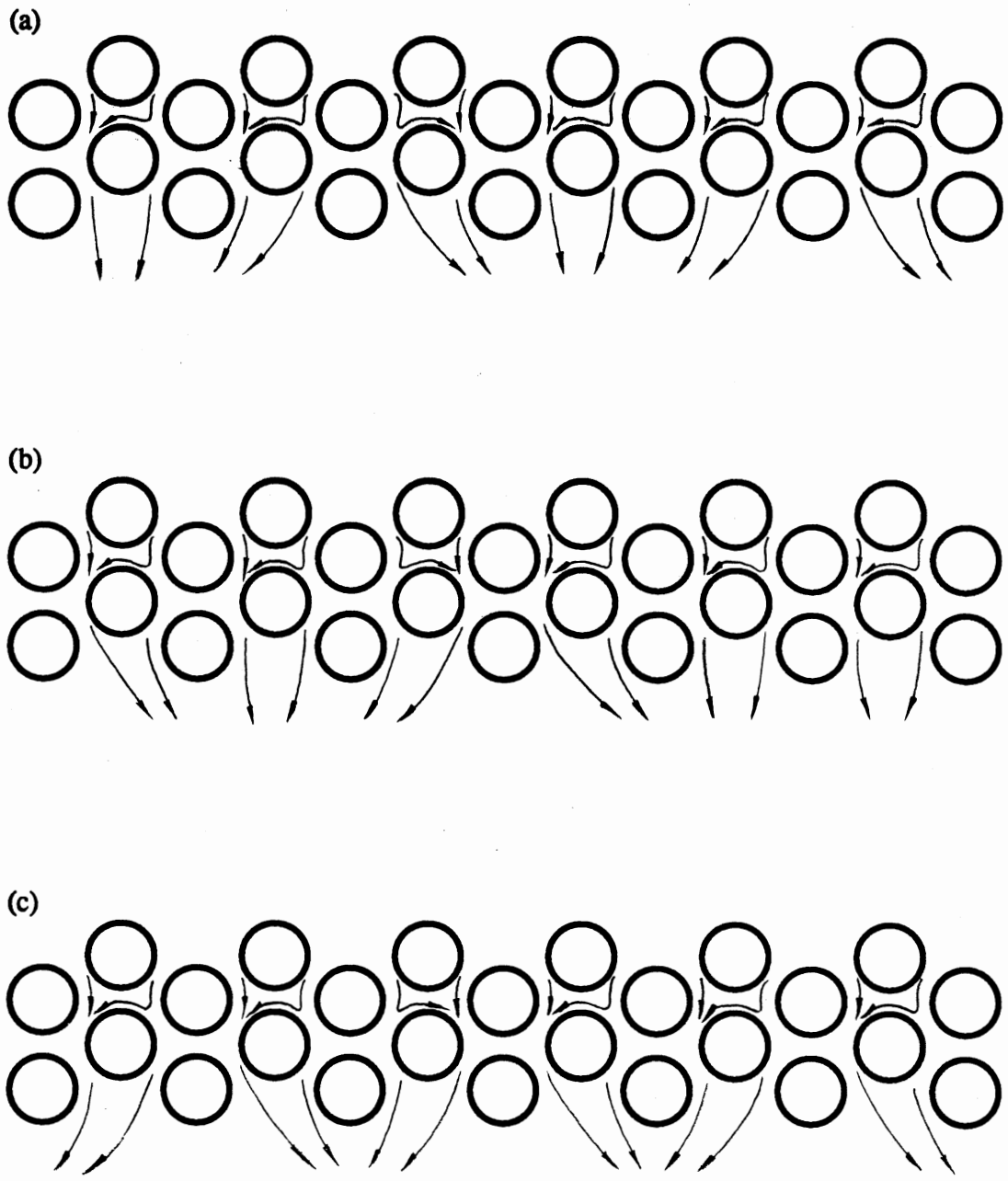

Figure 28. Flow Patterns of Tube Arrays with 60^{o} Arrangement and P/D=1.25. (a)-(i) Re=3000, (j)-(n) Re=6070, (o)-(t) Re=8340.

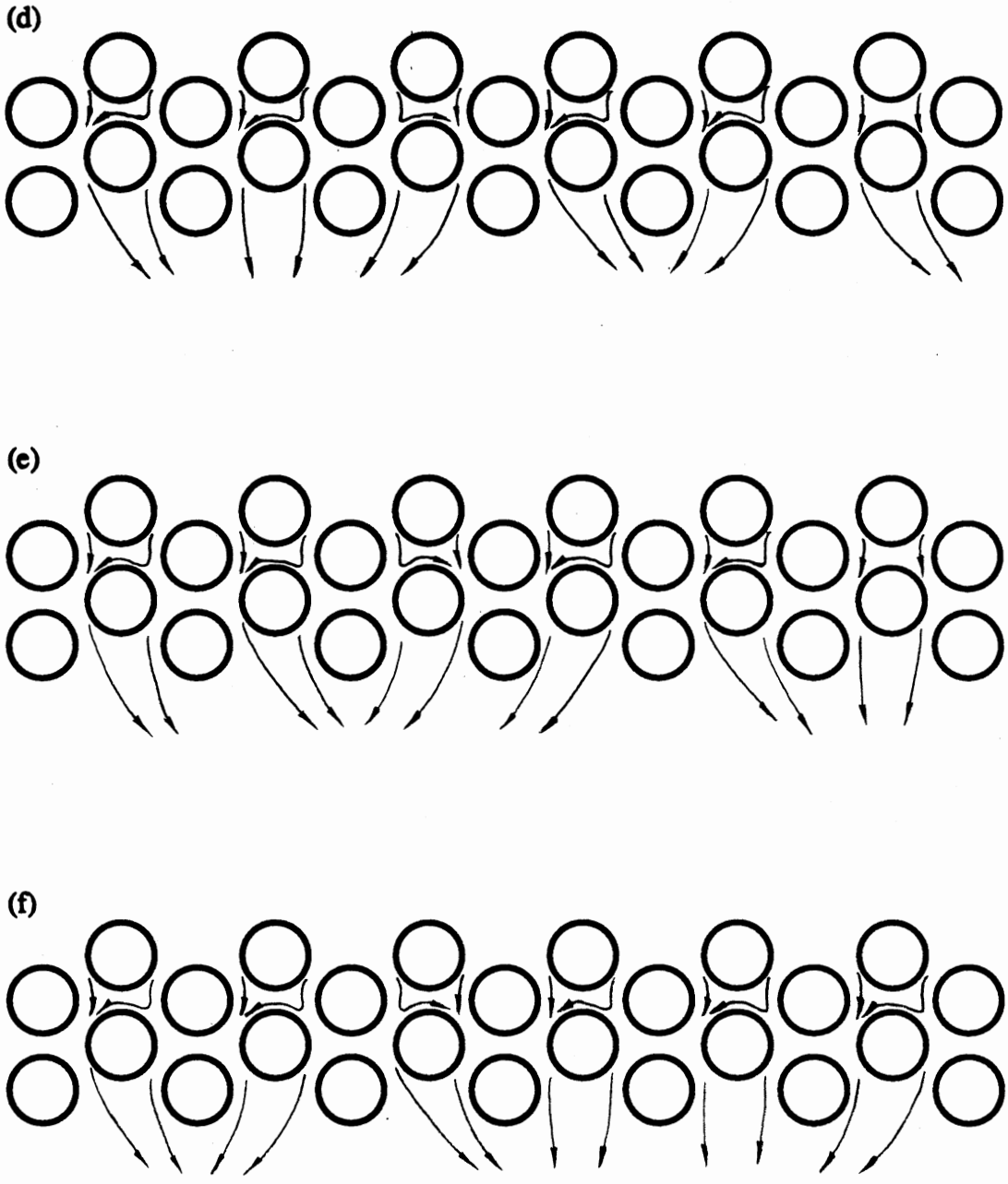

Figure 28. (Continued)

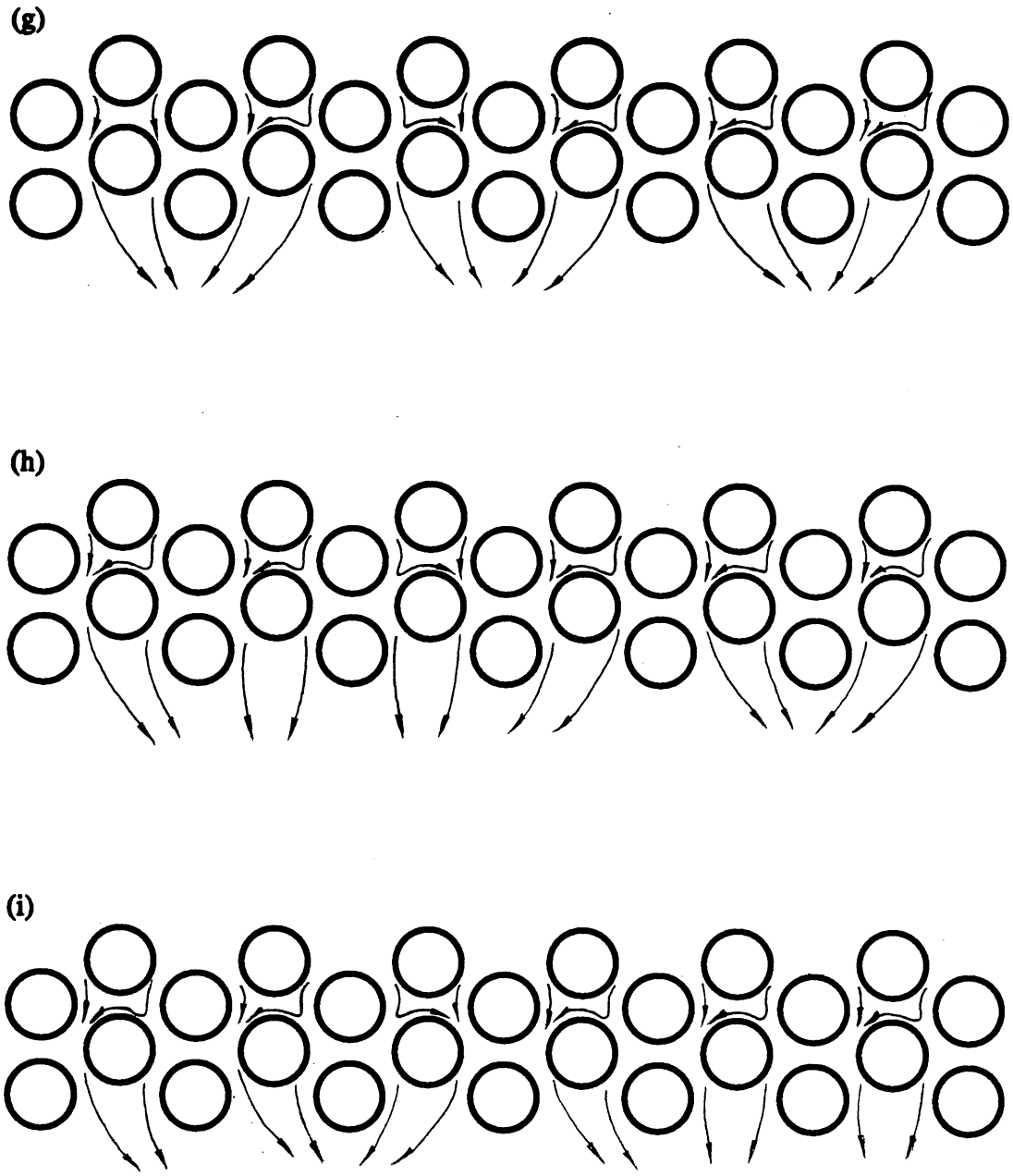

Figure 28. (Continued)

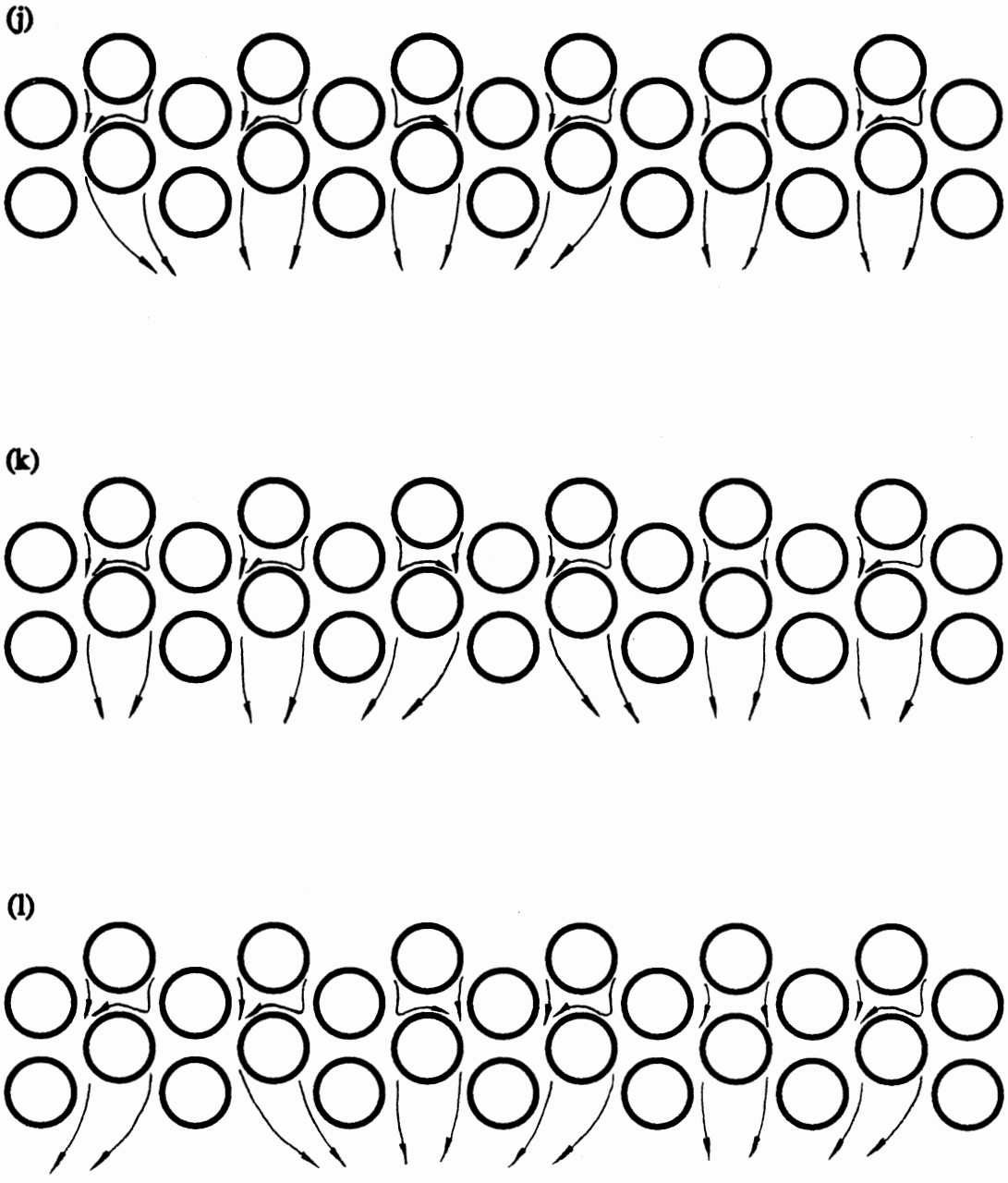

Figure 28. (Continued)

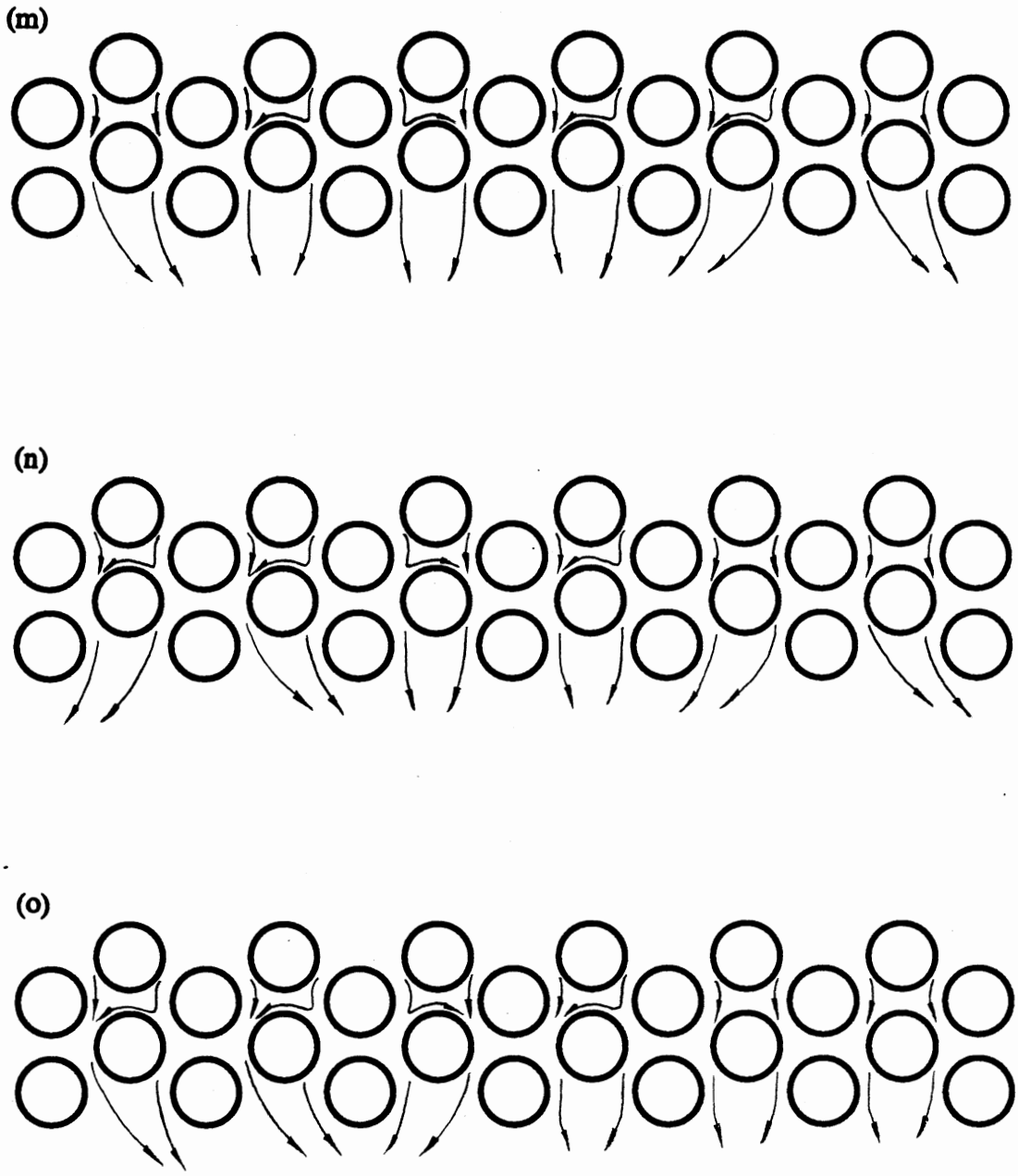

Figure 28. (Continued)

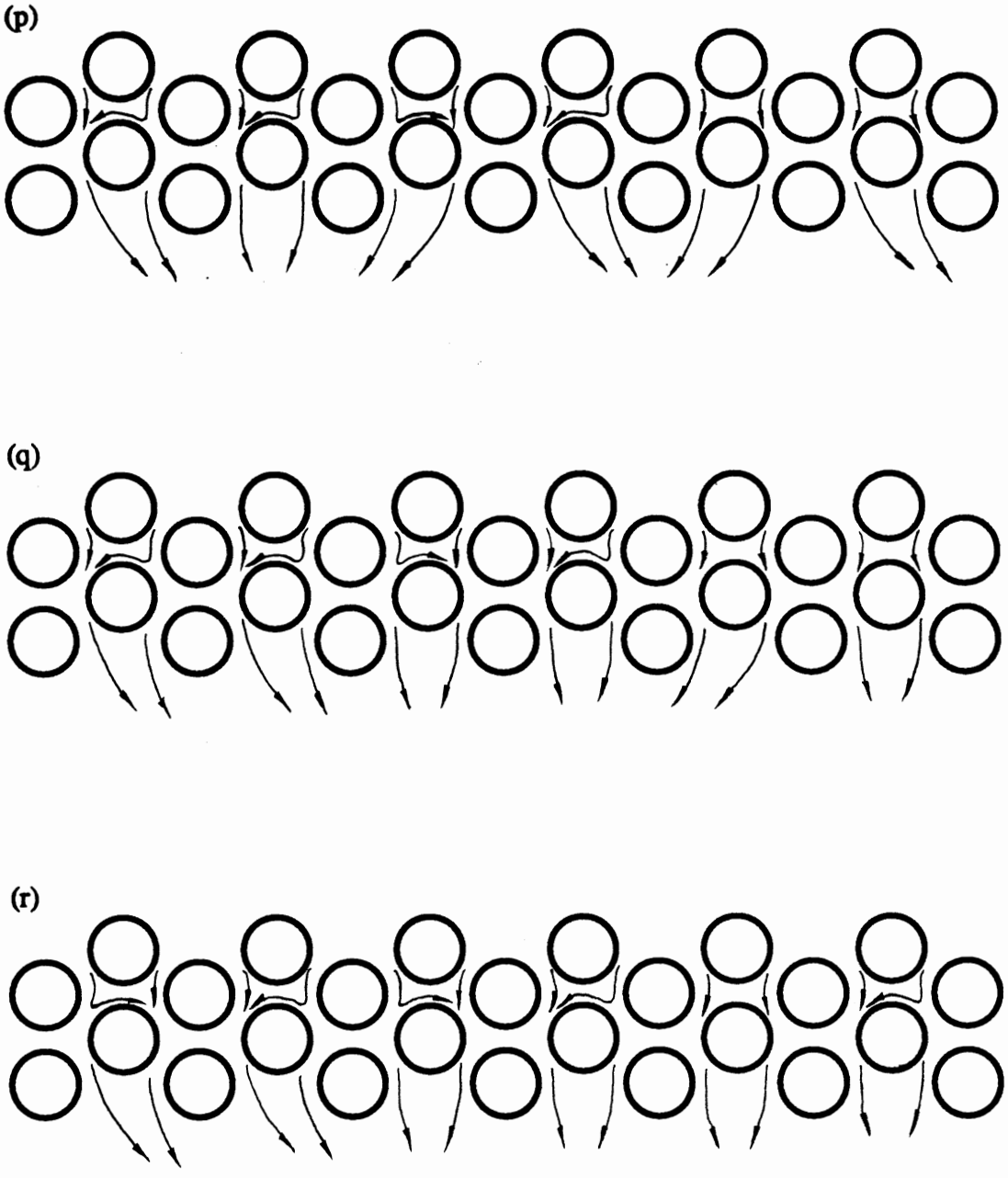

Figure 28. (Continued)

(s)

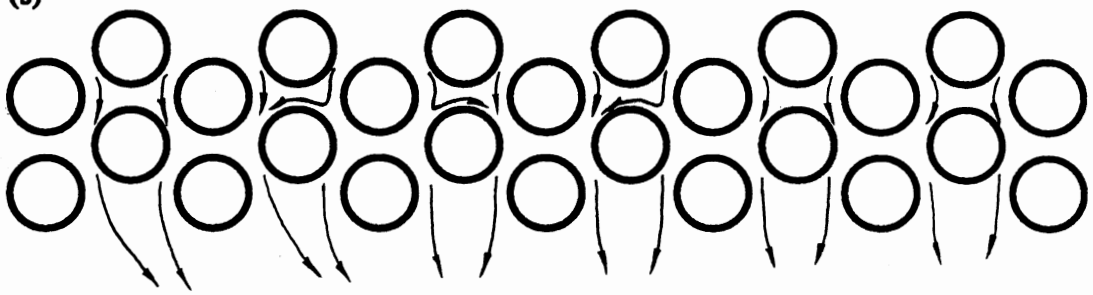

(t)

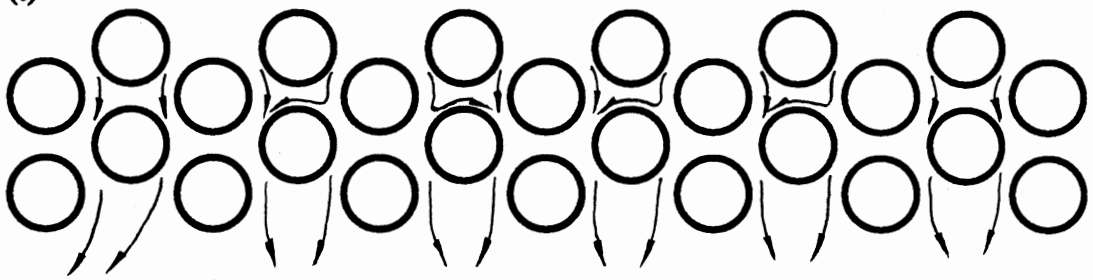

Figure 28. (Continued)

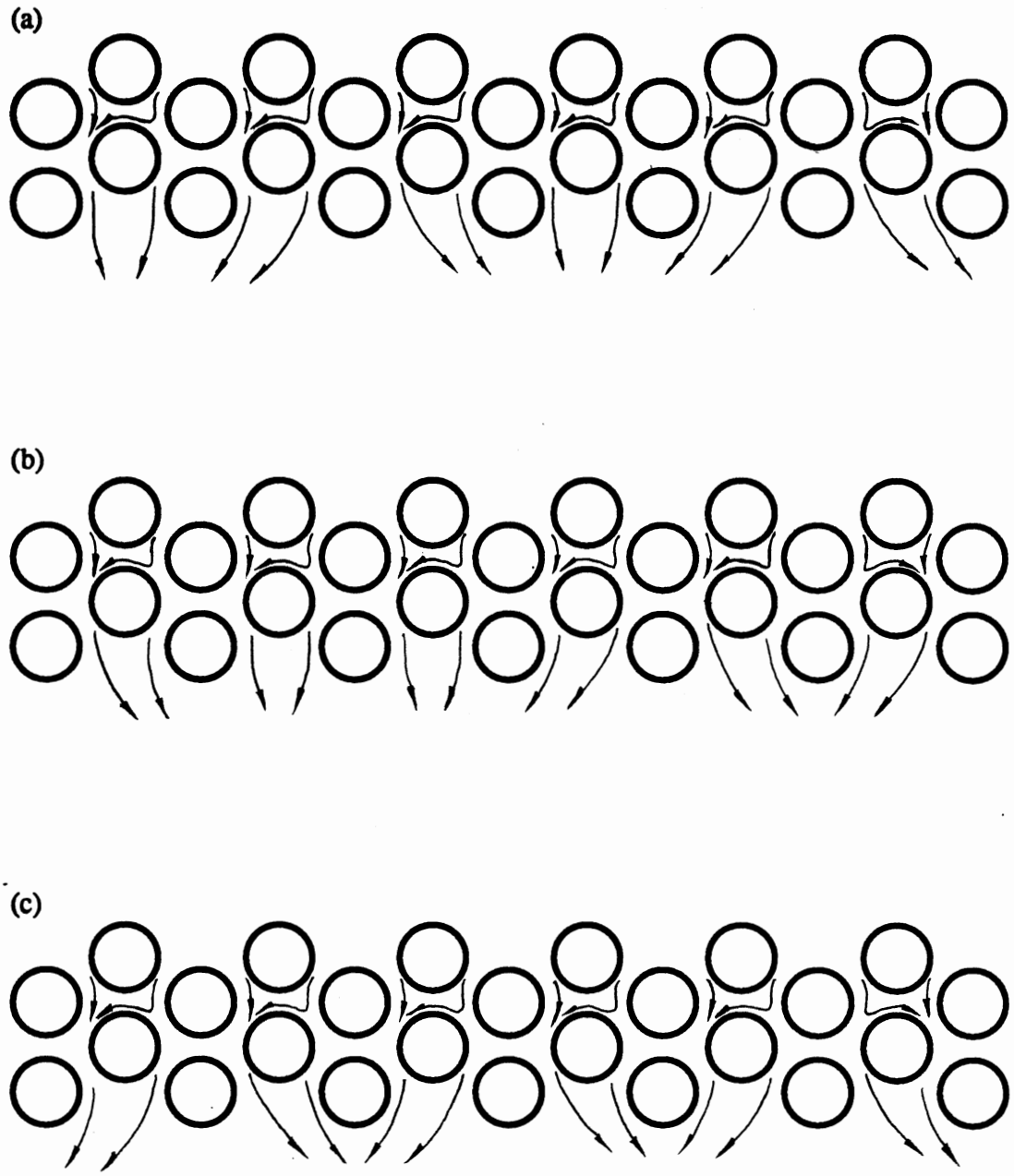

Figure 29. Flow Patterns of Tube Arrays with 60^{o} Arrangement and P/D=1.33. (a)-(g) Re=2500, (h)-(j) Re=4680, (k)-(m) Re=6930, (n)-(o) Re=7760.

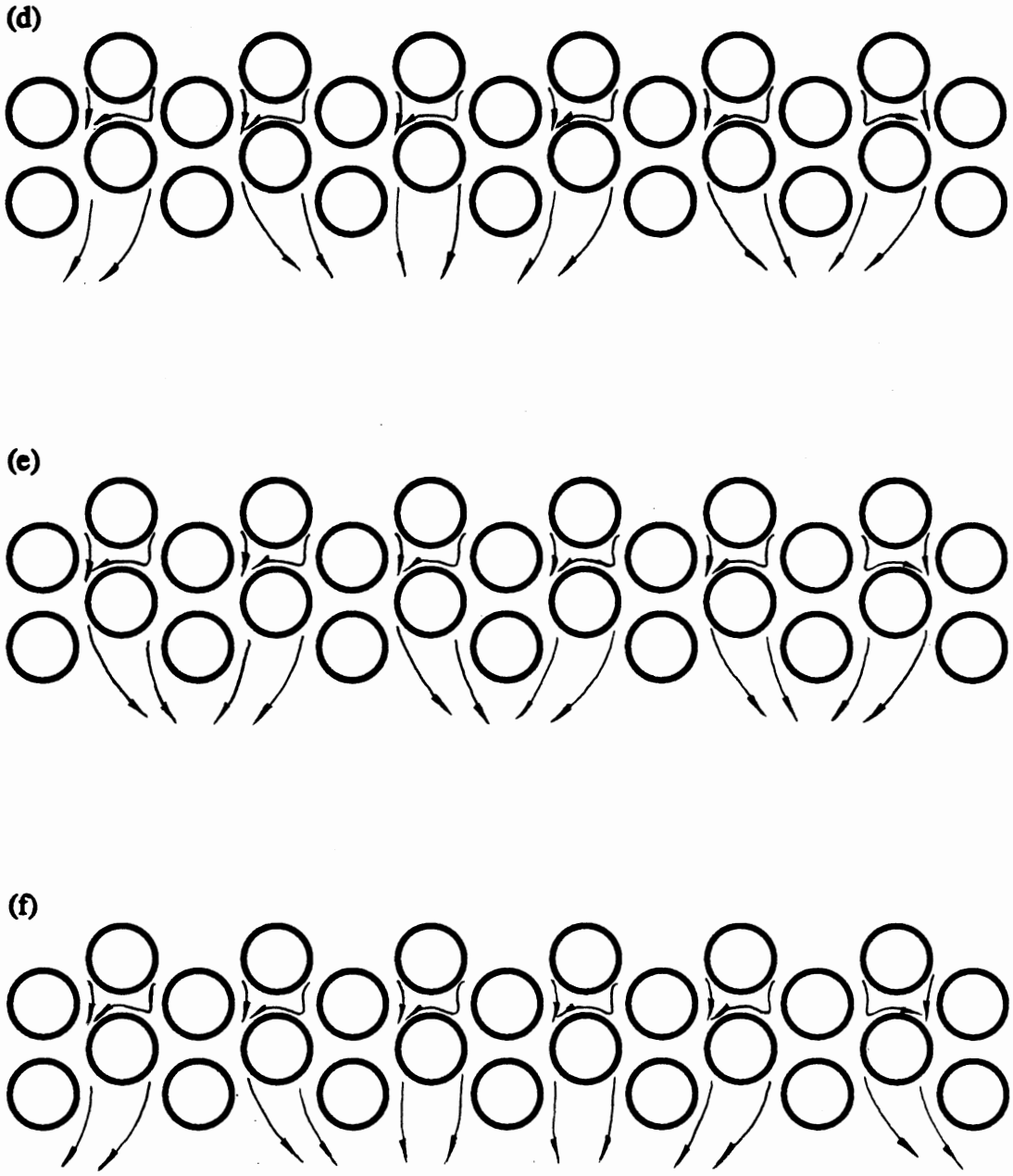

Figure 29. (Continued)

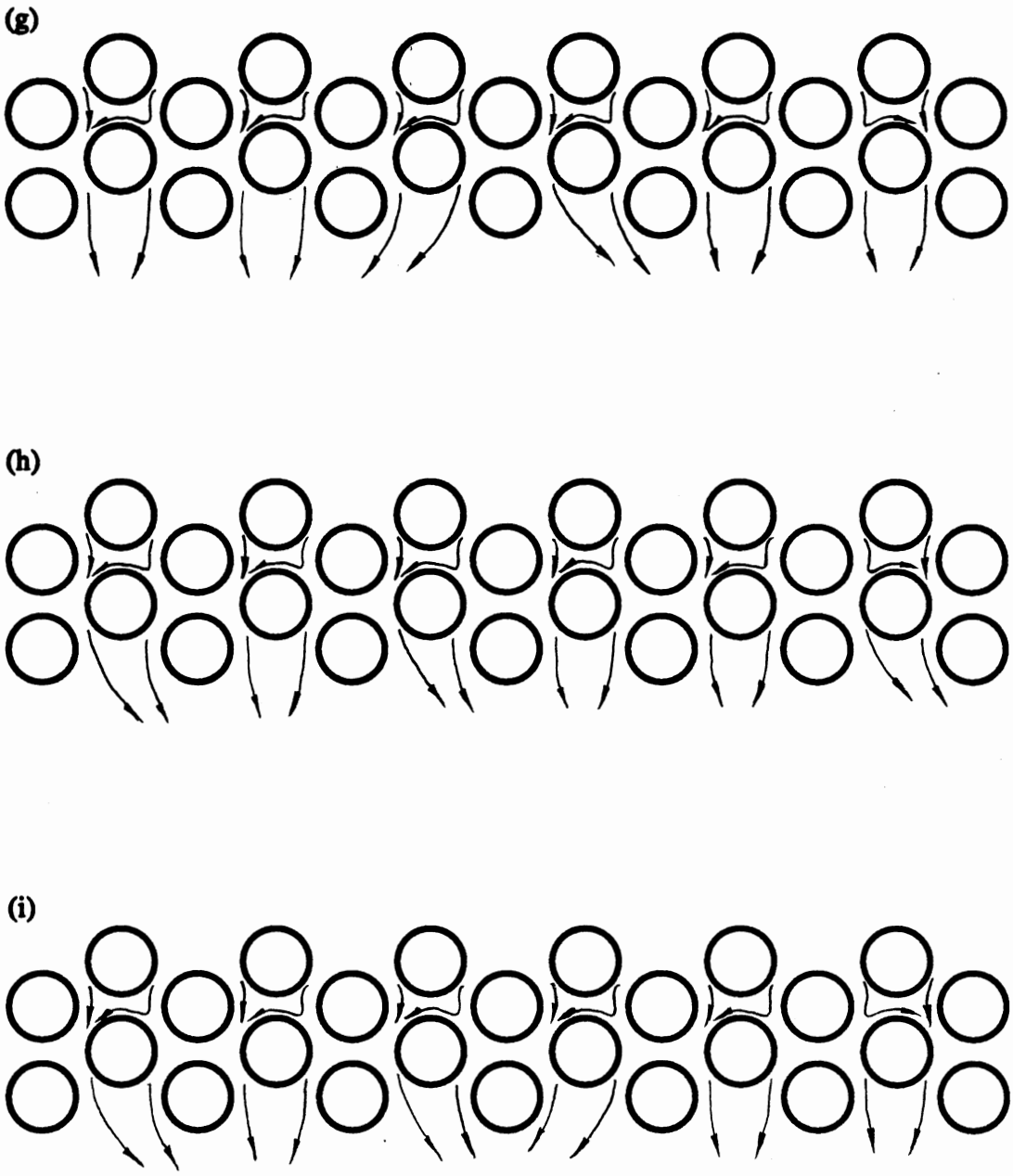

Figure 29. (Continued)

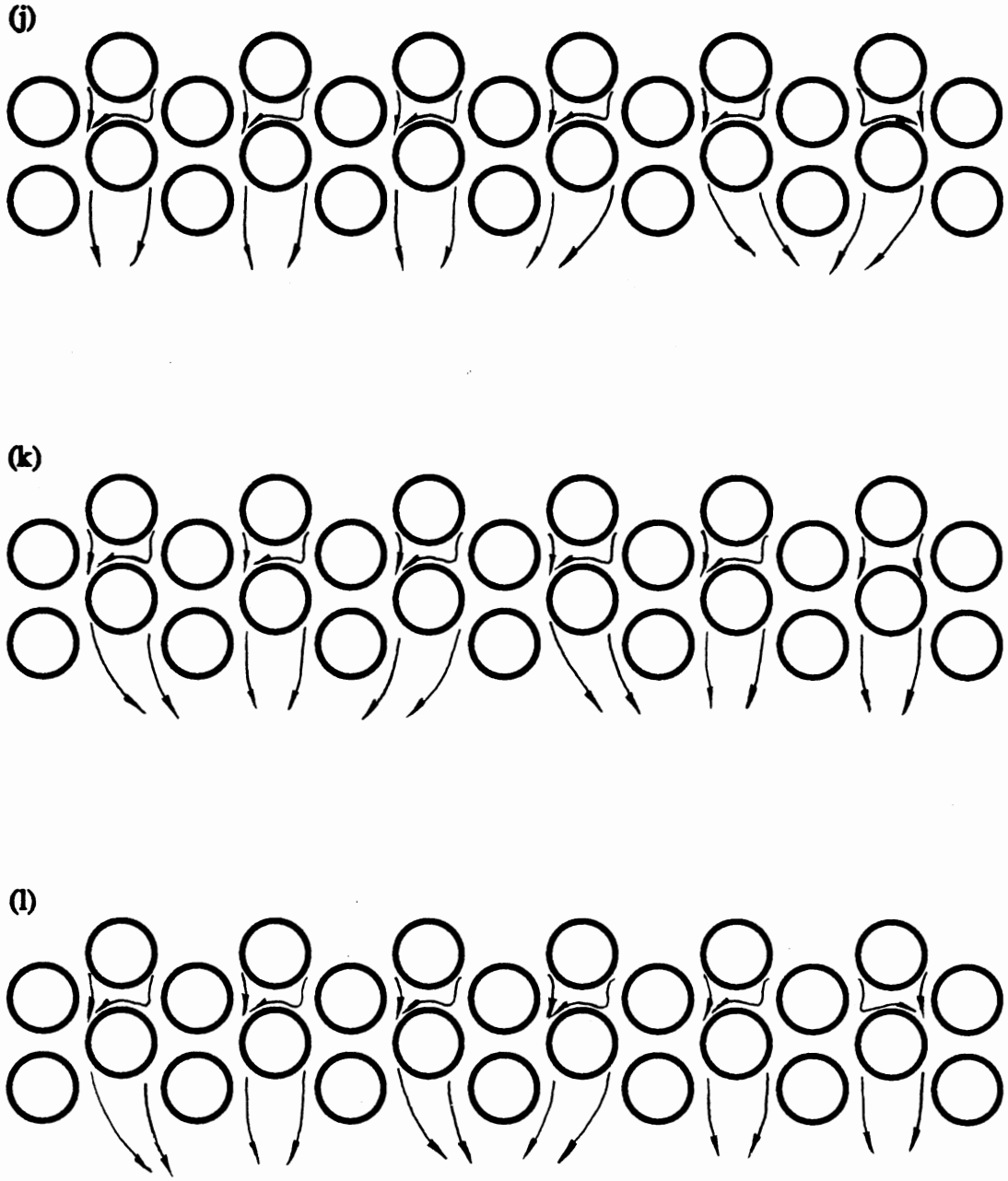

Figure 29. (Continued)

(m)

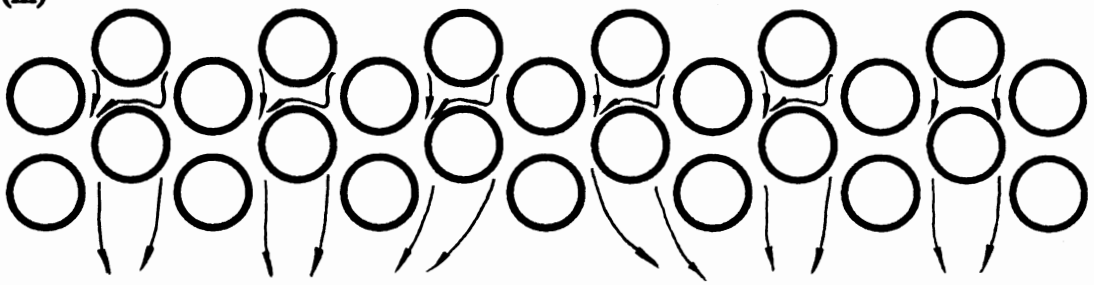

(n)

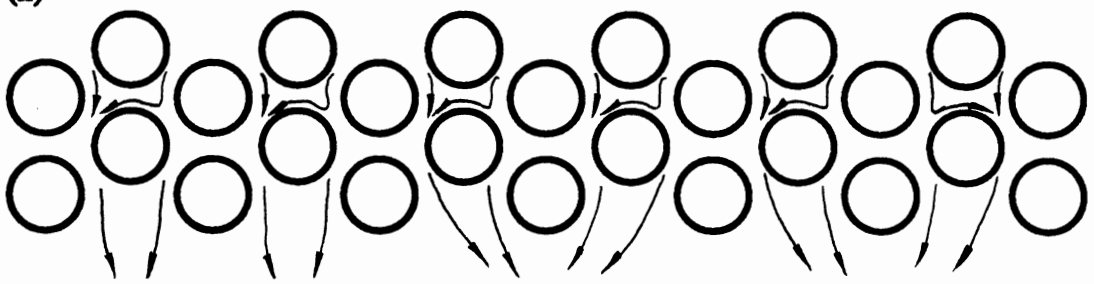

(o)

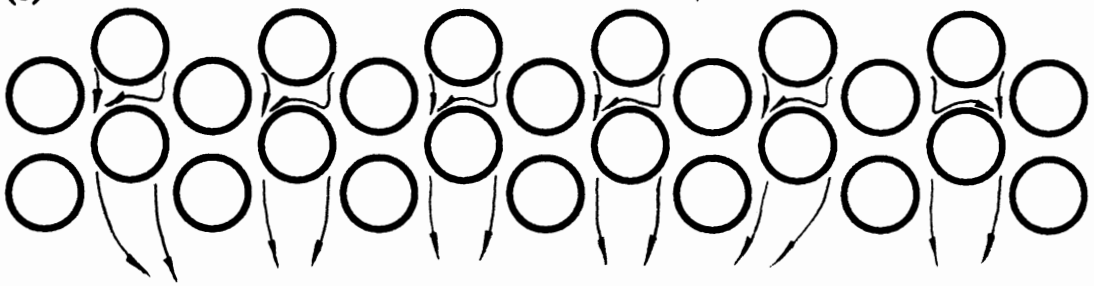

Figure 29. (Continued)

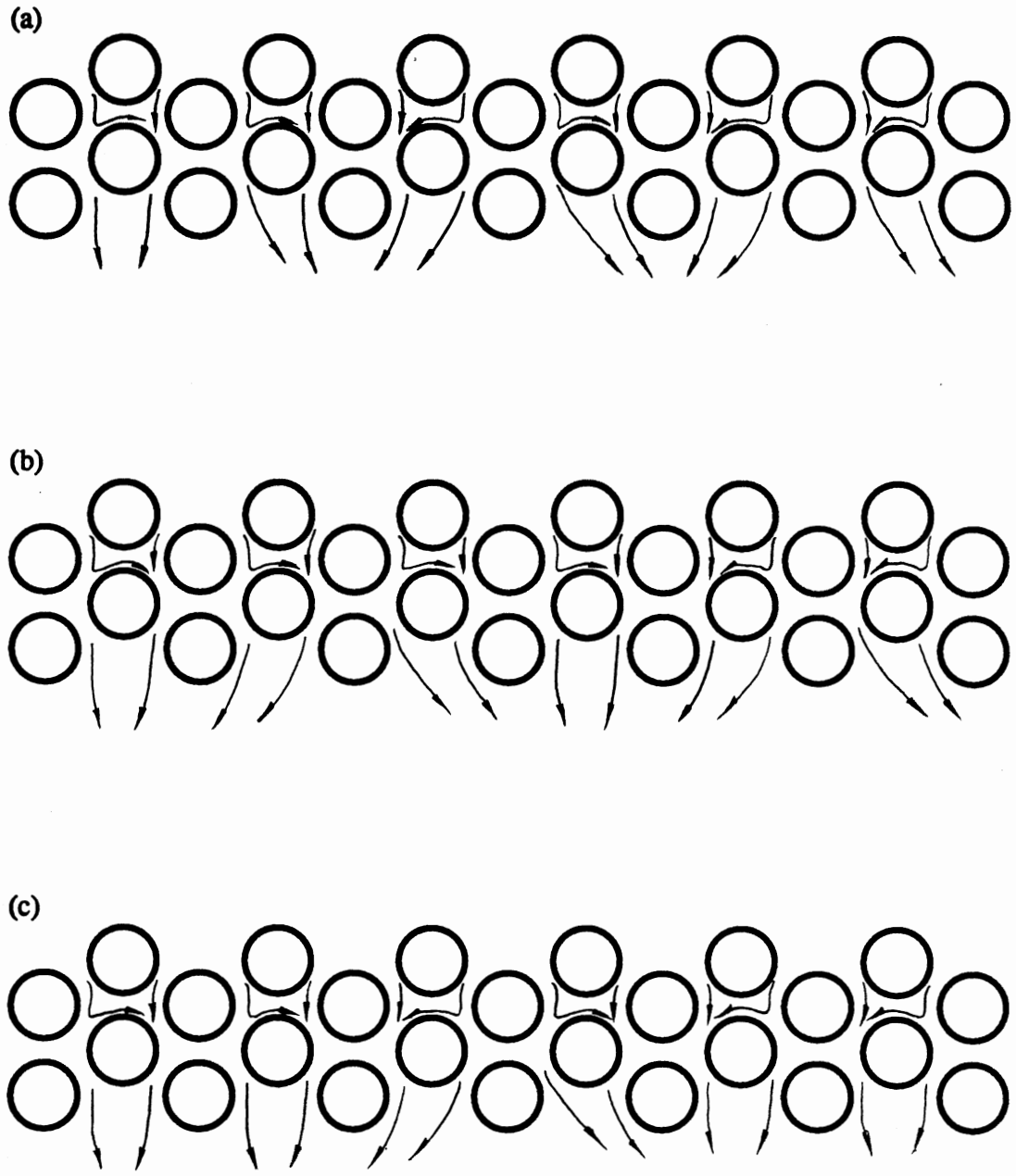

Figure 30. Flow Patterns of Tube Arrays with 60^{o} Arrangement and P/D=1.4. (a)-(d) Re=2160, (e)-(f) Re=4830, (g)-(i) Re=6760, (j)-(k) Re=7840.

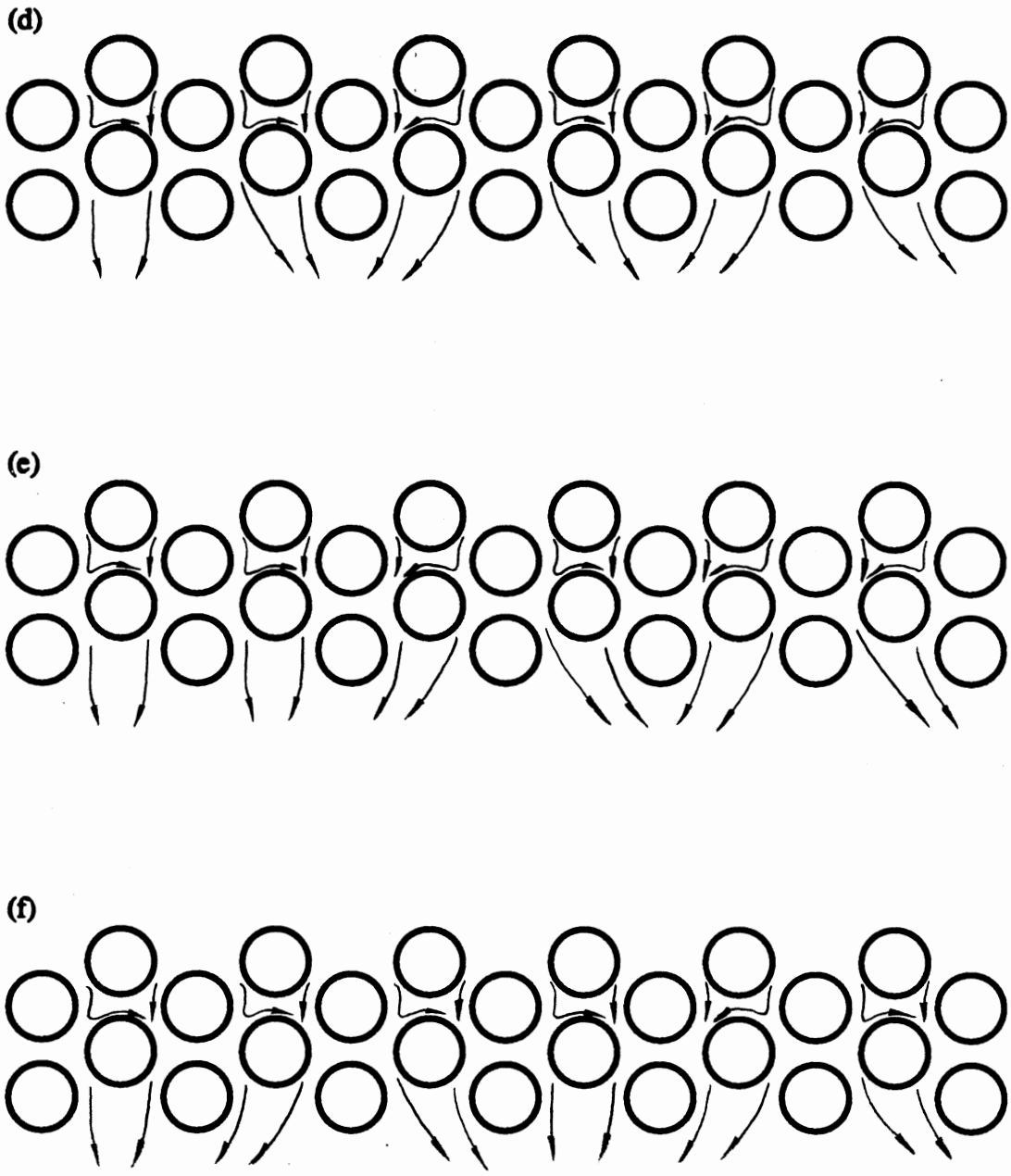

Figure 30. (Continued)

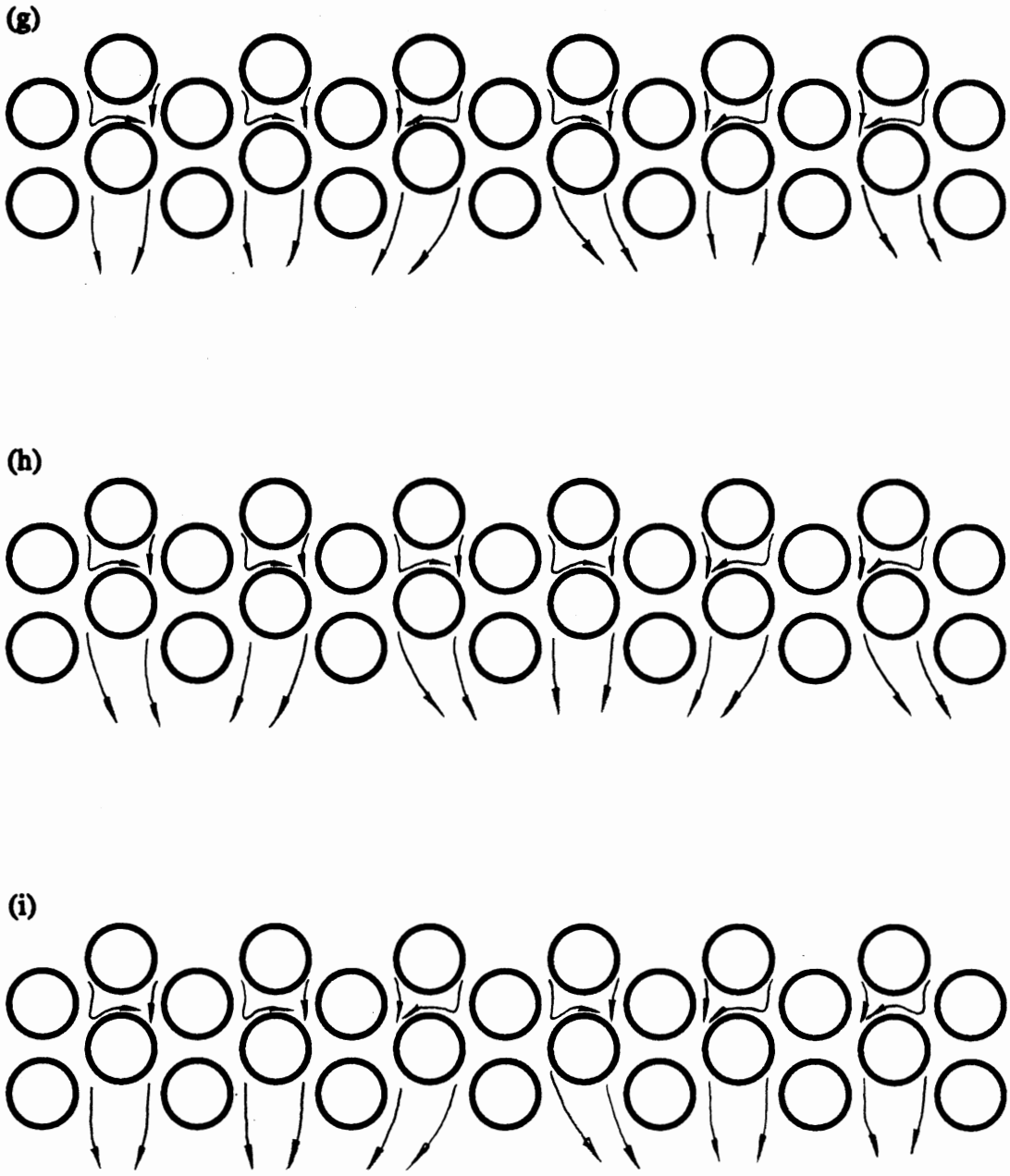

Figure 30. (Continued)

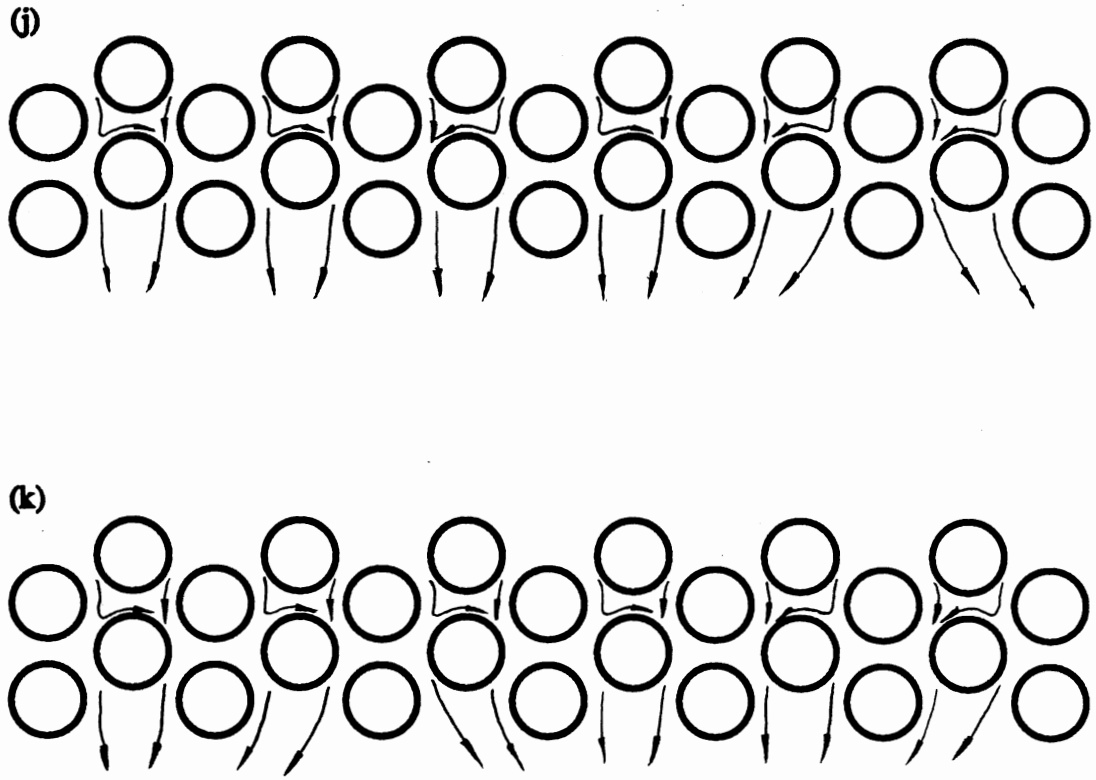

Figure 30. (Continued)

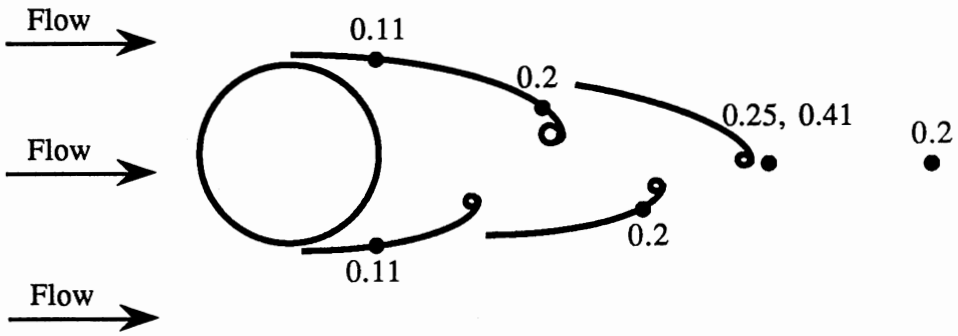

Figure 31. Strouhal Numbers of a Stationary Cylinder

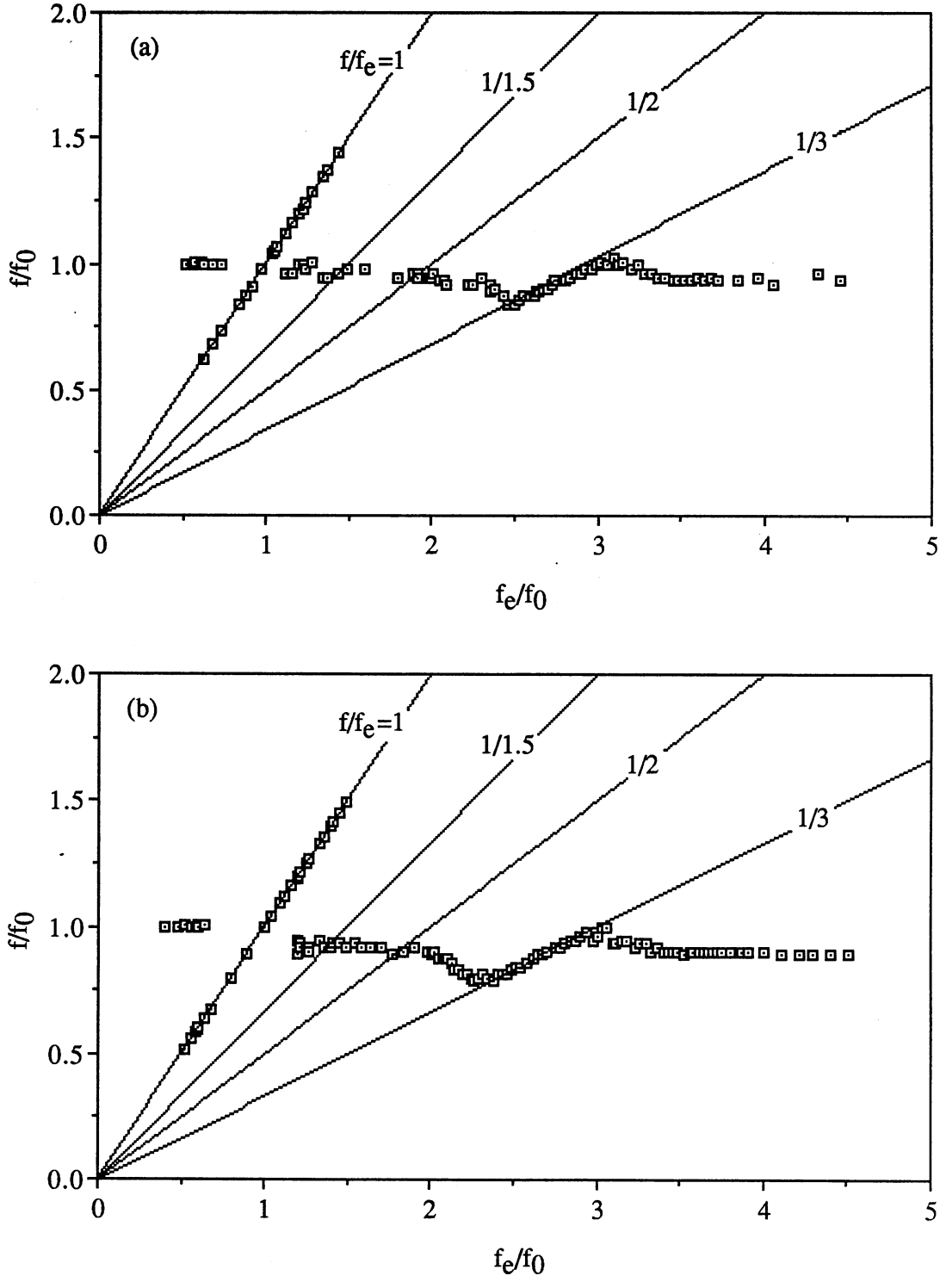

Figure 32. Variation of Shedding Frequency with Driving Frequency of a Single Cylinder in Uniform Flow for Re=1500, with (a) A/D=0.05, (b) A/D=0.145, (c) A/D=0.235

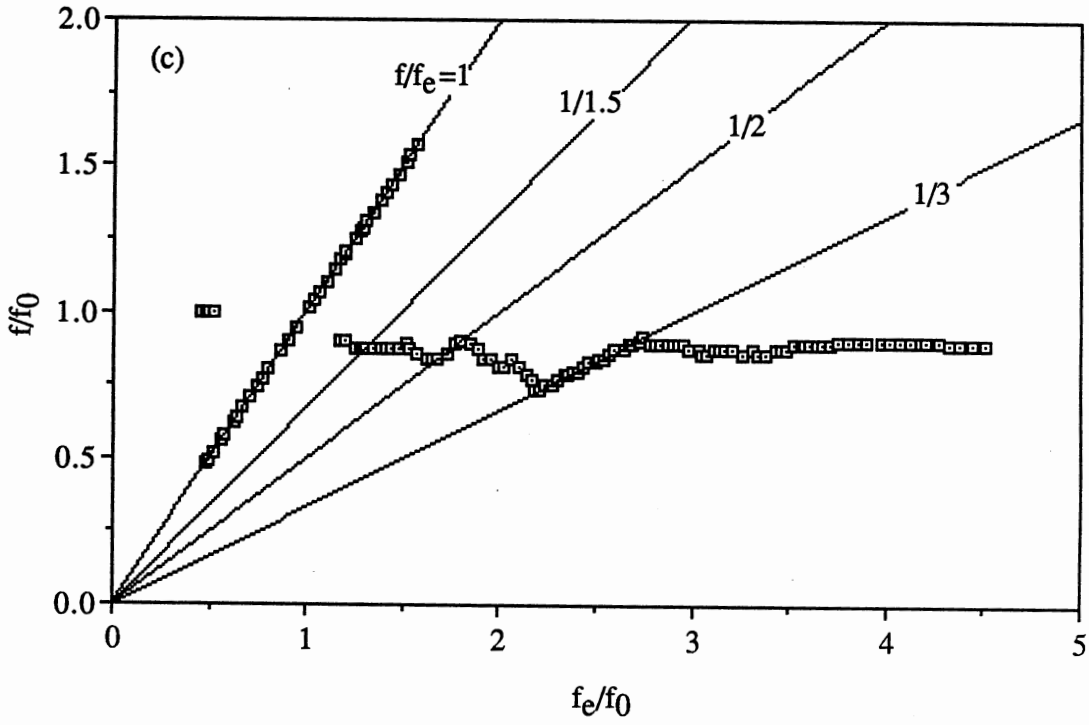

Figure 32. (Continued)

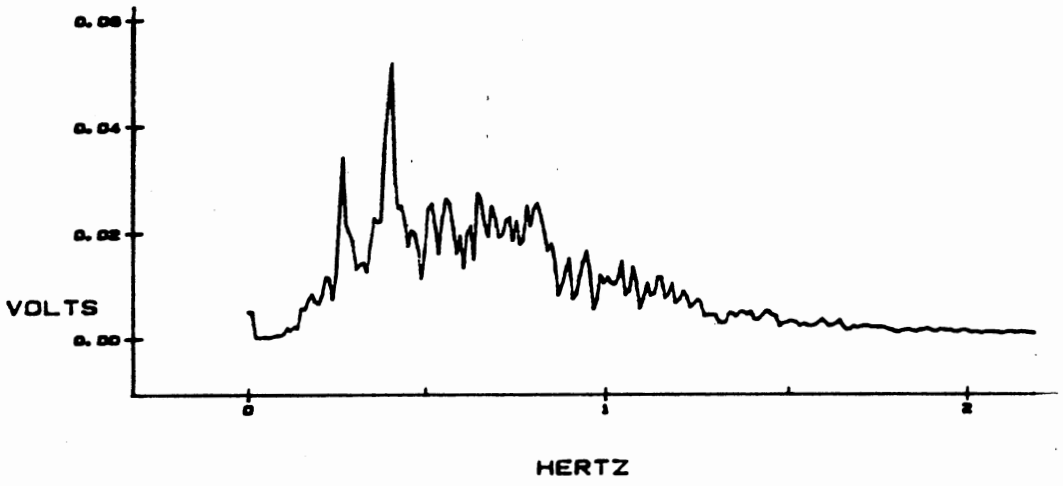

Figure 33. Frequency Specturm of a Single Cylinder with Forced Transverse Vibration in Double-Value Region

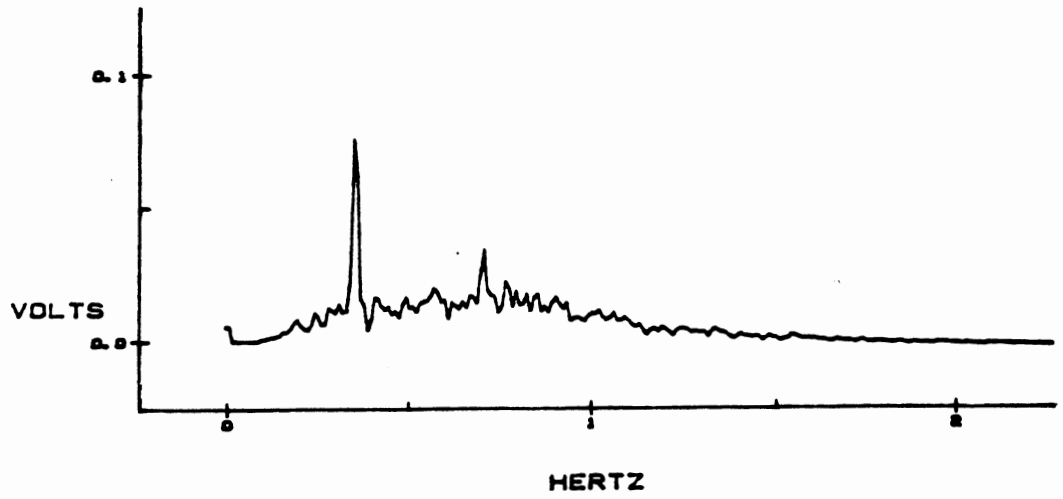

Figure 34. Frequency Spectrum of a Single Cylinder with Forced Transverse Vibration in Lock-In Region

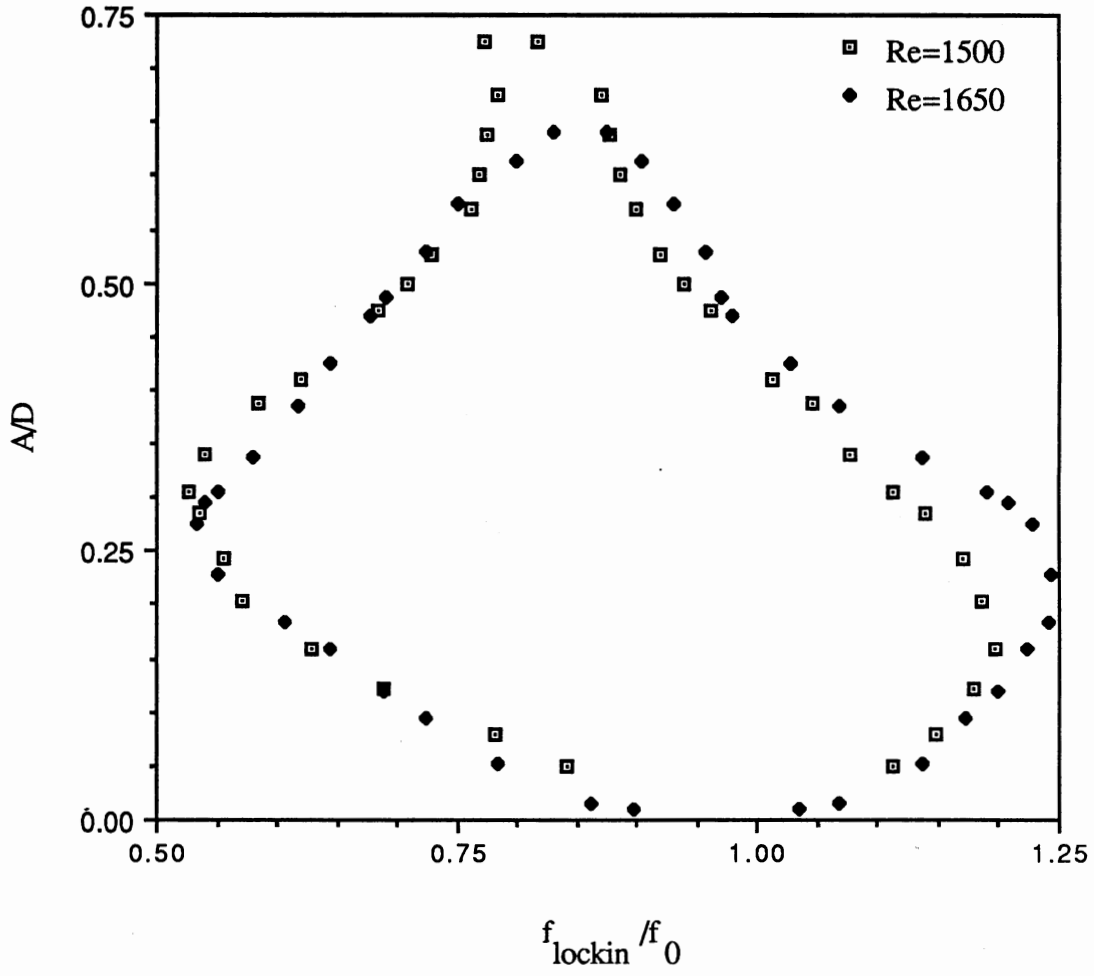

Figure 35. Primary Lock-in Bands of a Single Cylinder with Forced Transverse Vibration in Uniform Flow for Various A/D

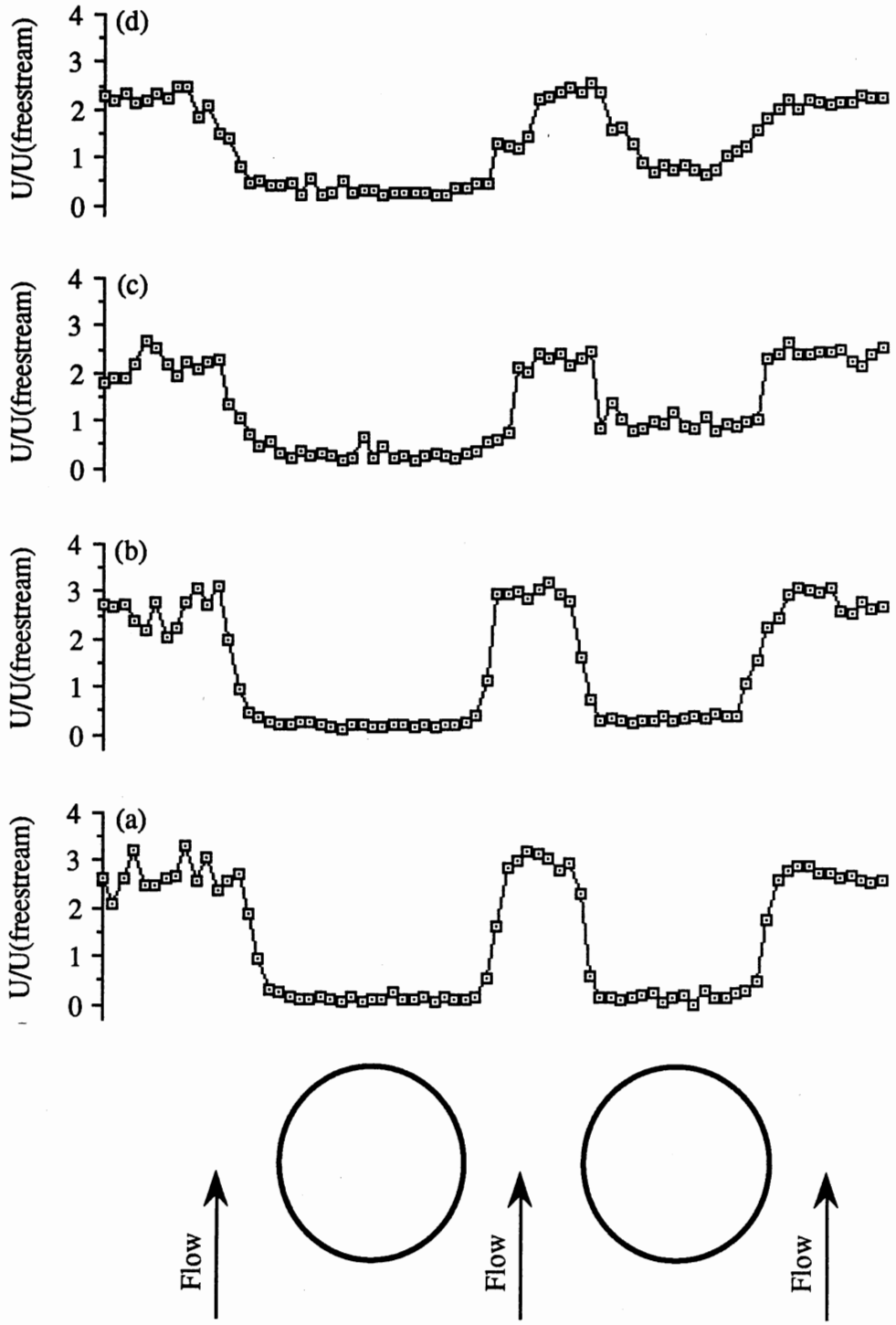

Figure 36. Time Mean Velocity Profiles of a Cylinder Pair with P/D=1.4 at Various Downstream Positions. (a) 0.5D, (b) 0.75D, (c) 1.0D, (d) 1.25D, (e) 1.5D, (f) 2.0D, (g) 2.5D, (h) 1.25D (2nd Test)

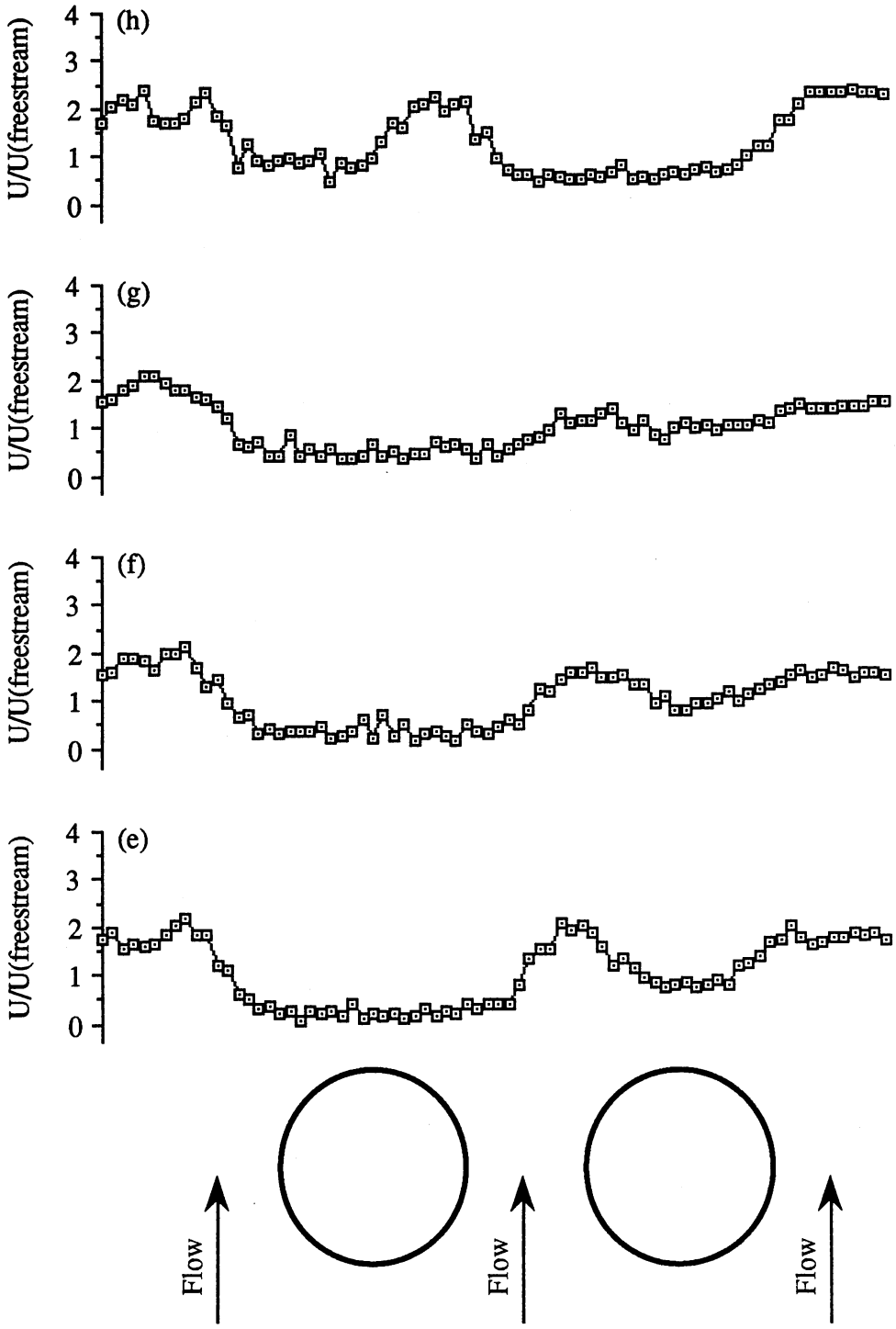

Figure 36. (Continued)

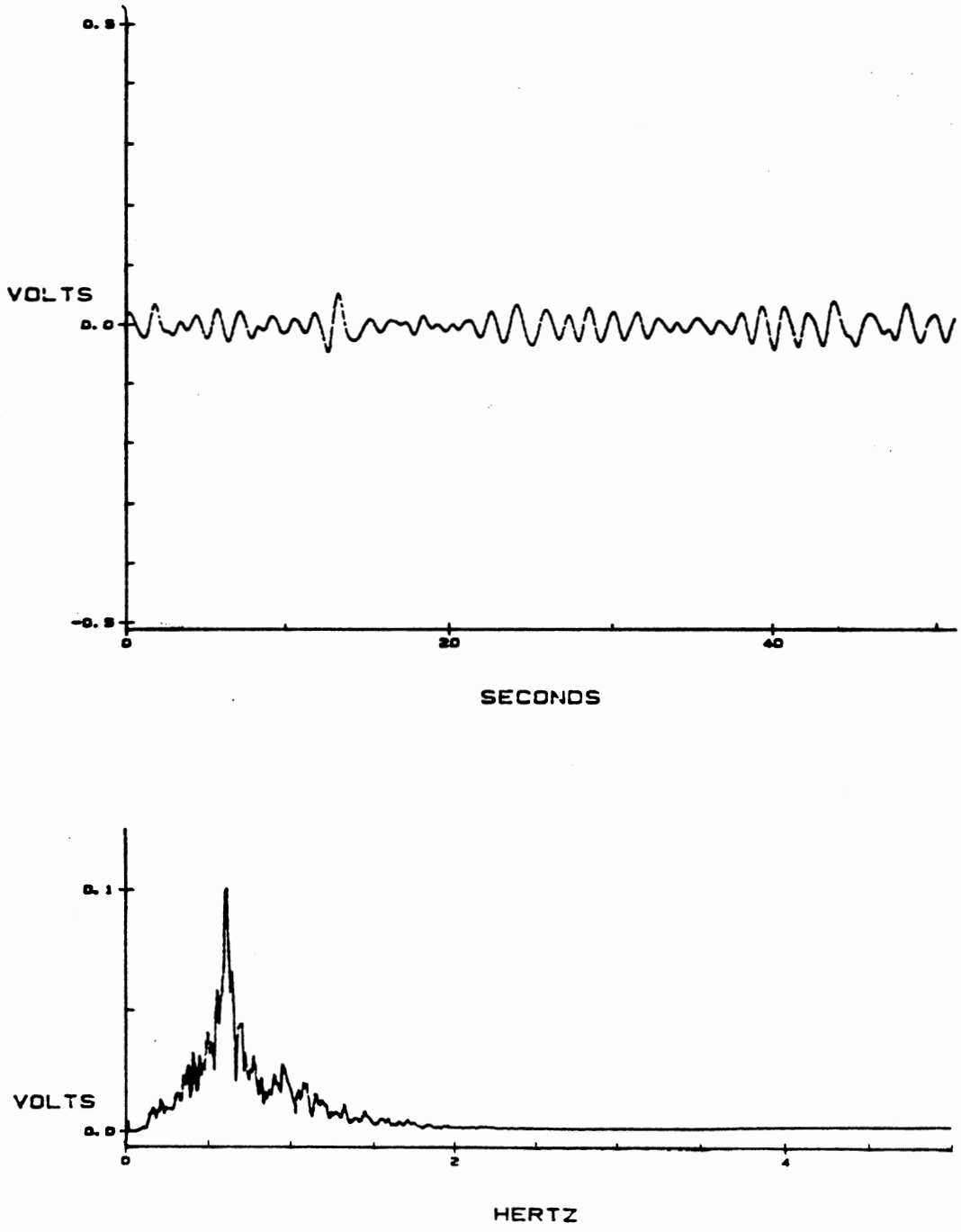

Figure 37. Oscillogram and Spectrum for the Narrow Wake of the Normal Cylinder Pair

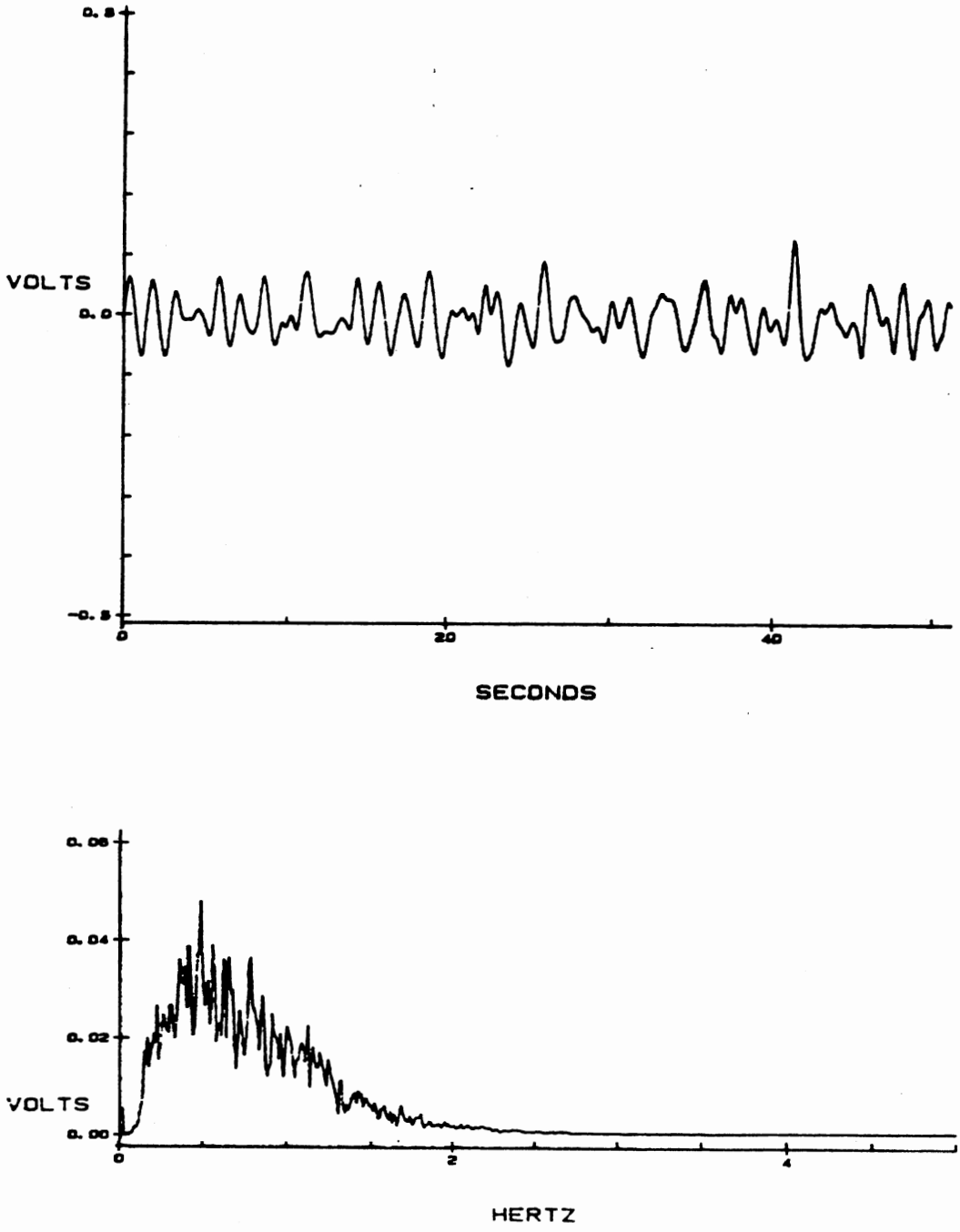

Figure 38. Oscillogram and Spectrum for the Wide Wake of the Normal Cylinder Pair

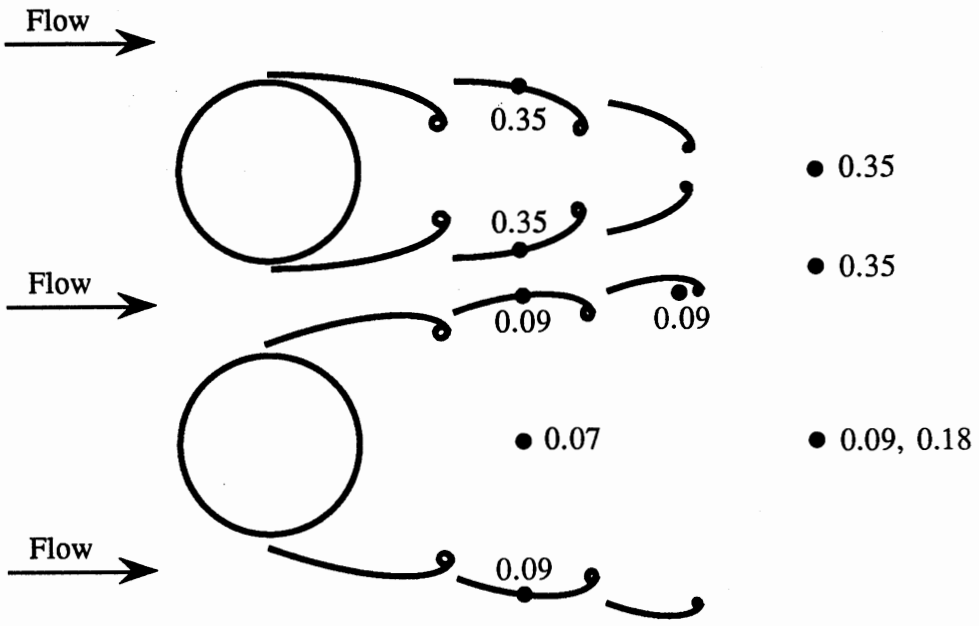

Figure 39. Strouhal Numbers of a Normal Cylinder Pair at P/D=1.5

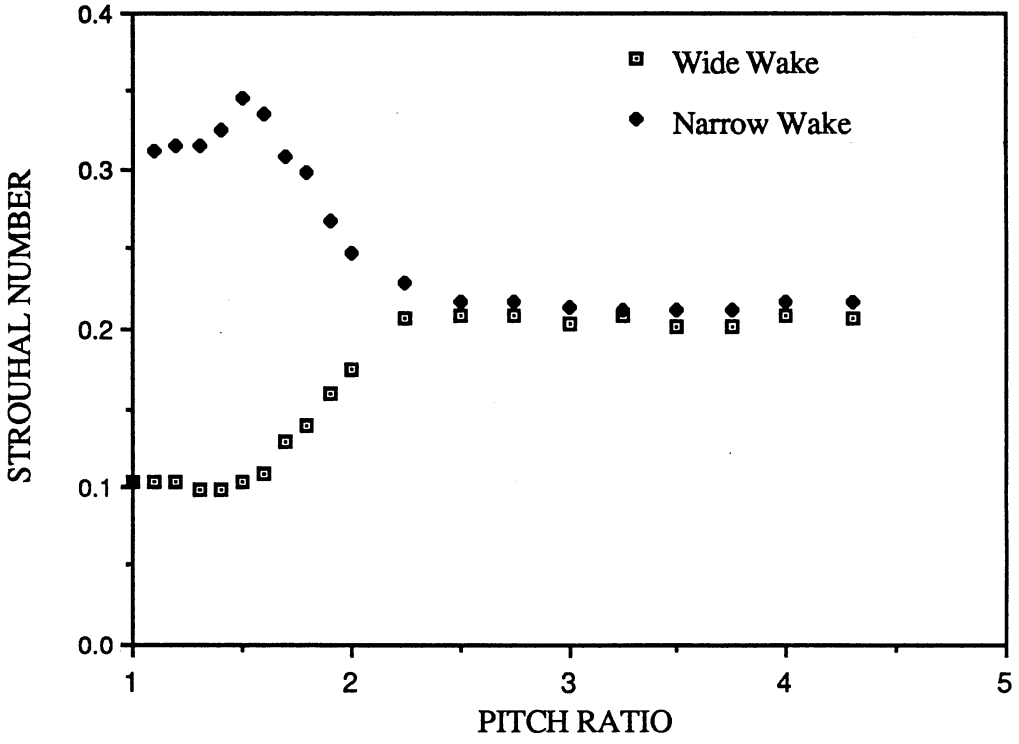

Figure 40. Strouhal Numbers about a Normal Cylinder Pair at Various Separation

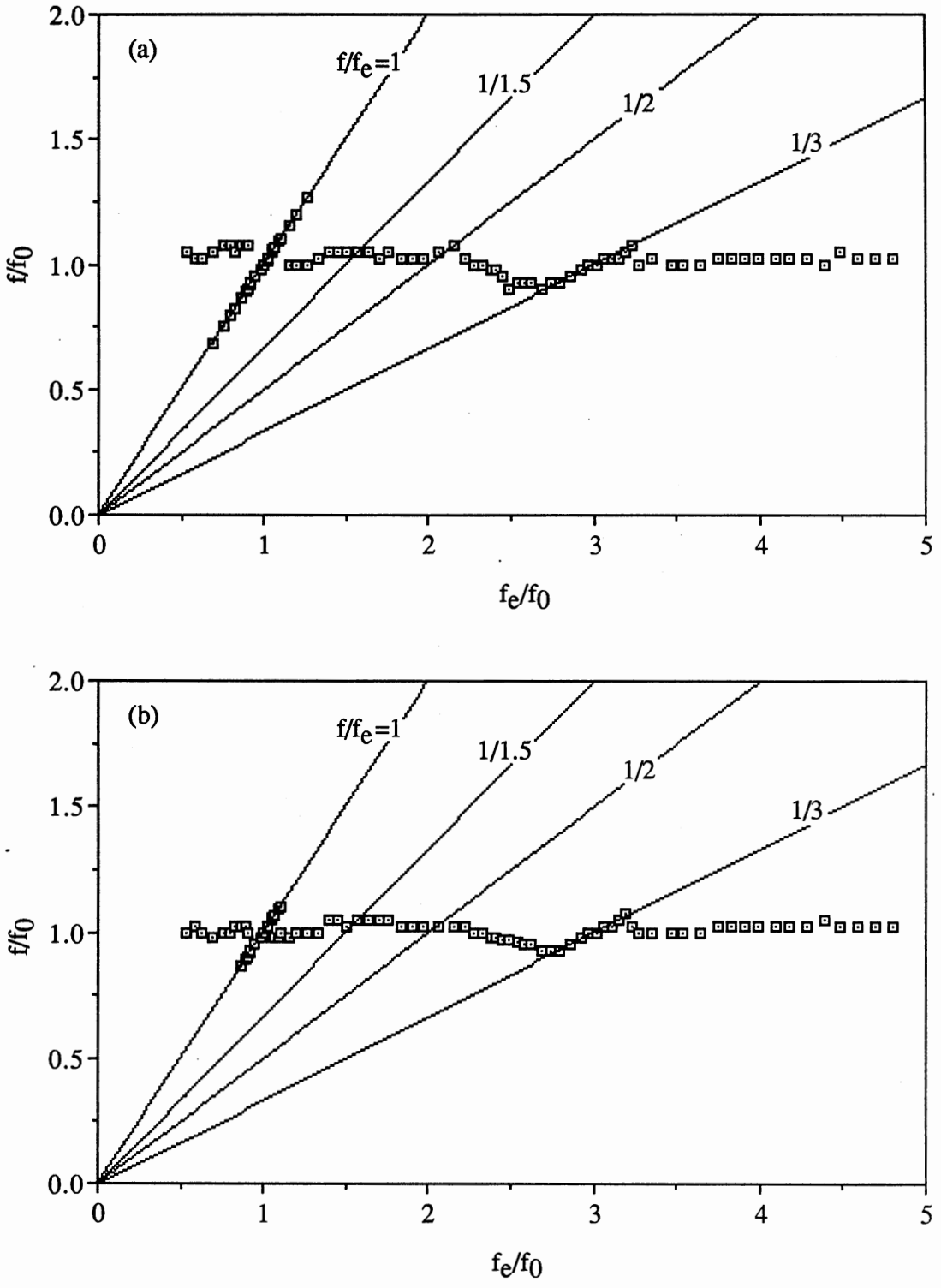

Figure 41. Variation of Shedding Frequency as a Function of Cylinder Forced Oscillation Frequency for a Normal Cylinder Pair Having P/D=3.0. (a) Fixed Cylinder, (b) Vibrating Cylinder

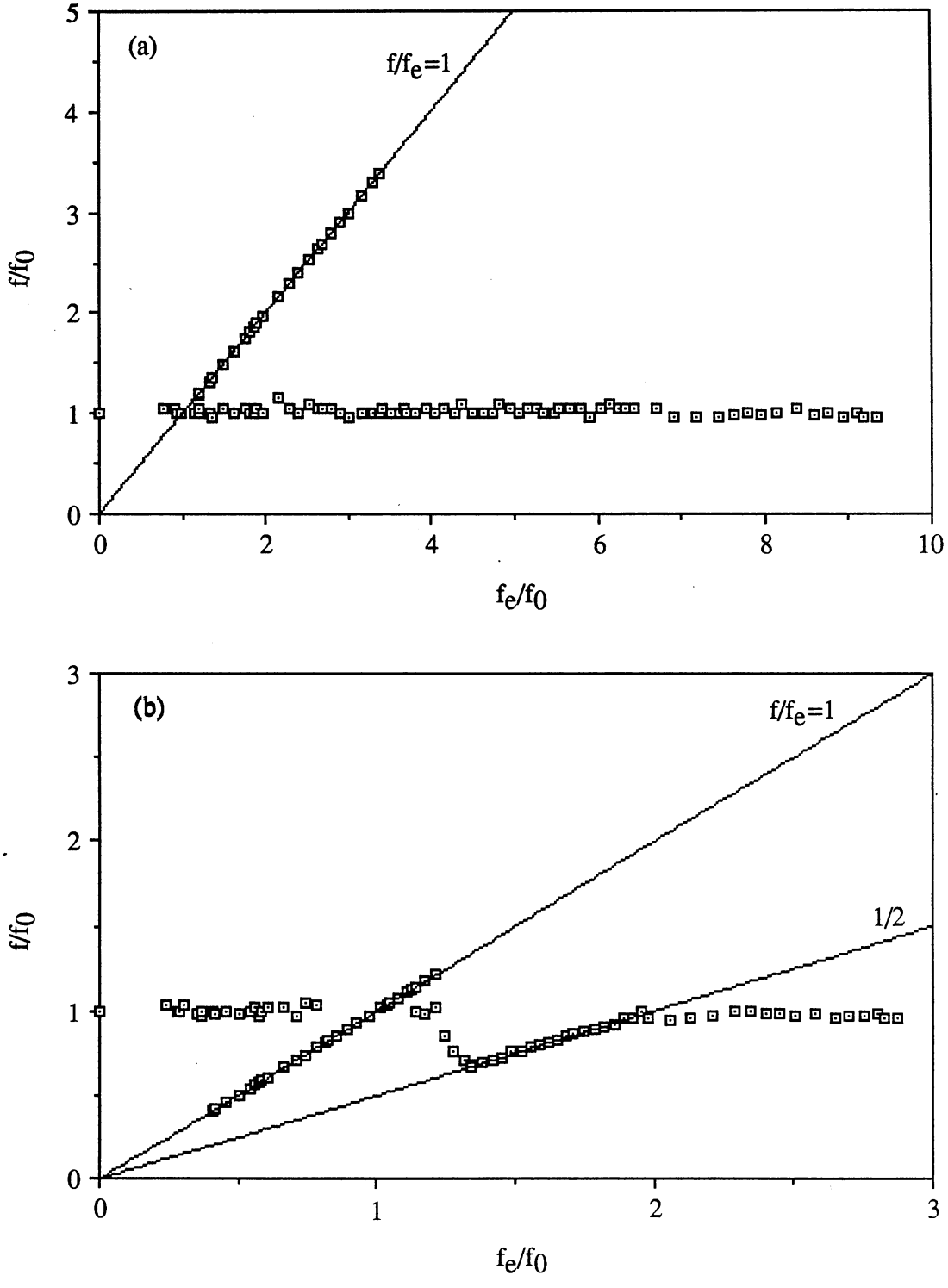

Figure 42. Variation of Shedding Frequency as a Function of Cylinder Forced Oscillation Frequency for a Normal Cylinder Pair Having P/D=1.5. (a) Wide Wake, (b) Narrow Wake

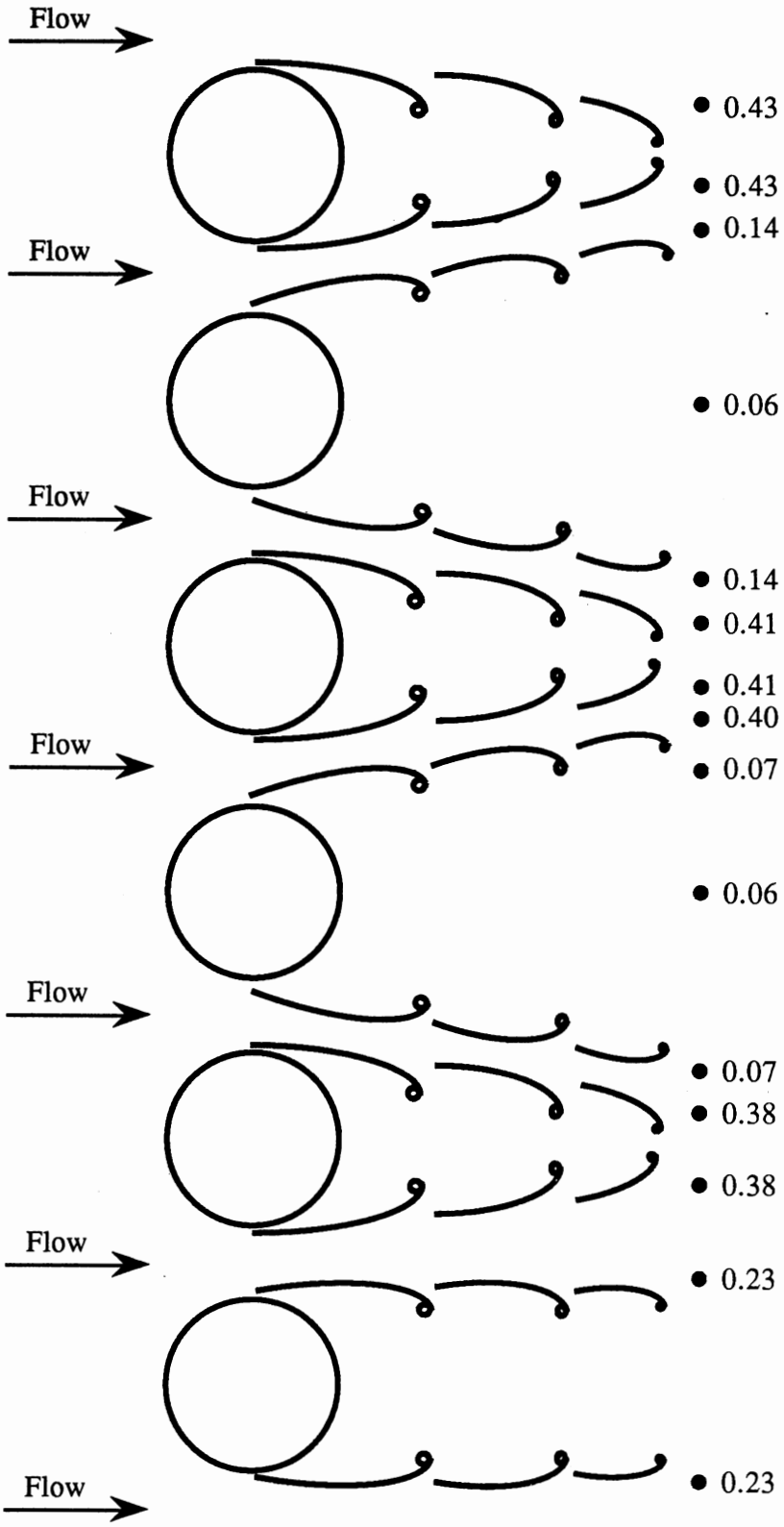

Figure 43. Strouhal Numbers of a Single Tube Row at P/D=1.4

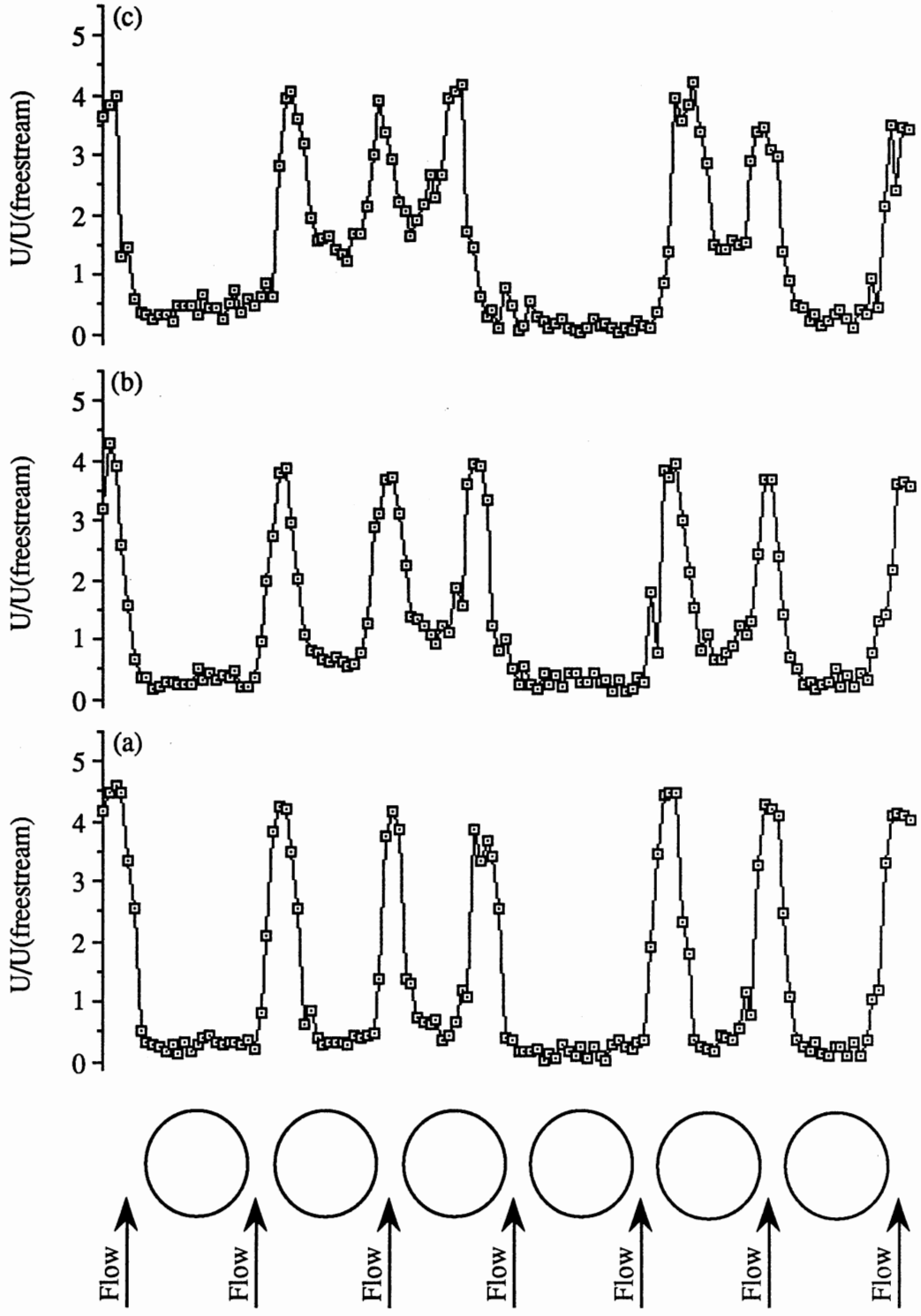

Figure 44. Time Mean Velocity Profiles of a Single Tube Row with P/D=1.25 at Various Downstream Positions. (a) 0.5D, (b) 0.75D, (c) 1.0D

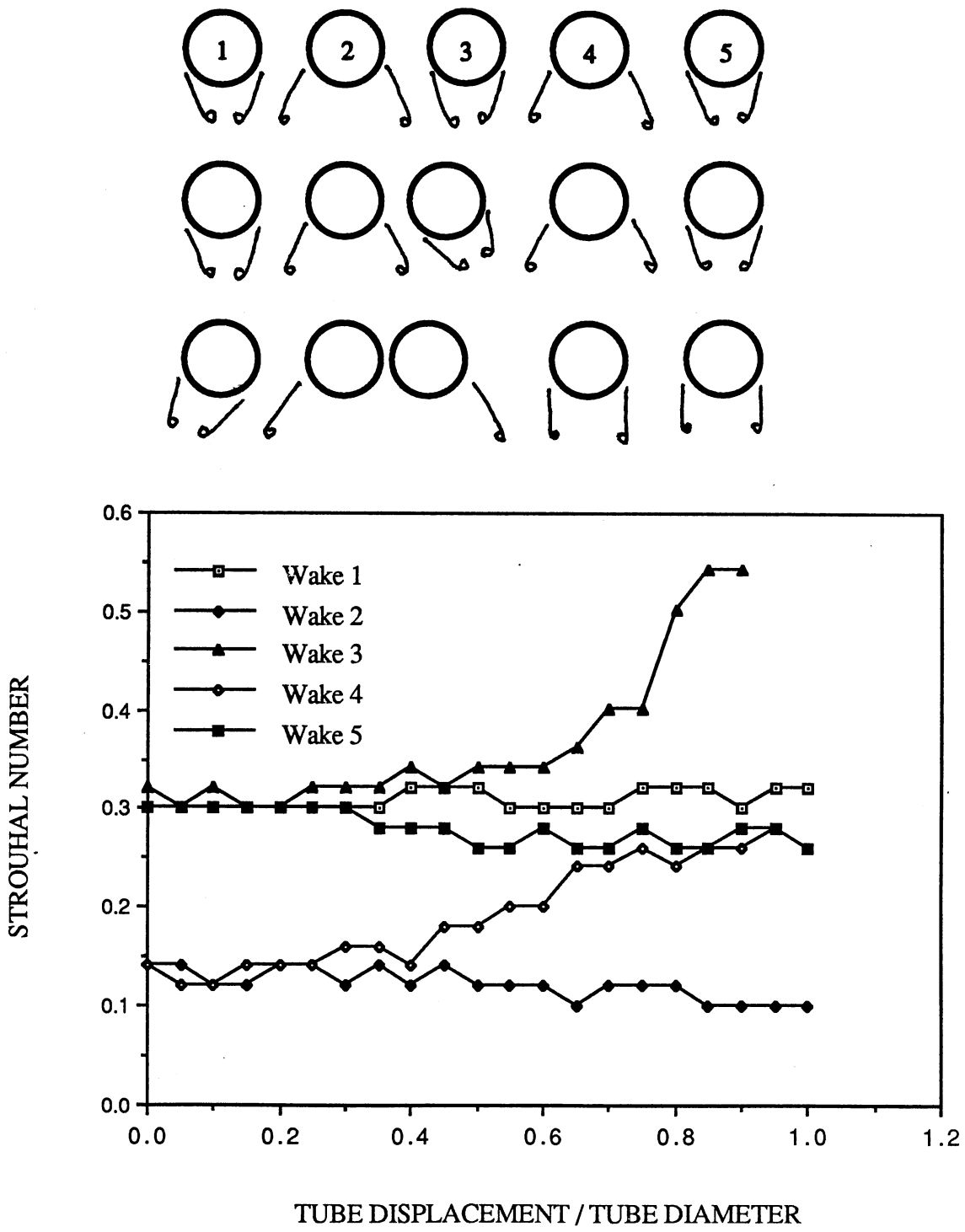

Figure 45. Strouhal Number vs. Static Tube Displacement in a Single Tube Row Having P/D=2.0 at Re=2040

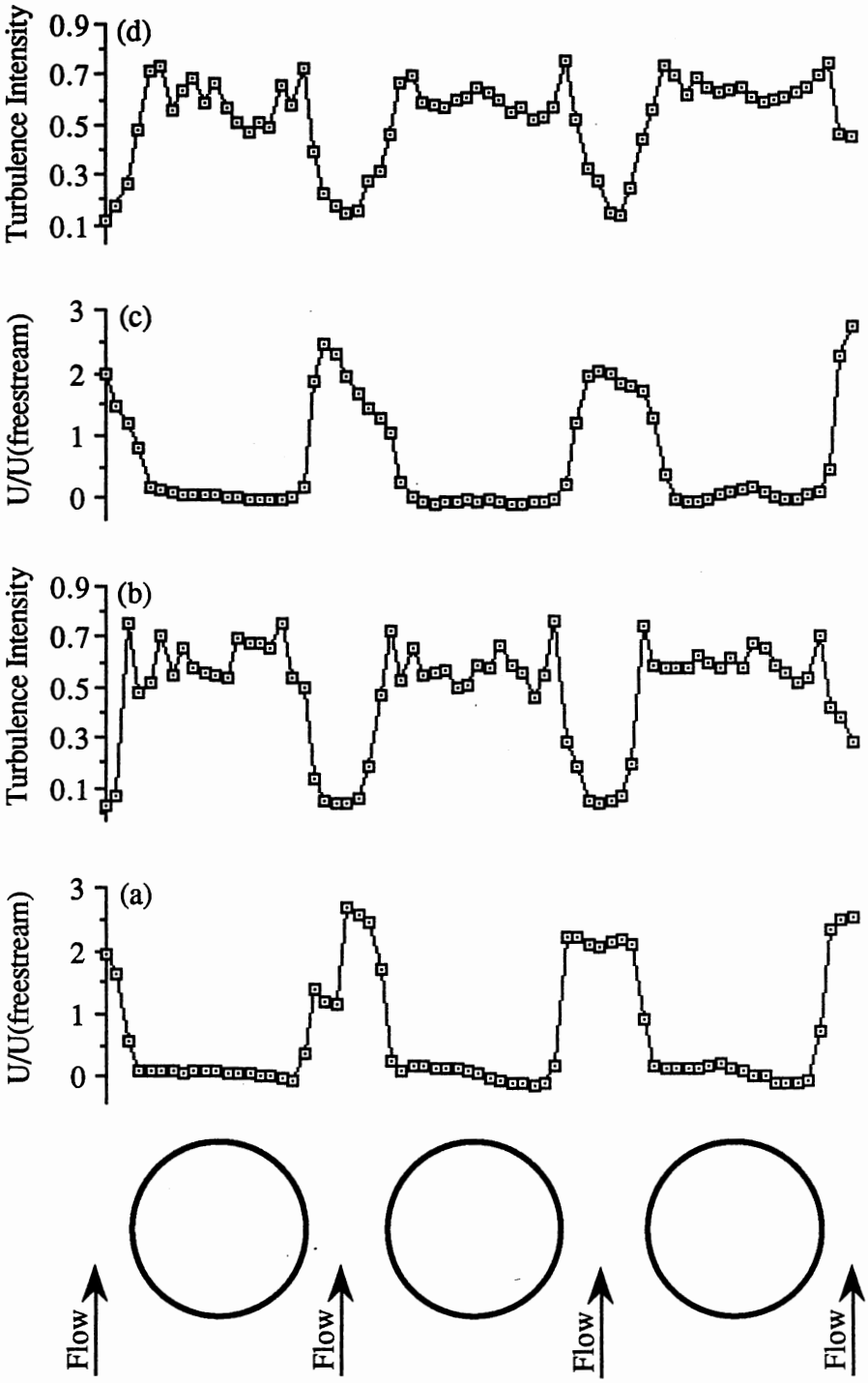

Figure 46. Time Mean Velocity and Turbulence Intensity Profiles in and behind a 90-degree Four-Row Tube Array with P/D=1.5. (a) & (b) between 1st and 2nd Rows, (c) & (d) between 2nd and 3rd Rows, (e) & (f) between 3rd and 4th Rows, (g) & (h) 1/8D Downstream of the Array, (i) & (j) 1D Downstream of the Array

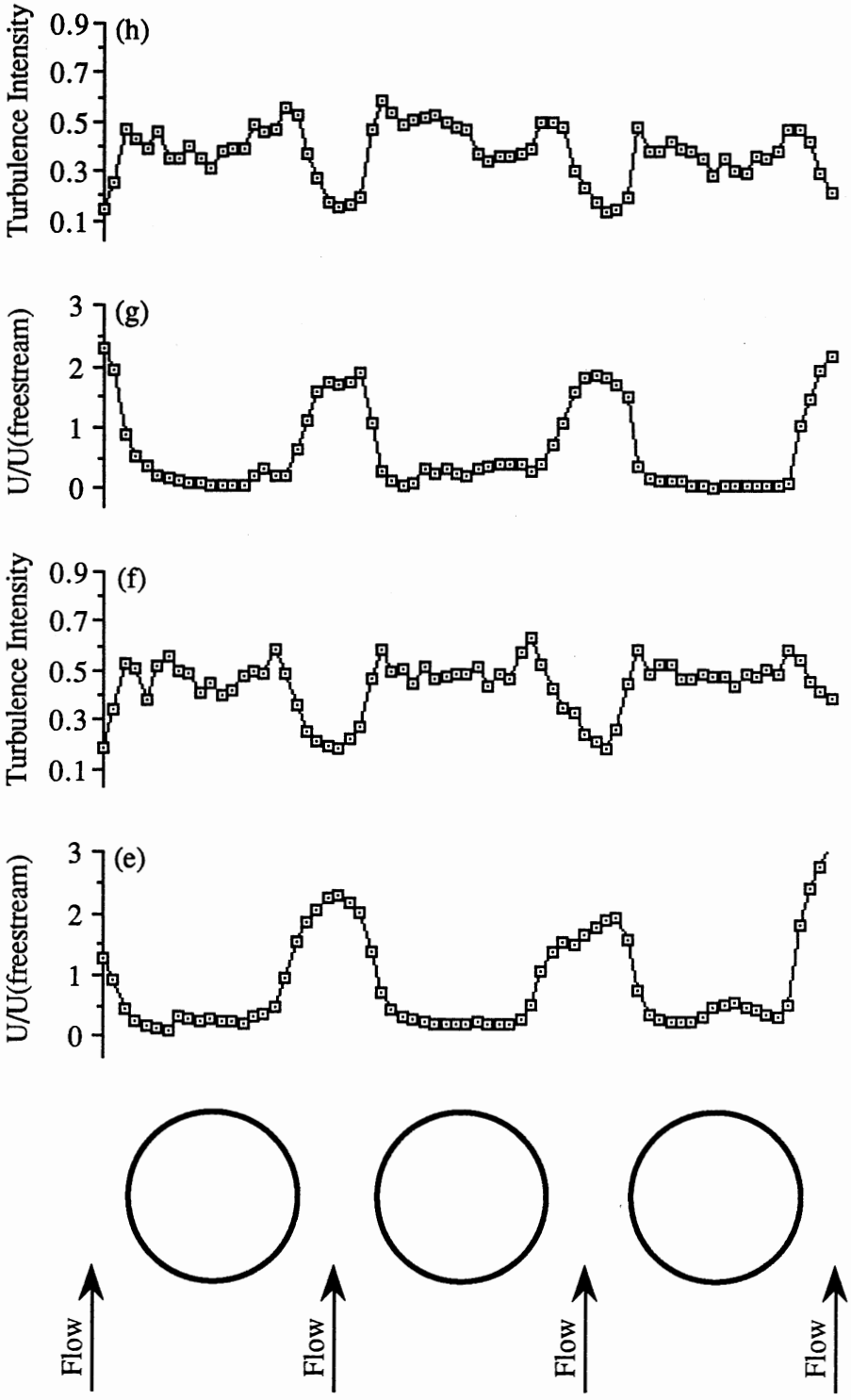

Figure 46. (Continued)

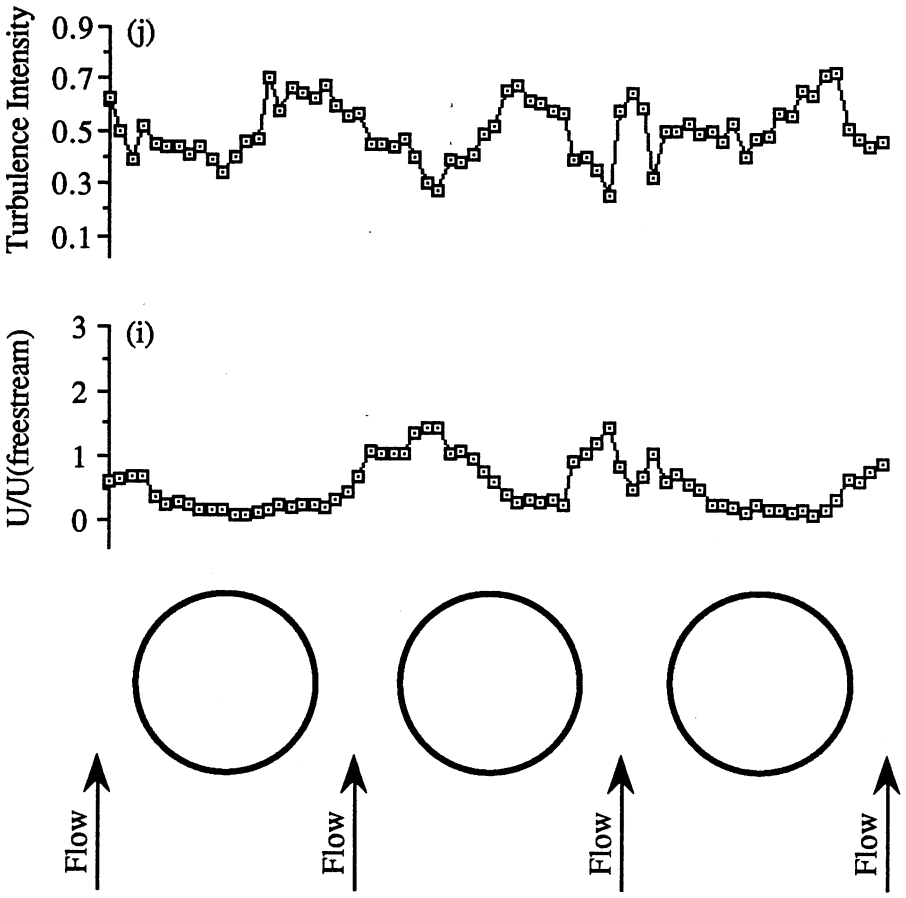

Figure 46. (Continued)

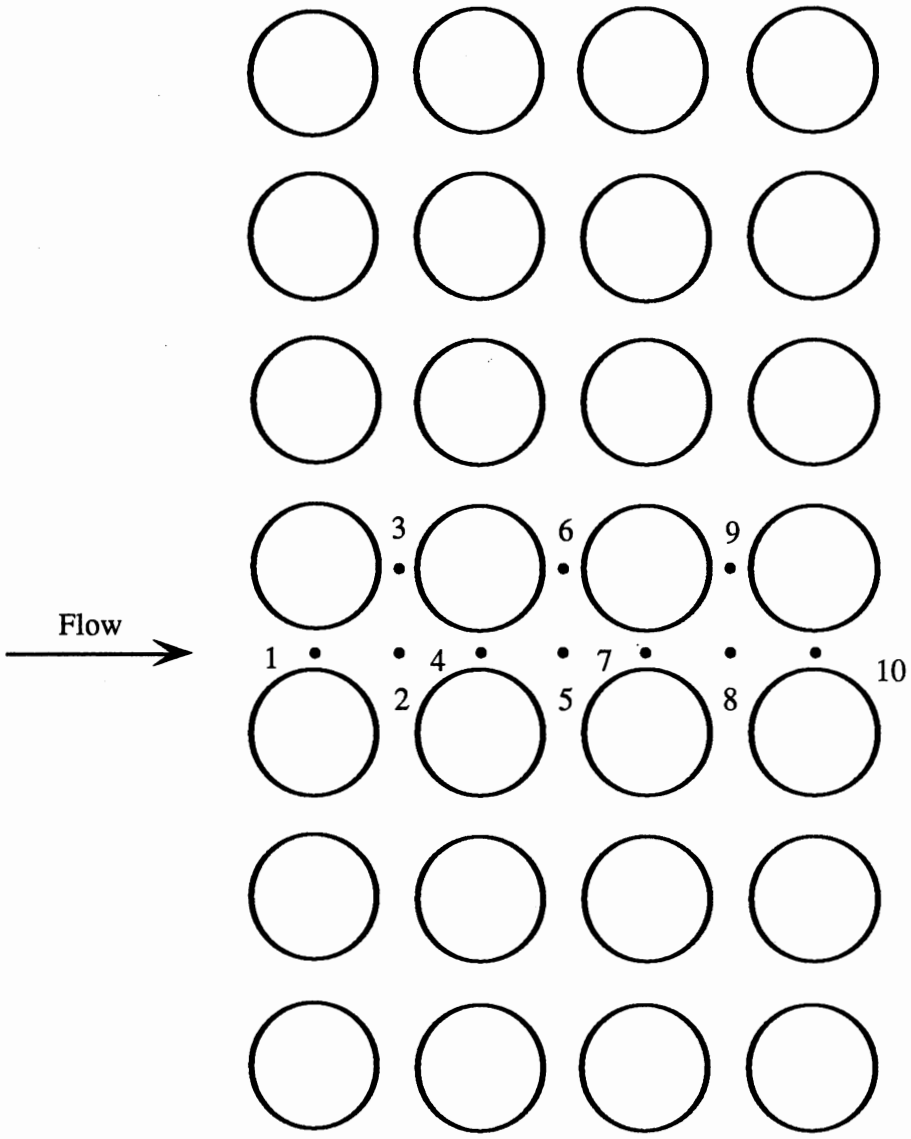

(a) MEASURING POSITIONS

Figure 47. Oscillograms and Spectra in 90-Degree Arrangement Tube Array at P/D=1.5

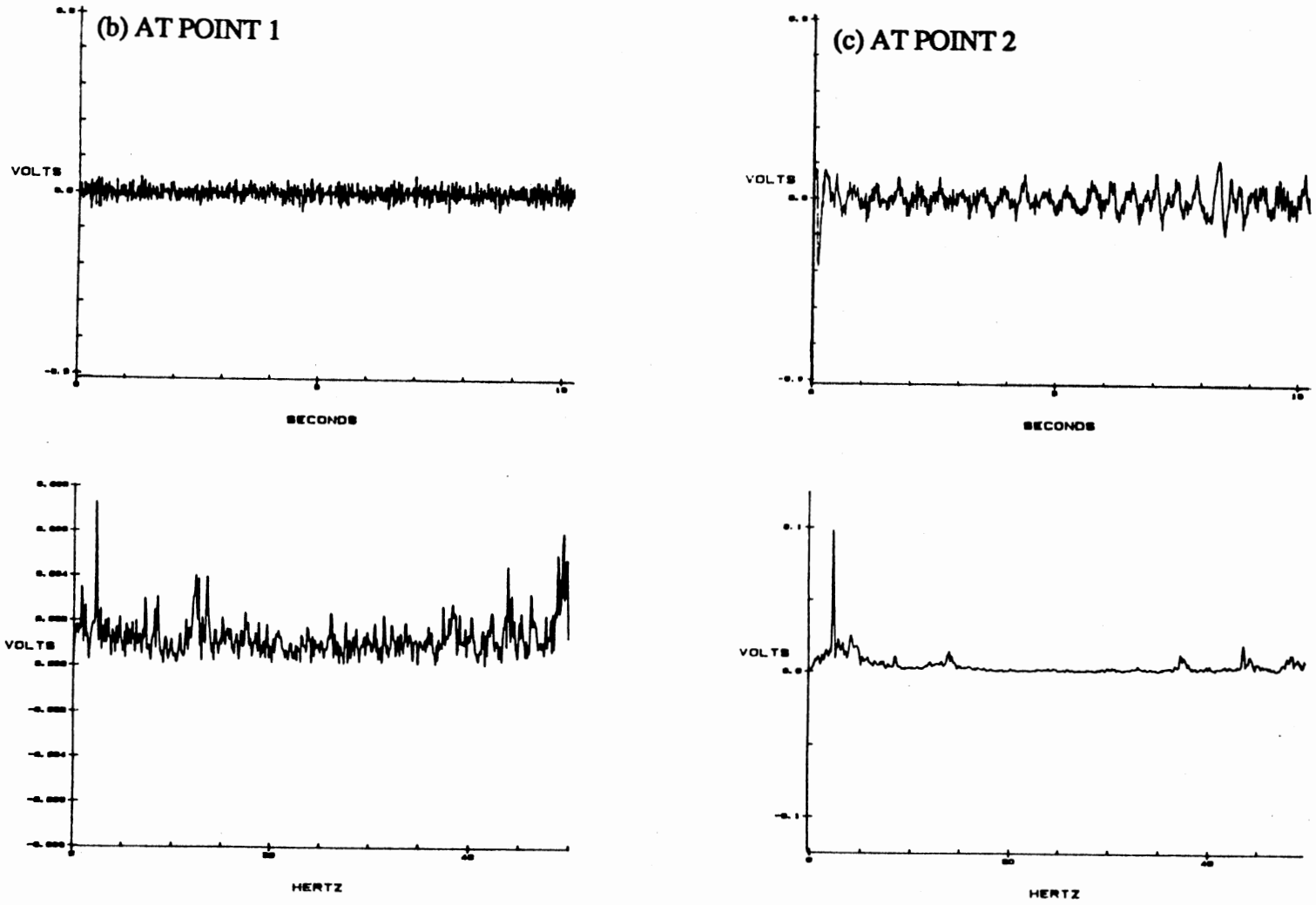

Figure 47. (Continued)

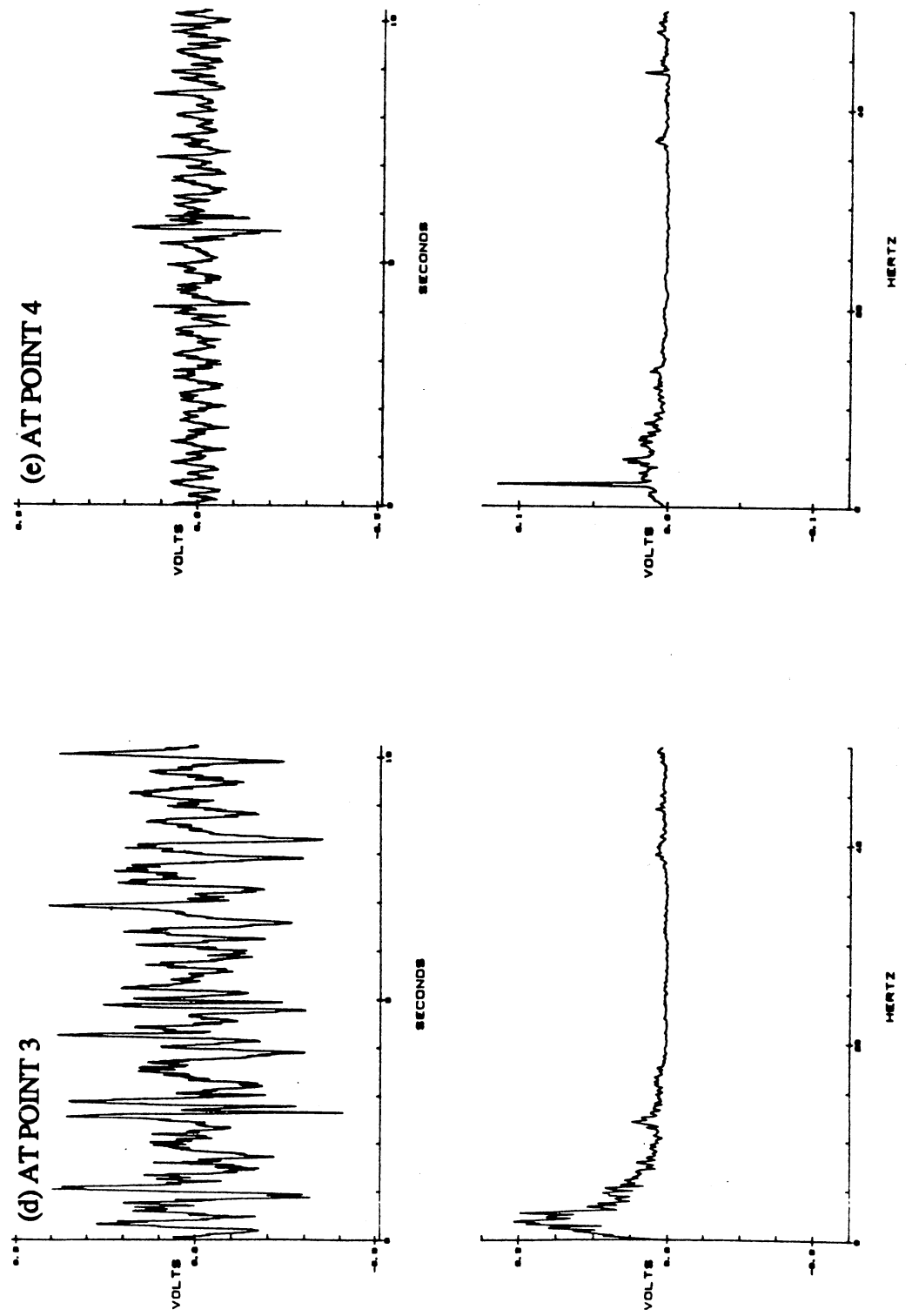

Figure 47. (Continued)

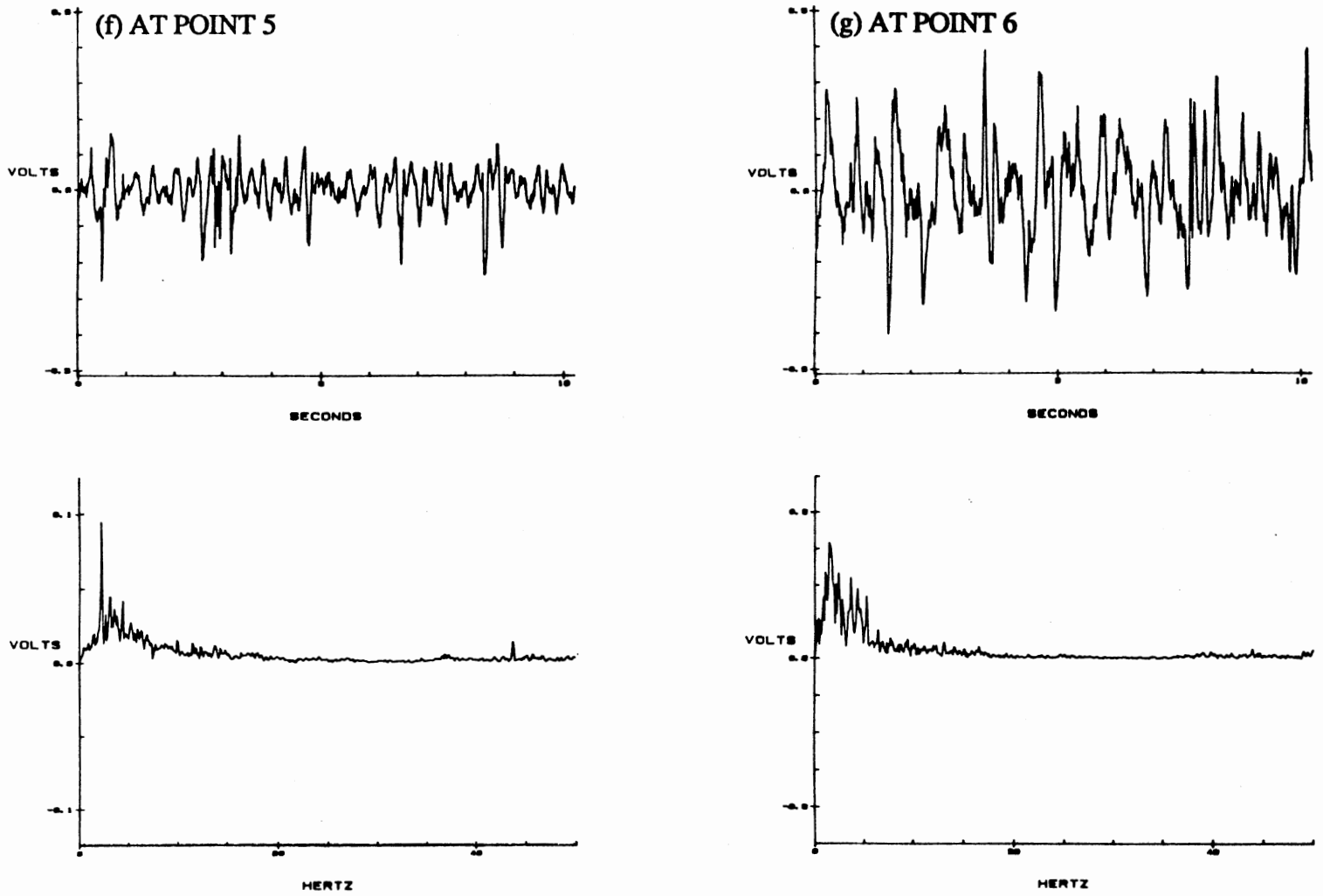

Figure 47. (Continued)

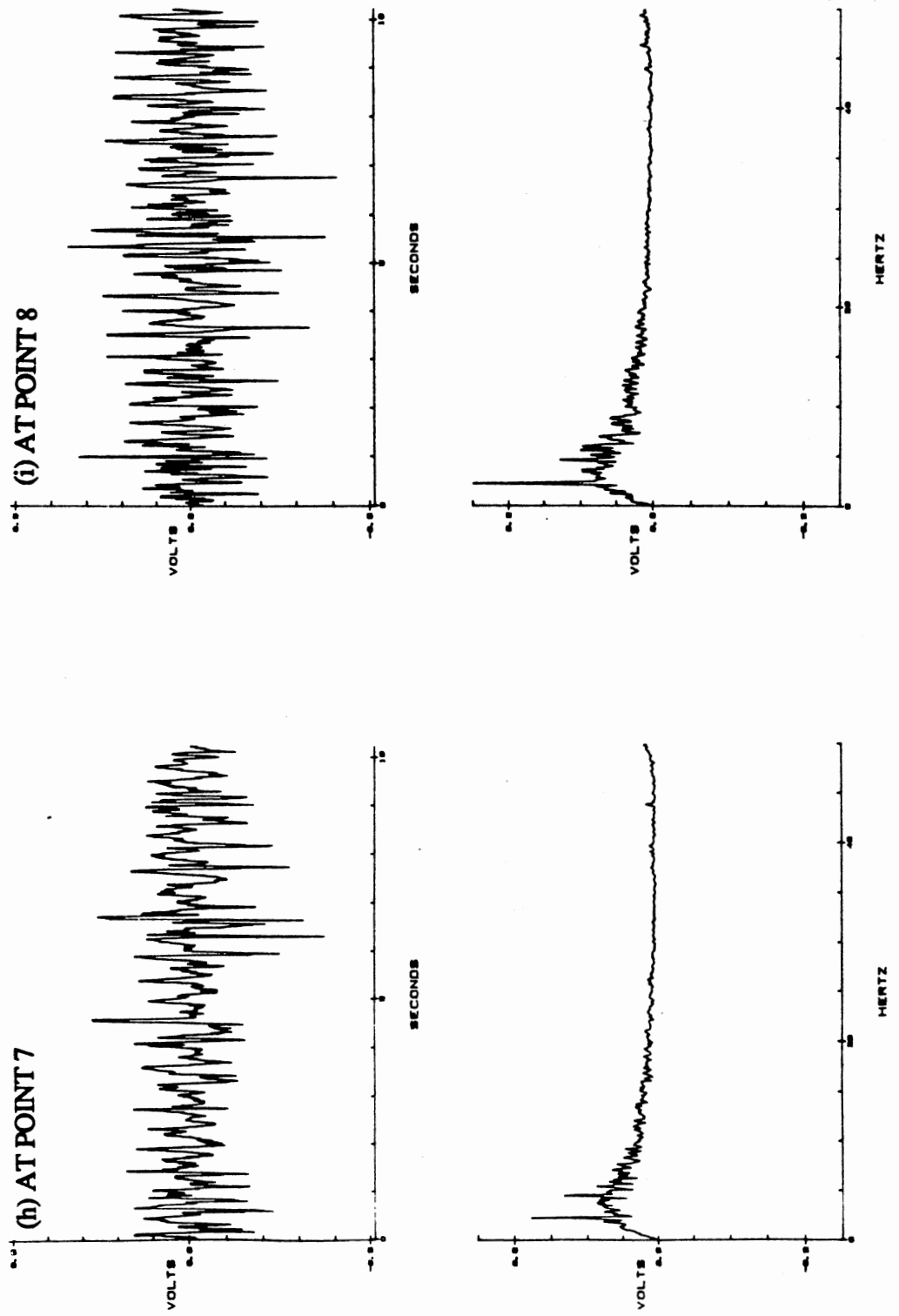

Figure 47. (Continued)

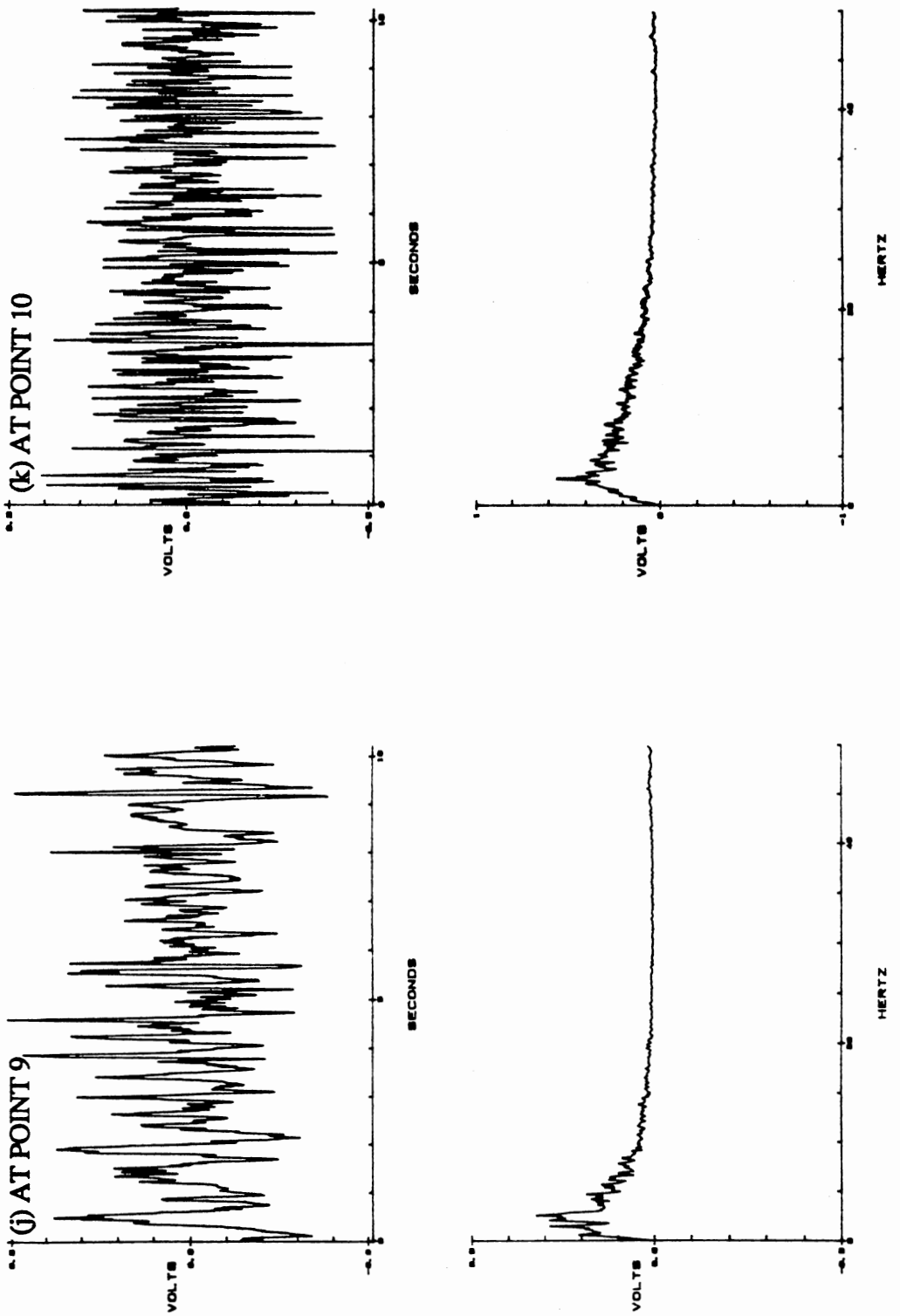

Figure 47. (Continued)

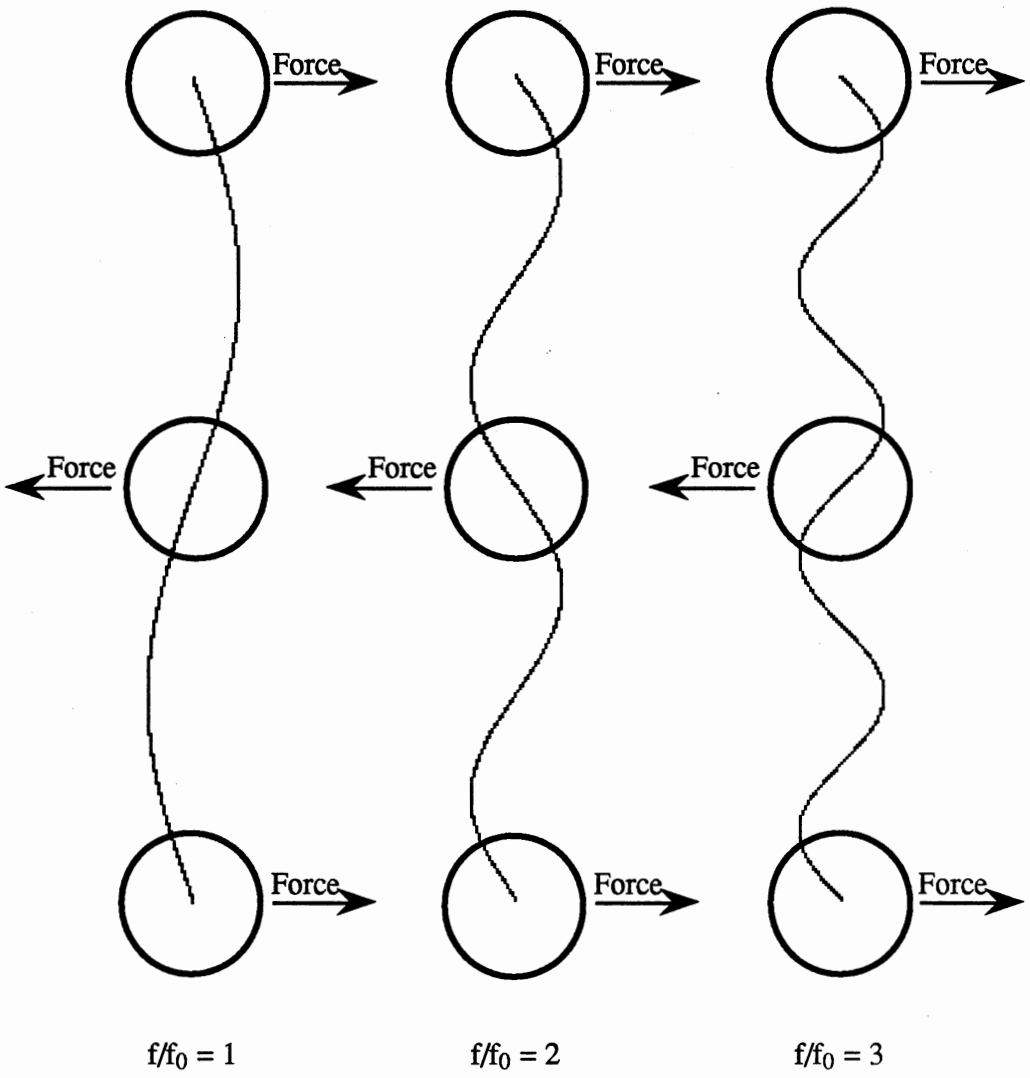

Figure 48. Odd-Number Harmonic Lock-in Effect

2

VITA

Minter Cheng

Candidate for the Degree of

Doctor of Philosophy

Thesis: INSTABILITY OF CROSS-FLOW THROUGH CIRCULAR CYLINDERS

Major Field: Mechanical Engineering

Biographical:

Personal Data: Born in Taiwan, Republic of China, December 3, 1957, the son of Yuan-Chi and Pi-Ann Cheng. Married to Suefen Chen on January 7, 1989.

Education: Graduated from High School of Taiwan Normal University, Taipei, Taiwan, R. O. C., in May, 1975; received Bachelor of Engineering degree in Mechanical Engineering from Feng Chia University at Taichung, Taiwan, R. O. C., in May, 1979; received Master of Science degree from Oklahoma State University in December, 1985; completed requirements for the Doctor of Philosophy degree at Oklahoma State University in May, 1991.

Honors: National Dean's List 1985-1986; Phi Kappa Phi; Pi Tau Sigma; Sigma Xi; Who's Who among International Students in American University and Colleges 1989.

Professional Society: The American Society of Mechanical Engineers

Professional Experience: Mechanical Engineer,Chinese Petroleum Corporation,Taipei, Taiwan, R. O. C., August 1981 to November 1981; Research Assistant, Chung Shan Institute of Science and Technology, Lung-Tan, Taiwan, R. O. C., November, 1981 to June, 1984; Teaching Associate, Department of Mechanical and Aerospace Engineering, Oklahoma State University, August, 1985 to January, 1988; Research Associate, Department of Mechanical and Aerospace Engineering, Oklahoma State University, January, 1988 to December, 1990.